150
6/14/79

DR. 2721

GEAP-23773-2
MARCH 1979

MASTER

DEMONSTRATION OF FUEL RESISTANT TO PELLET-CLADDING INTERACTION PHASE I FINAL REPORT

COMMONWEALTH RESEARCH CORPORATION
SUBCONTRACT 3-20-46
U.S. DEPARTMENT OF ENERGY
PRIME CONTRACT EN-77-C-02-4473

GENERAL ELECTRIC

DISCLAIMER

GEAP-23773-2
March 1979
UC-78
DRF No. J11-102

DEMONSTRATION OF FUEL RESISTANT TO PELLET-CLADDING INTERACTION

PHASE I
Final Report

Compiled by
H. S. Rosenbaum
Program Manager

Approved: J. S. Armijo 2/15/79

J. S. Armijo, Manager
Core Materials Engineering

Approved: R. G. Proebstle 3/6/79

R. A. Proebstle, Manager
Applied Metallurgy and Chemistry

Prepared for the
Commonwealth Research Corporation Under Subcontract 3-20-46
U.S. Department of Energy
Prime Contract EN-77-C-02-4473

Printed in the United States of America
Available from
National Technical Information Service
U.S. Department of Commerce
5285 Port Royal Road
Springfield, VA 22161
Price: Printed Copy $6.00, Microfiche $2.25

NUCLEAR ENERGY ENGINEERING DIVISION • GENERAL ELECTRIC COMPANY
SAN JOSE, CALIFORNIA 95125

GENERAL ELECTRIC

LEGAL NOTICE

This report was prepared by General Electric as an account of work sponsored by the U.S. Department of Energy ("DOE"). Neither DOE, members of DOE, nor GE, nor any person acting on behalf of either, including Commonwealth Edison Company and Commonwealth Research Corporation:

A. *Makes any warranty or representations, express or implied, with respect to the accuracy, completeness, or usefulness of the information contained in this report, or that the use of any information, apparatus, method, or process disclosed in this report may not infringe privately owned rights; or*

B. *Assumes any liabilities with respect to the use of, or for damages resulting from the use of, any information, apparatus, method, or process disclosed in this report.*

TABLE OF CONTENTS

		Page
	ABSTRACT	xi
	CONTRIBUTING AUTHORS	xii
	ACKNOWLEDGEMENTS	xiii
	HIGHLIGHTS	xiv
1.	INTRODUCTION	1-1
2.	SUMMARY FOR PHASE 1	2-1
	2.1 Design of Large-Scale Demonstration	2-1
	2.2 Support Tests for Large-Scale Demonstration	2-1
	2.3 Lead Test Assemblies	2-3
3.	PART 1. DESIGN OF LARGE-SCALE DEMONSTRATION	3-1
	3.1 Objectives	3-1
	3.2 Introduction	3-1
	3.3 Design Concept	3-1
	3.4 Core Performance—Steady-State Analyses	3-2
	3.5 Ramping Studies	3-2
	3.6 Bundle Design and Related Studies	3-3
	3.7 Core Response to Assumed Accidents and Transients	3-4
4.	PART 2. SUPPORT TESTS FOR LARGE-SCALE DEMONSTRATION	4-1
	4.1 Task 1.0 Laboratory Support	4-1
	4.2 Task 2.0 Licensing Tests	4-27
	4.3 Task 3.0 Fuel Irradiation Tests	4-40
5.	PART 3. LEAD TEST ASSEMBLIES	5-1
	5.1 Objectives	5-1
	5.2 Task 1.0 Design and Licensing	5-1
	5.3 Tasks 2.0 and 3.0 Fabrication, Characterization and Quality Assurance	5-2
	5.4 Task 4.0 Irradiation and Evaluation	5-4
6.	REFERENCES	6-1/6-2

LIST OF ILLUSTRATIONS

Figure	Title	Page
4.1-1	Comparison of Total Plastic Strain from Expanding Mandrel Tests on Irradiated Tubing: Zircaloy-2, Nonbonded Copper Plated on Zircaloy-2, and Iodide Zirconium Bonded on Zircaloy-2 in Cadmium and Flowing Iodine; and Bonded Copper Plated on Zircaloy-2 in Cadmium	4-11
4.1-2	Scanning Electron Micrographs (Secondary Electron Image) of the Inner Surface of SRP-3/15 (5 μm Electroplated and Nonbonded Copper Barrier on Zircaloy-2) Tested in 335°C Cadmium	4-12
4.1-3	Scanning Electron Micrograph (Secondary Electron Image) of the Fracture Surface of SRP-3/17-1 (0.076 mm Iodide Zirconium Liner on Zircaloy-2) Showing Ductile Morphology.	4-13
4.1-4	Scanning Electron Micrographs (Secondary Electron Image) of the Inner Surface of the SRP-3/17-1 (0.076 mm Iodide Zirconium Liner on Zircaloy-2) Showing Superficial Cracks	4-14
4.1-5	Scanning Electron Micrographs (Secondary Electron Image) of the Inner Surface of SRP-3/17-2 (0.076 mm Iodide Zirconium Liner on Zircaloy-2) Showing Incipient Cracks	4-15
4.1-6	Scanning Electron Micrographs (Secondary Electron Image) Showing the Fracture Surface of SRP-3/19-1 (0.076 mm Iodide Zirconium Liner on Zircaloy-2) Tested at 335°C, 40 Pa Iodine	4-16
4.1-7	Relative Concentrations of Fluorine in Copper-On-Zircaloy (CZ), Copper-On-Oxide (CA), and Copper-On-Zircaloy Plus Post-Plating Autoclave Treatment (CZA) as a Function of Depth from the Copper Surface	4-17
4.1-8	Bright-Field Images of Grains in 10 μm Thick Polycrystalline Plated Copper Barriers: (a) Vacuum Outgassed at 200°C for 16 Hours; (b) Vacuum Outgassed at 400°C for 16 hours; (c) Electrolytic (No Heat Treatment). Magnification 38,000X	4-18
4.1-9	Selected Area Electron Diffraction Patterns from Thin Regions Illustrated in Figure 4.1-1 for Copper Barriers: (a) Vacuum Outgassed at 200°C for 16 Hours (b) Vacuum Outgassed at 400°C for 16 Hours; (c) Electrolytic.	4-19
4.1-10	Bubbles in Copper Barriers Outgassed at (a) 200°C, (b) 400°C	4-20
4.1-11	Apparatus for Protecting the Inner Barrier Material Surface During Chemical Milling Operation	4-21
4.1-12	Radial Direction Pole Figure of the (0002) Plane of Tubing, Barrier-Low Oxygen Sponge Zirconium, Annealed 577°C. LD = longitudinal direction; TD = tangential direction	4-22
4.1-13	Radial Direction Pole Figure of the (1010) Plane of Tubing, Barrier-Low Oxygen Sponge Zirconium, Annealed 577°C	4-23
4.1-14	Radial Direction Pole Figure of the (0002) Plane of Tubing at Midwall, Barrier-Low Oxygen Sponge Zirconium, Annealed 577°C	4-24
4.1-15	Radial Direction Pole Figure of the (0002) Plane of Tubing at Inner Surface, Barrier-Low Oxygen Sponge Zirconium, Annealed 577°C	4-24
4.1-16	Inverse Pole Figure for Zr-lined Tubing: (a) Midwall of Zircaloy-2 Tubing, (b) Zirconium Barrier Surface of Low Oxygen Sponge, Annealed at 577°C	4-25

LIST OF ILLUSTRATIONS (Continued)

Figure	Title	Page
4.2-1	Schematic of LOCA Test Specimen	4-32
4.2-2	Temperature as a Function of Time for Simulated LOCA Testing	4-33
4.2-3	Longitudinal Section from Lower Portion of Cu on Unoxidized Zircaloy-2 Specimen. Note Wall-thickness Buildup from Molten Metal at A and B, the Wall Thinning Below B, and Metal Between Urania Pellets at E. Magnification 8X.	4-34
4.2-4	Post-Test Inner Surface (I.D.) Microstructure of Cu on Autoclaved Zircaloy-2 Specimen. Note Oxygen Stabilized α-Zirconium Phase A, β-Quenched Structure B, and Complex Interaction Layer Between A and B Regions. Magnification 500X.	4-35
4.2-5	Typical Post-Test Outer Surface (O.D.) Microstructure of Zircaloy-2 Cladding After Heating to 1204°C in Saturated Steam. Note ZrO_2 Layer A Oxygen Stabilized α-Phase B, and β-Quenched Structure C. Magnification 300X.	4-35
4.2-6	Longitudinal Section of Cu on Oxidized Cladding Showing Wall Thickness After 5.17 MPa (750 psi) Test. Note Variation in Thickness of Inner Surface (I.D.) Cu-Zr Interaction Layer. Magnification 100X.	4-36
4.2-7	Post-Test Microstructure at Inner Surface of Cu on Autoclaved Zircaloy-2 Tested at 5.17 MPa (750 psi). Note Complex Eutectic Structure and Absence of Oxygen Stabilized α-Phase Layer. Magnification 530X.	4-37
4.2-8	Post-Test Microstructure at Inner Surface of Cu on Autoclaved Zircaloy-2 Tested at 6.90 MPa (1000 psi). Magnification 530X.	4-38
4.3-1	Nondestructive Test Summary—Sound Electroless Cu-Barrier Rod CC-54A	4-50
4.3-2	Irradiation Growth of SRP-3 Fuel Rod Segments	4-51
4.3-3	Relative Power Attenuation Versus ^3He Pressure (for ~2.6% ^{235}U Enriched Fuel Rod)	4-52
4.3-4	Specified Ramp Test Sequence for Tests at the R-2 Test Reactor	4-53
4.3-5	Recorder Chart Output of Relative Rod Power and Loop Activity Level Indicating Failure of SRP-2/13	4-54
4.3-6	Preparation of SEM Sample (SRP-3/14, L-2)	4-55
4.3-7	Low Magnification (~30X) Composite SEM Micrograph Secondary Electron Image (SRP-3/14, L-2) Showing Areas for More Detailed Study	4-56
4.3-8	SEM Micrographs (Secondary Electron Images) of Cu-Barrier in Plenum Section (SRP-3/15)	4-57
4.3-9	Cu-Barrier in Fueled Section (SRP-3/15, B-5)	4-58
4.3-10	SEM Micrograph Fuel and Fission Product Deposits on Cu-Barrier at Pellet Interface Location (SRP-3/14, L-2)	4-59

LIST OF ILLUSTRATIONS (Continued)

Figure	Title	Page
4.3-11	X-ray Maps of Area Shown in Figure 4.3-10(a)	4-60
4.3-12	Fission Product X-ray Maps of Area Shown in Figure 4.3-10(a)	4-61
4.3-13	Cu-Barrier Surface Apparently Smeared or Flattened by Hard Interaction with Fuel Pellet (SRP-3/14, L-2)	4-62
4.3-14	Cu-Barrier Surface in Fueled Section Showing Flattened Area (SRP-3/15, G-2)	4-63
4.3-15	Break in Cu Layer (SRP-3/15, B-2) (Secondary Electron Image)	4-64
4.3-16	X-ray Maps of Area Shown in Figure 4.3-15(b)	4-65
4.3-17	Heavy Deposits on Cu-Barrier Surface at Pellet Interface Location (CC-44A, G)	4-66
4.3-18	X-ray Maps of Area Shown in Figure 4.3-17(a)	4-67
4.3-19	Fission Product X-ray Maps of Area Shown in Figure 4.3-17(a)	4-68
4.3-20	Deposit on Cu-Barrier Surface at Pellet Interface Location (SRP-3/15, B-5)	4-69
4.3-21	X-ray Maps of Area Shown in Figure 4.3-20(a)	4-70
4.3-22	Zr-Liner Surface in Plenum Section (SRP-3/18)	4-71
4.3-23	Zr-Liner in Fueled Section (SRP-3/18, H-2)	4-71
4.3-24	Deposit on Zr-Liner Surface at Pellet Interface Location (SRP-3/18, H-2)	4-72
4.3-25	Fission Product X-ray Maps of Area Shown in Figure 4.3-24(a)	4-73
5.1-1	Fuel Rod Serial Numbers and Locations of Fully Characterized Rods, Zirconium-Liner (Crystal Bar Zirconium) Coreduced with Zircaloy	5-5
5.1-2	Fuel Rod Serial Numbers and Locations of Fully Characterized Rods, Zirconium-Liner (Low Oxygen Sponge Zirconium) Coreduced with Zircaloy	5-6
5.1-3	Fuel Rod Serial Numbers and Locations of Fully Characterized Rods, Copper Barrier on Etched Zircaloy	5-7
5.1-4	Fuel Rod Serial Numbers and Locations of Fully Characterized Rods, Copper Barrier on Autoclave-Oxidized Zircaloy	5-8
5.1-5	Cross Section of Bundle with 2.82% Average Enrichment and 6 Rods with 2Wt % Gd_2O_3	5-9

LIST OF TABLES

Table	Title	Page
4.1-1	Summary of Expanding Mandrel Test Results for Irradiated Copper Plated Zircaloy-2, Iodide Zirconium Lined Zircaloy-2 and Zircaloy-2 Tubing	4-2
4.1-2	Relative Concentrations of Copper-On-Zircaloy Sample (at. %)	4-7
4.1-3	Inverse Pole Figure Orientation Parameters	4-9
4.2-1	Simulated LOCA Test Results on Reference and Barrier Zircaloy-2 Cladding	4-28
4.2-2	Planned RIA Tests	4-31
4.3-1	SRP Irradiation Status	4-41
4.3-2	Segments Retrieved During Third Reconstitution of Bundle SRP-2 (Monticello)	4-41
4.3-3	R2 Technical Data	4-42
4.3-4	R2 Loop 1 and 2 Technical Data Summary	4-43
4.3-5	Loop Instrumentation	4-43
4.3-6	Description of Segments Ramp Tested in R2	4-44
4.3-7	Pre-Ramp Standardization Phase Irradiation Summary	4-44
4.3-8	R2 Ramp Test—Results Summary	4-45
4.3-9	SEM Specimen Details	4-46
4.3-10	Summary of Fission Gas Release for SRP-III Rods Ramp Tested in GETR	5-4

ACKNOWLEDGEMENTS

A project as complex as this requires active support and help from many individuals representing many organizations. The contributing authors have cited those whose help they acknowledge, and their acknowledgements appear separately at the end of the various subsections of this report. In addition, acknowledgements are due to those whose efforts have made this entire project a reality. The invaluable contributions of the following people are gratefully acknowledged:

GE Nuclear Technology Department:

J. S. Armijo, for his encouragement and leadership throughout this effort and for his helpful comments and critical review of reports.

L. D. Noble for his helpful advice and his review of the manuscript.

S. Y. Ogawa for helping to plan the characterization and evaluations of the lead test assemblies.

R. A. Proebstle for his active encouragement and support.

Commonwealth Edison Company:

W. M. Kiefer for encouragement in starting this project and for his participation in the Program Steering Committee.

D. R. O'Boyle for his active support and for his help in representing the viewpoint of the Commonwealth Edison Company and the Commonwealth Research Corporation in this program.

U.S. Department of Energy:

P. M. Lang for his active interest and support and for participation in the Program Steering Committee.

D. W. Ujifusa for his support and help during the formative stages of this project.

GE Corporate Research and Development:

M. G. Benz and H. W. Schadler, for their interest in making available the expertise and the facilities of the GE Corporate Research and Development Center for the work of this project.

GE Installation and Service Engineering:

H. A. Zimmerman for his help in resolving administrative details between GE and the Commonwealth Edison Co. regarding this work.

HIGHLIGHTS

- Results of the generic nuclear design indicate that a demonstration irradiation of a PCI-resistant fuel is feasible in a commercial power reactor (BWR/3 type) which has a steady-state core. The barrier fuel can be power ramped to demonstrate resistance to PCI with minimum risk to conventional fuel in the core.

- Nuclear design of the demonstration irradiation has been focused on a demonstration involving 132 bundles of PCI-resistant fuel. Of these, 64 will be a special nuclear design to assure adequate power peaking during the power ramp tests.

- Analyses of core energy throughout the demonstration cycles have proved to be favorable; transient and accident analyses have shown the nuclear design to provide adequate margins for commercial power operations. Furthermore, the core performance at rated power is essentially unchanged from that of a normal reload design.

- In power ramp tests of fuel rods irradiated in commercial BWR's and subsequently tested in a test reactor, the Cu-barrier fuel of the type presently considered for the demonstration successfully resisted PCI at burnup = 12.4 MWd/kg-U; the Zr-liner fuel resisted PCI at burnup = 16.6 MWd/kg-U.

- Four lead test assemblies of barrier fuel were successfully fabricated. Each was of a somewhat different barrier type:

  —Cu-barrier plated on etched Zircaloy
  —Cu-barrier plated on autoclave-oxidized Zircaloy
  —Zr-liner (crystal bar zirconium) coreduced with Zircaloy
  —Zr-liner (low oxygen sponge zirconium) coreduced with Zircaloy.

  These four barrier fuel bundles were inserted into the core of Quad Cities-1 for irradiation in Cycles 5 through 8. Irradiation was begun in February, 1979.

- Simulated loss of coolant accident (LOCA) tests have been done to compare the behavior of the barrier fuels to that of conventional fuel. The resulting data provide background information to be used in licensing the advanced fuel concepts and indicate that the deformation behavior of the barrier fuel cladding during severe LOCA transients is not markedly different from that of standard fuel cladding.

- Expanding mandrel tests which attempt to simulate the stress and corrosion conditions of PCI show that both copper-plated Zircaloy and zirconium-lined Zircaloy tubing (unfueled) are superior to reference Zircaloy. Such tests have been done with both irradiated and unirradiated cladding samples.

- Liquid cesium saturated with cadmium was found to be a very aggressive environment in laboratory tests which simulate PCI.

1. INTRODUCTION

Experience in the nuclear industry with fuel rods of Zircaloy-clad urania has brought to light several causes of fuel rod failure. Most of these causes have been corrected by innovative design modifications and by improvements in manufacturing processes. However, there persists one class of fuel failures which has yet to be eliminated and which presently is controlled by reactor design and operational constraints. These failures are caused by the direct interaction between the irradiated urania fuel, including its inventory of fission products, and the Zircaloy fuel sheath, or cladding. This phenomenon is called "fuel/cladding interaction" or "pellet-cladding interaction" (PCI). The incidence of such failures is closely linked to the power history of the fuel rod and to the severity and duration of power changes. Pellet-cladding interaction fuel failures have occurred in all types of water-cooled reactors that are fueled with urania which is sheathed in Zircaloy: boiling water reactors (BWR), pressurized water reactors (PWR), Canadian deuterium-moderated reactors (CANDU), and the steam generating heavy water reactor (SGHWR).

Recently, national policy regarding light water reactor (LWR) technology has focused on the goal of improved uranium utilization in a fuel cycle that does not depend upon fuel reprocessing. Higher burnup can improve uranium utilization, but the design of fuel for high burnup service requires an acceptable resistance to PCI at those high burnup levels.

Of more immediate concern for utilities are the operational constraints which have been imposed on commercial power reactors to ameliorate the PCI phenomenon. While these operational procedures have been successful in reducing the incidence of fuel failure, the procedures constrain certain reactor operations and are costly in terms of capacity factor. There is a strong incentive to provide a remedy, *i.e.,* a fuel which is resistant to the PCI failure mechanism and which can be operated to high burnup with improved plant capacity factors.

Building upon the General Electric Company's extensive previous efforts (1969 — 1977) to understand the PCI phenomenon and to develop potential remedies, this program was designed to exploit two remedies which General Electric (GE) had already identified as having good potential for success: (a) Cu-barrier fuel and (b) Zr-liner fuel. Copper-barrier fuel has a Zircaloy sheath with a very thin layer of copper plated on the inner surface. Zirconium-liner fuel has a Zircaloy fuel cladding with a metallurgically bonded layer of zirconium on the inner surface. Both the Cu-barrier fuel and the Zr-liner fuel are known collectively as "barrier fuel".

The ultimate objective of this program is to realize demonstration of the PCI-resistance of a fuel based on one of these potential PCI remedies. The demonstration will be in a commercial BWR and it is intended to test a sufficient quantity of fuel to form a reliable data base regarding the performance characteristics of the new fuel. While it is not yet known in which reactor the actual demonstration will occur, it probably will be in a reactor of the BWR/3 type with a steady-state core, where the barrier fuel will be introduced as part of a reload batch.

Prior to the actual demonstration there must be an adequate data base to enable design and licensing; fabrication and quality assurance problems must be addressed; and there must be extensive nuclear physics, fuel management, and power history analyses so that the experimental fuel is properly tested with minimum risk to other fuel in the core. Consequently, the program has been structured to consider each of these aspects.

This program leads ultimately to the large-scale demonstration of one of the two remedy concepts discussed here: Cu-barrier or Zr-liner. The overall program has been divided into three phases:

PHASE 1. Design and Supporting Tests
PHASE 2. Large-Scale Demonstration
PHASE 3. Demonstration Extending to High Burnup

PHASE 1 now has been completed and includes all work from July 1, 1977, through February 28, 1979. PHASE 1 included:

1. A generic nuclear engineering study to show that the demonstration is feasible in a reactor of the BWR/3 type.

2. Laboratory and reactor tests to verify the PCI resistance of the Cu-barrier and the Zr-liner fuel types.

3. Laboratory tests simulating loss-of-coolant accident (LOCA) conditions.

4. Design, licensing documentation, fabrication and pre-irradiation characterization of four lead test assemblies (LTA's) for irradiation in the Quad Cities Nuclear Power Station, Unit 1, beginning in Cycle 5.

PHASE 2 will continue the work of PHASE 1, and it will also include:

1. Selection of the remedy fuel for the demonstration.

2. Nuclear design and core management of the demonstration, expanding from the generic feasibility study in PHASE 1 to a specific reactor and target cycle, including bundle nuclear designs.

3. Design, licensing documentation, and manufacturing of the demonstration fuel.

4. The demonstration *per se; i.e.,* the irradiation (including specially designed power ramps to test PCI resistance) and the evaluations. As presently perceived, PHASE 2 will include the irradiation through September 30, 1984.

5. Continued irradiation and evaluation of the four LTA's.

PHASE 3 is intended to extend the demonstration to high burnup. It is contingent on successful completion of PHASES 1 and 2, and details of the scope have yet to be defined.

This report is the Final Report for PHASE 1 of this program. It covers progress since the last progress report,[1] as well as a summary of the entire PHASE 1 effort (Section 2).[1,2]

2. SUMMARY FOR PHASE 1

2.1 DESIGN OF LARGE-SCALE DEMONSTRATION

Using Unit 1 of the Quad Cities Nuclear Power Station at the beginning of Cycle 6 as an example, the feasibility of the demonstration irradiation was determined. Quad Cities 1 is an operating commercial power reactor of the BWR/3 type with a steady-state core. The power density and other design features of a BWR/3 make such a reactor well-suited for the demonstration, but the results of the demonstration should be applicable generally to LWR's.

The demonstration, as presently perceived, will involve the insertion of the advanced, PCI-resistant fuel as part of a normal reload batch. The demonstration has been so designed that (a) the PCI resistance of the advanced fuel can be demonstrated by suitable power increases on certain nodes (*i.e.*, axial locations) of the advanced fuel bundles; (b) simultaneously, the power limits and power changes on the conventional, non-remedy fuel are held within limits specified to minimize the risk to the conventional fuel; (c) the demonstration does not inhibit unduly the reactor performances as a central station power plant; and (d) the operational procedures are compatible with the needs and capabilities of the utility which operates the plant. The demonstration plan which has been developed fulfills these goals.

The demonstration nuclear core design involves the use of test cells which contain the barrier fuel assemblies and which are symmetrically placed in the core. Each test cell contains four barrier fuel assemblies surrounding one cruciform control blade. The test cells are operated with their control blades inserted 60 to 100% of their length during most of the reactor cycle. Near the end of the cycle the control blades of the test cells are withdrawn in a stepwise fashion to impart a rapid increase in power in the barrier fuel to test its resistance to PCI. The test cells are surrounded by a buffer of high exposure (~20 MWd/kg-U) fuel bundles. This buffer zone serves to isolate the increase in power due to the withdrawal of the test cell control blades and thereby to protect the standard fuel in the core. The entire process has been analyzed to compare the suggested operation using the demonstration fuel and the demonstration mode of operation to what would normally be expected for Cycles 6 through 13. The demonstration mode produces very nearly the same energy as the normal mode of operation, but the extra neutron absorption of the copper barrier (~0.25% reactivity penalty) results in ~0.14% energy penalty for the demonstration. Use of Zr-liner fuel results in no energy penalty. Power ramp simulation analyses using a 3-dimensional coupled nuclear-thermal hydraulic simulation have shown that the demonstration is feasible, providing both adequate design margin and a good demonstration of PCI resistance of the barrier fuel, while protecting the conventional fuel bundles in the core from power changes likely to produce fuel cladding penetrations by PCI. Also, margins for transient and accident situations were shown to be adequate in the demonstration mode.

2.2 SUPPORT TESTS FOR LARGE-SCALE DEMONSTRATION

2.2.1 Laboratory Tests

2.2.1.1 Expanding Mandrel Tests

Expanding mandrel tests provide a controlled, localized, noncompliant stress system on cladding specimens along with exposure to temperature and corrosive environments that produce stress corrosion effects in Zircaloy. Thus, the expanding mandrel tests constitute a laboratory simulation of PCI. Such tests were done with both irradiated and with unirradiated barrier cladding and with suitable control specimens. The expanding mandrel tests were used to compare the stress corrosion resistance of irradiated Cu-barrier, Zr-lined and conventional cladding. Tests were done also with unirradiated materials to explore the effects of fabrication parameters.

Unirradiated specimens were tested in several environments: (a) flowing iodine (I_2) in a carrier gas of argon, (b) pure cadmium (either above or below the melting temperature), and (c) liquid cesium saturated with cadmium (Cs/Cd). Cold-worked Zircaloy reference specimens were consistently embrittled in such tests. While some tests were done with unirradiated Cu-barrier tubing, the emphasis was on Zr-lined tubing, where the effects of liner thickness, purity (oxygen content), and grain size were explored. It was found that in the unirradiated condition the resistance of

Zr-lined Zircaloy tubing to simulated PCI is insensitive to either the thickness or the purity of the liner. However, if the grain size of the zirconium liner was allowed to grow to >35 μm, the resistance to PCI was degraded. In tests with unirradiated Cu-barrier Zircaloy tubing it was shown that the PCI-resistance of the Cu-barrier tubing could be degraded if the Cu-barrier tubing is given an anneal sufficient to significantly interdiffuse the copper and the Zircaloy.

Irradiated specimens were obtained mainly from the unfueled plenum regions of test fuel rods (removable segments from segmented fuel rods) which had been irradiated in commercial BWR's and subsequently power ramp tested for PCI in a test reactor. Expanding mandrel tests were done at reactor temperatures (300 to 335°C) in atmospheres containing either I_2 vapor or pure Cd. These tests at burnup levels up to ~10 MWd/kg-U (fluences up to 2.4×10^{21} n/cm^2, E>1 MeV) showed that when the copper barrier had been diffusion-bonded, the Cu-barrier tubing lost much of its PCI resistance. Irradiated Zircaloy tubing having either an unbonded copper barrier or a zirconium liner showed good resistance to simulated PCI at these fluence levels.

2.2.1.2 Barrier Characterization and Stability

Although the early experiments were done by General Electric on electroplated Cu-barrier tubing, the Lead Test Assemblies (LTA's) (see Part 3) were prepared by an electroless copper plating method. The electroless technique was thought to have advantages both in ease of fabrication and in product uniformity. Much of the effort in this subtask was devoted to chemical and metallurgical characterization of the electroless copper barrier. The Zr-lined Zircaloy tubing was characterized with respect to crystallographic texture.

The electroless copper barrier was found to have very fine grain size (mean intercept distance <0.5 μm). Chemical analyses by means of ion microprobe showed the major impurities of the electroless product to be hydrogen and carbon. The crystallographic texture of the zirconium liner and the Zircaloy tube in which it was bonded was not markedly different from that of standard Zircaloy tubing.

The Cu-barrier tubing received further attention with respect to its stability, especially its behavior in the presence of steam-hydrogen mixtures as might occur in a fuel rod with a cladding penetration. It was found in laboratory experiments that the presence of the copper barrier promoted the absorption of hydrogen by the Zircaloy in an environment of steam and hydrogen. The use of copper plated on oxidized Zircaloy (a thin layer of zirconia separating the copper and the Zircaloy) tended to retard the absorption of hydrogen, but did not prevent it entirely.

2.2.1.3 Effects of Irradiation on Zirconium of Various Purities

Irradiated specimens of zirconium (flat stock) of different purity levels were tested for resistance to stress corrosion cracking (or embrittlement) in environments of pure cadmium or liquid cesium saturated with cadmium (Cs/Cd). The intention was to determine the influence of purity on the resistance of irradiated zirconium to stress corrosion and thereby to PCI. With sheet specimens the strain rate can be directly controlled and varied by orders of magnitude. Results showed that both crystal bar zirconium and sponge zirconium retain a high degree of resistance to embrittlement in these environments at strain rates ~0.01 min^{-1}, but at much higher strain rates (~0.1 min^{-1}) some embrittlement was seen.

2.2.2 Licensing Tests

2.2.2.1 Simulated Loss-of-Coolant Accident (LOCA)

Laboratory experiments were done to compare the behavior of barrier fuel with that of reference fuel under simulated LOCA conditions. These experiments involved the use of cladding with urania dummy fuel pellets; the cladding was subjected to a pressure/temperature transient expected in a postulated LOCA situation. In terms of overall cladding deformation and tendency for perforations to occur, the behavior of barrier cladding (both Cu-barrier and Zr-lined) was not markedly different from that of reference Zircaloy cladding. Under the extreme temperatures involved with a LOCA the copper barrier and the Zircaloy interacted in a eutectic reaction as had been expected.

2.2.2.2 Reactivity Initiated Accident

Reactivity Initiated Accident (RIA) comparisons between barrier fuel and reference fuel are to be done at the Nuclear Safety Research Reactor (NSRR) in Tokai, Japan. Barrier and reference cladding samples were supplied to Battelle Pacific Northwest Laboratory where special fuel pins were fabricated and shipped to Japan. Tests are scheduled to occur in 1979 and will be reported in PHASE 2.

2.2.3 Fuel Irradiation Tests

This task addresses directly the question of PCI resistance. It involves the irradiation of experimental fuel rods and subjects them to power ramp tests in a test reactor especially equipped for such tests. In PHASE 1 such tests were done at burnup levels ranging to ~16 MWd/kg-U under power history and power ramp conditions that consistently produce cladding perforations by PCI in conventional fuel (i.e., fuel with nonbarrier reference Zircaloy cladding) of equivalent burnup.

At burnup levels up to 10 MWd/kg-U both the Cu-barrier fuel and the Zr-liner fuel demonstrated superior resistance to PCI. Not only did these barrier fuel rods remain sound after a ramp to high powers, but careful post-test nondestructive and destructive examinations revealed no incipient cracks of the barrier cladding. Tests at higher burnup showed that while all of the barrier configurations appeared to be superior to conventional fuel, cladding failures did occur in fuel with certain copper barrier configurations. Copper barrier fuel with 5 μm thick copper failed as did the diffusion-bonded Cu-barrier fuel. Copper barrier cladding with 10 μm thick copper which had not been diffusion bonded during fabrication continued to resist failure by PCI at a burnup of 12.5 MWd/kg-U (rod average). In tests thus far the Zr-liner fuel has resisted failure by PCI to burnups up to 16.6 MWd/kg-U (rod average) and linear powers as high as 59.1 kW/m (18 kW/ft).

Fuel ramp testing is scheduled to continue in PHASE 2 to support the large-scale demonstration in a commercial power reactor.

2.3 LEAD TEST ASSEMBLIES

The actual demonstration of the Cu-barrier and the Zr-liner fuel concepts starts with the fabrication, irradiation and evaluation of lead test assemblies (LTA's). The LTA's have full sized fuel rods in an 8x8 array and are intended to provide both fabrication experience and lead irradiation experience for the barrier fuels. Thus, the LTA's will start their irradiation before the large-scale demonstration fuel is inserted into a reactor, and the LTA's will lead the large-scale demonstration in burnup. No special power maneuvers are anticipated for the LTA's; their function is to be irradiated under service conditions like that of conventional BWR fuel and to be evaluated for licensing purposes with respect to dimensional stability and ability to perform at relatively high power ratings. In PHASE 1 the LTA's were designed and fabricated. Irradiation was initiated in Cycle 5 of the Quad Cities-1 power reactor beginning in February, 1979. Their continued irradiation and evaluations are scheduled for PHASE 2 and PHASE 3.

Four LTA's have been fabricated, two with Cu-barrier fuel and two with Zr-liner fuel as follows:

—Copper barrier plated on etched Zircaloy
—Copper barrier plated on autoclave-oxidized Zircaloy
—Zirconium liner (crystal bar zirconium) coreduced with Zircaloy
—Zirconium liner (low oxygen sponge zirconium) coreduced with Zircaloy

Each LTA contains 60 full-length fuel rods, two water rods, and two rods which are segmented. The segmented rods were included as a contingency; they each are composed of four short (~1 m long) fuel rod segments which can be readily disassembled for detailed examinations or for fuel power ramp tests in a test reactor should such tests be deemed desirable.

The LTA's were designed for inclusion in symmetric locations in the core of Quad Cities Unit 1, at the start of Cycle 5. Fabrication was completed and the LTA's were delivered to the Quad Cities Nuclear Power Station in December 1978 in time for the scheduled refueling outage (starting January 1979) prior to the start of Cycle 5 (February 27, 1979).

During the fabrication of the LTA's they were thoroughly characterized to facilitate evaluations at subsequent refueling outages of the Quad Cities 1 power plant. Also, preliminary work was done at the Quad Cities Nuclear Power Station to assure the availability of a thorough and complete power history record to aid in the performance evaluations of the LTA's.

3. PART 1. DESIGN OF LARGE-SCALE DEMONSTRATION

(R. E. Brown and S. R. Specker, NTD)

3.1 OBJECTIVES

1. Design a large-scale demonstration experiment to test unambiguously the resistance of the barrier fuel to PCI, while minimizing the risk to the other fuel in the core.

2. Select a reactor for the demonstration and obtain concurrence from the reactor owner.

.3 Design the nuclear aspects of the demonstration fuel bundles, including fuel rod enrichments, rod locations, and distribution of gadolinia.

4. Establish the patterns for loading, discharge, and repositioning of fuel assemblies.

5. Specify reactor operational variables as required to satisfy the needs of both the demonstration and the reactor owner/operator.

3.2 INTRODUCTION

The nuclear design effort in PHASE 1 was directed toward verifying the feasibility of the large-scale demonstration in a BWR/3 type plant. This was accomplished by developing a generic nuclear design of the demonstration and performing detailed analyses to determine the expected core performance. The predicted core performance was then compared with the demonstration goals and the design constraints. The primary criterion was that the design must satisfy the demonstration goals while not unduly restricting the normal plant operational goals or energy generation capability.

To this end, a generic design was developed for a demonstration in Quad Cities Unit 1 (BWR/3, 2411 MWt plant) beginning in Cycle 6 and ending in Cycle 9. The design consisted of fuel loading and movement strategies and operational procedures for the four demonstration cycles. Coupled three-dimensional nuclear-thermal hydraulic calculations were performed to predict the core performance of the design. These included calculations of cycle exposure capability, reactivity margins, critical rod patterns, core response to assumed accidents and transients, and core response to the ramping of the demonstration test fuel assemblies. Scoping calculations were performed to determine what types of changes in the standard reload bundle designs would be required for the demonstration test fuel.

The results of all calculations have been reported in an earlier report.[1] The following key design features and conclusions are based upon these results.

3.3 DESIGN CONCEPT

The loading strategy for the demonstration cycles developed in PHASE 1 is as follows. The PCI-resistant fuel assemblies (either Zr-liner or Cu-barrier) are loaded in the first demonstration cycle. A total of 132 test fuel assemblies are loaded, of which 64 bundles to be ramp tested are divided into four groups of 16; one group will be ramped per cycle. The test assemblies to be ramped in a given cycle are moved into test cells. Each test cell has four fuel bundles clustered about a single control blade. The remaining groups to be ramped are located in low power regions of the core near the periphery. Following the ramp testing, the fuel bundles in the test cells are moved to other locations in the core and are replaced by the assemblies in the next group to be ramped.

The test cells are partially isolated from the remainder of the core by a ring of low power (high exposure, ~20 MWd/kg-U) bundles. This buffer zone is necessary to minimize the power impact of the ramp testing on the high power nonremedy bundles near the test cells.

The operational procedure consists of two parts. During the majority of the cycle [from the beginning of the cycle (BOC) to 12 to 20 full power days before end of full power capability] the control blades in the test cells are inserted between 60% and 100%. This limits the power in the demonstration test fuel in these cells to less than 26.2 kW/m (8 kW/ft.). During this portion of the cycle other control blades are used to control the excess reactivity and the power shape. This mode of operation is used until near the end of cycle when the control blades in the test cells are withdrawn 40% and all other control blades are fully withdrawn. Power ramping of the test fuel bundles in the test cells begins at this point in the cycle.

The ramp testing is achieved by allowing the core power to coast down from 1% to 5%, then withdrawing the control blades in the test cells 0.457m (1.50 ft) each. The amount of coastdown required is determined by the expected core power increase following control blade withdrawal. This is repeated, coastdown followed by control blade withdrawal, until all the control blades are fully withdrawn, which is the end of full power capability.

3.4 CORE PERFORMANCE — STEADY-STATE ANALYSES

The expected steady-state core performance (at rated conditions) was calculated using a three-dimensional coupled nuclear-thermal hydraulic model. The important core performance parameters (exposure capability, thermal margins, power distributions, etc.) were calculated and compared to the design criteria and similar calculations for a normal reload design when the latter was available. The following conclusions were made based upon these calculations:

1. **Exposure Capability.** An exposure comparison was made between a normal reload and the demonstration reload design. This comparison showed that for the eight cycles analyzed (four cycle demonstration plus four cycles follow-on) only a small exposure penalty existed. The total energy produced by the fuel being discharged from these eight cycles was the parameter compared. The results indicated that the Zr-liner demonstration and the normal reload cases produced essentially the same energy, while the Cu-barrier demonstration produced 0.14% less energy. This loss can be associated with the reactivity penalty of 0.25% $\Delta k/k$ due to the Cu-barrier.

2. **Thermal Margins.** The thermal margin parameters minimum critical power ratio (CPR), maximum linear heat generation rate (LHGR), and maximum average planar heat generation rate (APHGR) were calculated based upon critical control rod patterns developed for the demonstration cycles. The design criteria for these parameters were met in all cycles.

3. **Follow-on Cycle Core Performance.** The core performance in the cycles following the demonstration will not be degraded because of the demonstration. This conclusion is based upon the results of Haling Analyses[3] of the fuel cycles mentioned in item 1. Comparison of the power distributions and exposure capability showed very little difference between the two cases.

3.5 RAMPING STUDIES

Detailed three-dimensional calculations were performed to calculate the core performance during the ramp testing of the demonstration test fuel assemblies. The purpose of these analyses was to determine the degree to which the test fuel could be ramped, the effect of the ramp testing on the nonremedy fuel and the operational aspects of the ramp testing. The following conclusions can be made based upon these analyses:

1. The ramp testing will subject the demonstration test fuel to power ramps to 44.0 kW/m (13.4 kW/ft) for low exposure fuel (6 MWd/kg-U), to 38.4 kW/m (11.7 kW/ft) for medium exposure fuel (12 MWd/kg-U) and to 32.8 kW/m (10 kW/ft) for high exposure fuel (25 MWd/kg-U). The powers quoted are for the maximum power fuel rod in the test assemblies ramped.

2. A core power level change of up to 5% of rated can be expected due to the withdrawal of all test cell blades 0.457 m (1.50 feet) during the ramping. Thus, a coastdown of up to 5% is required prior to withdrawing the bank of test cell control blades for each 1.50 foot (0.457 m) increment. The power level change is determined by the reactivity worth of the blade withdrawal.

3. The nonremedy bundles used in the buffer zone will be subjected to a power increase of no more than 8.2 kW/m (2.5 kW/ft). However, the expected peak LHGR will always be less than 26.2 kW/m (8 kW/ft).

3.6 BUNDLE DESIGN AND RELATED STUDIES

3.6.1 Bundle Design Studies

The design of the demonstration test fuel assemblies which are to be ramp tested will be done in PHASE 2. These designs will be based upon the current standard 8x8D retrofit reload designs. The 68 PCI-resistant fuel assemblies which are not currently scheduled to be ramped will employ the standard nuclear design. All demonstration fuel bundles will retain the standard hardware design and standard fuel rod enrichments. The only changes will be in the fuel rod enrichment distribution within the bundle which will be required to obtain the desired assembly local power distribution, and only those assemblies scheduled to be ramped will have such changes.

The demonstration test fuel was simulated in all PHASE 1 calculations with the standard reload bundles. Scoping studies of possible design changes were performed to provide the expected local power distributions. The design changes investigated involved increasing the enrichment of the wide-wide corner rod and the distribution of fuel rod enrichments in the rods near the wide-wide corner. These rods will be those which experience the greatest power ramp. This is due to the control blade history effect.

The extent to which the wide-wide corner rod and surrounding rod enrichments can be raised (to increase the severity of the test) is limited by several considerations. Of primary importance is the constraint that the power in these rods not exceed 26.2 kW/m (8 kW/ft) during the period prior to the ramp test. Also, the critical power ratio of a bundle is reduced if the local power distribution becomes strongly peaked in a localized area.

The enrichment of the fuel rods in the wide-wide corner can be increased significantly and still maintain the power in these rods below 26.2 kW/m (8 kW/ft) if the bundle is oriented in the core in a particular manner. The majority of the demonstration test fuel (75%) spends at least one cycle near the core periphery prior to being moved into a test cell for ramping. The neutron flux in this region is rapidly decreasing as a function of distance from the center of the core. Thus, if these bundles are oriented with the wide-wide corner toward the periphery, then the power in this corner will be reduced relative to what it would be with the opposite orientation. This allows increased enrichments while still maintaining the power in these rods below 26.2 kW/m (8 kW/ft).

The final bundle designs will be developed in PHASE 2 once the host reactor and cycle are selected.

3.6.2 Detailed Power Distribution Analyses

Several two-dimensional quarter core fine mesh multigroup diffusion theory calculations were performed in PHASE 1. The cases investigated were the following: (1) calculation of the local power distribution in the test fuel bundles which reside near the core periphery; and (2) calculation of the detailed local power and average power of the test fuel bundles in the test cells and in the nonremedy fuel bundles in the buffer zone. The first case was performed to provide a benchmark for an approximate technique developed to predict the local power distribution in a bundle which resides near the core periphery. The second case was performed to determine the ability of the standard design methods to predict the power of bundles in and around the test cells.

Case 1: The preliminary results indicate that the standard design calculations adequately predict the peak power in the test fuel assemblies near the periphery. However, the details of the local power distribution in these assemblies also must be accurately predicted for this demonstration. Specifically, the power in the fuel rods near the wide-wide corner (which will ultimately be ramped to the highest power) must be accurately predicted to assure that these rods do not exceed 26.2 kW/m (8 kW/ft) prior to ramping.

The standard fine mesh (single bundle) multigroup diffusion theory calculation is not valid for predicting the details of the local power distribution in the test fuel assemblies located near the core periphery. This is because the standard calculation assumes an infinite array of the lattice being analyzed which does not account for the strong

neutron flux gradients near the core periphery. However, the standard methods can be used to accurately predict the details of the local power distributions in the test fuel assemblies in this core region if the infinite lattice assumption is replaced by a technique which adjusts the boundary conditions to account for the flux gradients. The boundary conditions are based upon the flux distribution from the standard one-group coarse mesh diffusion theory calculation of the core power distribution. This technique was used to predict the power in the test fuel assemblies and compared to the quarter core fine-mesh multigroup calculation (benchmark). The results indicated that good agreement can be obtained in most cases. However, further investigation of this method is necessary and will be performed in PHASE 2 prior to development of the final demonstration test fuel bundle designs.

Case 2: The standard design method for calculating the core power distribution (bundle average power) is a coarse mesh one-group diffusion theory model. The comparison of the power predicted by this method and the detailed calculation indicated that:

1. The standard design method predicts the power in the nonremedy buffer zone fuel within 1% to 3% of that predicted by the detailed method.

2. The standard design method predicts the power in test fuel in the test cell to within 2% to 4% of that predicted by the detailed method.

3.7 CORE RESPONSE TO ASSUMED ACCIDENTS AND TRANSIENTS

Several three-dimensional calculations were performed to assess the impact of the demonstration nuclear design on the core response to assumed accidents and transients. These calculations included the response to a fuel loading error, rod withdrawal error, control rod drop accident, scram at full power and the response of the Rod Block Monitor (RBM) system to the withdrawal of a test cell blade. The details and results of these calculations have been reported[1] and are summarized below.

1. **Fuel Loading Error.** The fuel loading error (FLE) analysis was performed for the first demonstration cycle. The assumed error was that one of the high enrichment demonstration test fuel bundles was erroneously loaded into an unmonitored location in the central region of the core in which a low power assembly should have been loaded. The predicted minimum CPR and maximum LHGR of the misloaded bundle, based upon the symmetric monitored bundle parameters, were within the design criteria for this assumed accident. The case analyzed should represent the worst case involving a test fuel bundle because these bundles reach maximum reactivity in the first demonstration cycle if misloaded.

2. **Rod Withdrawal Error.** The core response to a rod withdrawal error (RWE) involving a test cell control blade was analyzed for the second demonstration cycle. The point selected was based upon the calculated reactivity worth of fully withdrawing the selected control rod, which was maximum at the full power condition, early in the second demonstration cycle.

3. **Control Rod Drop Accident.** The control rod drop accident (CRDA) involving a test cell control blade was analyzed for the second demonstration cycle. As with the RWE, the point at which to perform this analysis was based upon the reactivity worth of the dropping rod. The point analyzed for the CRDA was the hot startup condition at a cycle exposure of 2.2 MWd/kg-U. This is believed to be the limiting situation for the example chosen in this generic study. The situation will be reconsidered for the specific demonstration core in PHASE 2. The design criterion for this accident is that the peak fuel enthalpy must not rise above 280 cal/g due to a control rod dropping from fully inserted to its maximum withdrawn position. This position is determined by the position of the other rods in the same rod bank. The case analyzed allowed the test cell blade to drop from fully inserted to fully withdrawn. The results indicated that the design criterion was not violated.

4. **Scram Reactivity.** The scram reactivity was calculated at the end of full power capability for each demonstration cycle. The design criterion was met in each case. The scram reactivity was also calculated for a normal reload design and compared to that calculated for the demonstration cycles. The compari-

son showed that the scram was not adversely impacted by the demonstration, as each case showed that the scram response was slightly better for the demonstration cycles.

5. **Rod Block Monitor Response.** The RBM response during a test cell control blade withdrawal of 1.50 feet (0.457m) was calculated to assure that a rod block would not occur which would prevent ramping. The case analyzed was for a withdrawal of a test cell blade from 50% withdrawn to 62.5% withdrawn during the first demonstration cycle ramp. This case was expected to cause the highest RBM response. The calculations indicated that for a rod block set point of 107% no rod block would result.

ACKNOWLEDGEMENTS

The authors wish to acknowledge the contributions made by the following individuals in the PHASE 1 design effort in the areas noted:

R. R. Galer and L. E. Fennern for design and analysis of the generic fuel loading strategies.

G. C. Hopkins for the analysis of the ramp testing and control rod drop accident.

P. O. Wei for the bundle design scoping studies.

M. J. Colby, M. J. Ferrazano and P. C. Wang for assistance in the fine mesh multigroup studies.

B. L. Sorensen for assistance in computations.

Also, the authors wish to acknowledge R. L. Crowther for the general design concept and advice throughout the entire design effort. All those acknowledged here are with the Nuclear Technology Department.

4. PART 2. SUPPORT TESTS FOR LARGE-SCALE DEMONSTRATION

4.1 TASK 1.0 LABORATORY SUPPORT (R. B. Adamson, NTD)

4.1.1 Subtask 1.1 Expanding Mandrel Tests

4.1.1.1 Objectives

1 Verify the applicability of the expanding mandrel test as a valid simulation of PCI for unirradiated and for irradiated Zircaloy and barrier modified (*i e*, Cu-barrier and Zr-liner) Zircaloy tubing

2 Evaluate the PCI-resistance of irradiated barrier-modified Zircaloy tubing

3 Explore design and fabrication parameters with respect to their effects on PCI resistance

4.1.1.2 Irradiated Material (S. B. Wisner and G. H. Henderson, NTD)

The environmental and mechanical aspects of the PCI failure mechanism for irradiated Zircaloy-2 and barrier-modified Zircaloy-2 cladding have been studied under controlled laboratory conditions using the expanding mandrel test technique The experimental apparatus has been described previously [1 2 4]

Expanding mandrel tests were conducted on specimens taken from the plenum sections of segmented fuel rods (so-called SRP rods) and on unfueled specimens that were irradiated at 326°C in the Big Rock Point (BRP) commercial power reactor All copper barriers had been produced by an electroplate process in 1974 and 1975 at the Vallecitos Nuclear Center

Progress in Current Report Period

During this reporting period, 10 expanding mandrel tests (6 on SRP unfueled plenum specimens and 4 on BRP specimens) were conducted in selective aggressive environments Table 4 1-1 provides a complete summary for all the tests run for this work * In Figure 4 1-1 the data are presented in a bar graph form which compares the total plastic diametral strain in expanding mandrel tests both in iodine and in cadmium The strain values were obtained from load-deflection curves that were generated for each test The given values provide a good qualitative measure of relative performance It is seen that there is marked improvement in resistance to environmental embrittlement for the nonbonded copper plated and crystal bar zirconium-lined cladding compared to bonded copper plated and Zircaloy-2 cladding The nonbonded copper barrier and zirconium liner tubes are resistant to iodine stress corrosion cracking at 4 Pa iodine pressure, whereas the zirconium liner is susceptible to stress corrosion fracture in iodine at high pressure (40 Pa) Because of the high reaction rates, it was not feasible to test the copper barrier cladding at the higher iodine pressure

For tests in cadmium environments, the nonbonded copper barrier is extremely resistant to liquid metal embrittlement (LME) compared to bonded copper which suffered low ductility failures [1] One zirconium-lined specimen failed in cadmium, but in a ductile fracture mode, two others did not fail

Figure 4 1-2 is a scanning electron micrograph (SEM) showing a typical locally stressed inner surface of SRP 3/15-1 (5 μm copper plate) specimen that was tested in molten cadmium No large cracks were seen There are superficial cracks in the cadmium enriched zone which do not appear to penetrate into the cladding However, in one instance a small crack was seen with what appeared to be a tight crack in the layer immediately under the

* The estimated burnups for the SRP specimens were obtained from ^{137}Cs gamma scans of the exposed rods The fast fluences (n/cm^2 E>1 MeV) were then estimated to be $2\,41 \times 10^{17}$ E where E is the burnup (exposure) in units of kWd/kg-U The fast fluences for the BRP specimens were determined from radiochemical analysis of flux monitor dosimeters that were located in selected axial positions for each BRP corner rod

Table 4.1-1
SUMMARY OF EXPANDING MANDREL TEST RESULTS FOR IRRADIATED COPPER PLATED ZIRCALOY-2, IODIDE ZIRCONIUM LINED ZIRCALOY-2 AND ZIRCALOY-2 TUBING (CROSSHEAD SPEED — 0.025 mm min^{-1}, 335°C FOR I_2 AND LIQUID Cd, 300°C FOR SOLID Cd)

Source	Material	Estimated Burnup (MWd/kg-U)	Estimated Fast Fluence $n/cm^2(E>1\ MeV)$	Environment	Average Total Diametral Strain (%)	Plastic Strain (%)	Comments
SRP3/2-1	Zircaloy + 5 μm Cu EP.BND.[a]	4.2	1.01×10^{21}	Liq. Cd	1.4	0.5	SCC Fracture
SRP3/2-2	Zircaloy + 5 μm Cu EP.BND.	4.2	1.01×10^{21}	Liq. Cd	0.8	0.3	SCC Fracture
SRP3/13-1	Zircaloy + 5 μm Cu EP.UNB[a]	8.1	1.95×10^{21}	Liq. Cd	4.2	3.6	No Fracture
SRP3/13-2	Zircaloy + 5 μm Cu EP.UNB.[a]	8.1	1.95×10^{21}	Liq. Cd	3.8	2.5	No Fracture
SRP3/14-1	Zircaloy + 5 μm Cu EP.UNB.	10.0	2.41×10^{21}	I_2 at 4 Pa	4.2	3.0	No Fracture
SRP3/14-2	Zircaloy + 5 μm Cu EP.UNB.	10.1	2.41×10^{21}	Liq. Cd	4.4	3.0	No Fracture
SRP3/15-1	Zircaloy + 5 μm Cu EP.UNB.	9.1	2.19×10^{21}	Liq. Cd	4.2	2.9	No Fracture
SRP3/17-1	Zircaloy +0.076 mm α Zr	7.9	1.90×10^{21}	Liq. Cd	3.5	2.8	Fracture
SRP3/17-2	Zircaloy +0.076 mm α Zr	7.9	1.90×10^{21}	I_2 at 4 Pa	4.3	3.3	No Fracture
SRP3/18-1	Zircaloy +0.076 mm α Zr	10.1	2.43×10^{21}	Sol. Cd	4.1	2.8	No Fracture
SRP3/18-2	Zircaloy +0.076 mm α Zr	10.1	2.43×10^{21}	I_2 at 4 Pa	4.4	3.1	No Fracture
SRP3/19-1	Zircaloy +0.076 mm α Zr	8.8	2.12×10^{21}	I_2 at 40 Pa	2.0	1.1	SCC Fracture
BRP	Zircaloy-2	8.8	3.7×10^{20}	I_2 at 40 Pa	1.8	0.5	SCC Fracture
BRP	Zircaloy-2		3.7×10^{20}	I_2 at 4 Pa	2.6	1.1	SCC Fracture
BRP	Zircaloy + 10 μm Cu EP.UNB.[b]		5.4×10^{20}	Sol. Cd	3.7	2.5	No Fracture
BRP	Zircaloy + 0.076 mm α Zr		4.4×10^{21}	Sol. Cd	4.6	2.9	No Fracture

SRP = Thick wall specimens—0.028 inches (0.71 mm)
BRP = Thin wall specimens—0.0165 inches (0.42 mm)
EP = Electroplated
BND = Diffusion bonded during fabrication
UNB = Not diffusion bonded
[a] = Nominal plating thickness is 5 μm; actual thickness varies from 5 to 17 μm around the circumference.
[b] = Ramp at 0.025 mm·min^{-1} to 0.015 inches (0.38 mm) diametral expansion and hold for 4 hours.

cadmium-enriched zone. A zirconium-lined specimen (SRP 3/17-1) that was tested in molten cadmium is shown in Figure 4.1-3. Approximately one-half of the fracture region is presented in the micrograph. The fracture morphology appears to be totally ductile. The failure might have been due to a local material flaw or defect which allowed ductile failure to occur. Figure 4.1-4 illustrates a typical stressed region in another area of SRP 3/17-1. It is seen that there are only superficial cracks in the cadmium-rich layer, indicating a lack of aggressive cadmium attack. In SRP 3/18-1 (0.076 mm zirconium liner) that was tested in 300°C (solid) cadmium, the inner surface of the stressed region appeared similar to the unfailed regions of SRP 3/17-1. There was no evidence of embrittlement by the cadmium and only superficial cracks in the cadmium-rich zone were seen. Another specimen from the same plenum segment, SRP 3/17-2, was tested in low pressure (4 Pa) iodine. One stressed region out of four had stress corrosion cracks as shown in Figure 4.1-5. This specimen did not suffer a through-wall fracture; the depth of the incipient cracks is not known.

Cracking was visible in the fracture region of SRP 3/19-1 (0.076 mm zirconium liner) tested in high pressure (40 Pa) iodine. It appears the stress corrosion cracking attack becomes increasingly aggressive with higher iodine pressure. The fracture surface of SRP 3/19-1 is shown in Figure 4.1-6. At the inner surface the fracture morphology is typical of iodine embrittled Zircaloy with cleavage facets and fluting visible.

The inner surface of a stressed region for a thin (0.42 mm) wall BRP (0.076 mm zirconium-lined) specimen tested in 300°C (solid) cadmium showed no evidence of embrittlement. There were no cracks, and the surface integrity was excellent. These results are similar to those of SRP 3/18-1.

Conclusions

1. Unbonded 5 μm electroplated copper and 0.076 mm crystal bar zirconium liners on Zircaloy-2 cladding irradiated to a fluence of $\sim 5 \times 10^{20}$ to 2×10^{21} ($E > 1$ MeV) exhibit immunity to embrittlement by liquid or solid cadmium when tested in the expanding mandrel configuration.

2. Irradiated nonbonded copper barriers are resistant to iodine stress corrosion cracking in the expanding mandrel test.

3. Irradiated diffusion-bonded electroplated Cu-barrier tubing is susceptible to embrittlement by cadmium.

4. Irradiated zirconium liners are susceptible to high or low pressure iodine stress corrosion cracking but exhibit greater resistance to cracking than standard irradiated Zircaloy-2.

4.1.1.3 Unirradiated Material (R.P. Gangloff, CRD)

The salient features of this work have already been reported.[1,2] Here the results of this effort are summarized.

The expanding mandrel technique[5] was employed to evaluate the PCI resistance of unirradiated zirconium and copper barrier fuel cladding. A range of test conditions, shown to produce severe embrittlement of standard Zircaloy-2 and including I_2 at 4 Pa, pure cadmium, and molten cadmium-saturated cesium, were employed for barrier screening. Iodide purity zirconium-lined and copper-plated barrier cladding exhibited large improvements in resistance to simulated PCI fracture for each aggressive environment compared to Zircaloy-2 reference tubing.

In iodine environments recrystallized iodide zirconium-lined Zircaloy-2, heat treated at 853 K (580°C), was equally resistant to stress corrosion fracture compared to cold worked barrier tubing of the same type. In contrast a large grain size liner (grain size estimated to be >35 μm), produced by heat treatment at 953 K (680°C), provided less improvement in fracture resistance compared to cold worked Zircaloy-2. Brittle low strain cleavage cracking proceeded both in the large grained zirconium liner and in the underlying Zircaloy-2. Select purity and commercial purity sponge zirconium-lined Zircaloy-2 were equally resistant to stress corrosion fracture compared to the high purity iodide material. Mean fracture strains were statistically equal on a 95% confidence level for each of the three zirconium barrier systems exposed to I_2, and were qualitatively equivalent for both cadmium-containing test conditions. Each purity of zirconium liner was embrittled by I_2 and Cs/Cd at high strain levels based on fractographic

observations. Reductions in the standard 75 μm liner thickness to 20 μm had no deleterious influence on barrier performance for select and commercial sponge zirconium-lined Zircaloy-2 tubing tested with I_2, Cd and Cs/Cd environments. The diametral fracture strain increased moderately with increasing liner thickness for Cs/Cd test conditions. Expanding mandrel tests established that the PCI resistance of Zr-barrier tubing was not affected adversely by variable liner thickness, including local thin spots, characteristic of both as-received and chemically polished composite tube samples. Scatter which is associated with the high fracture strain in the expanding mandrel tests complicated the quantitative analysis of zirconium liner purity and thickness effects on resistance to stress corrosion. Nonetheless, the superior PCI resistance exhibited by each composition and thickness of zirconium-lined Zircaloy-2 qualifies these barrier systems for more complex irradiation evaluations.

Electroless copper plated barrier tubing exhibited equivalent high diametral fracture strains compared to the electroplated material for each embrittling environment. Copper layers, 5 μm, 7 μm and 10 μm thick, were equally protective. Copper-zirconium interdiffusion limited the performance of barrier tubing. For all cases examined, brittle cracks formed in the interfacial intermetallic phases. In those cases where the residual copper layer was ruptured by intermetallic cracking, clad embrittlement was favored. For Cs/Cd conditions, one of two samples was embrittled, while ductile clad behavior was observed for pure Cd. This latter effect was related to alloying between the Cu-barrier and the Cd deposit to alter the transport processes during embrittlement. The presence of Cs eliminated the protective "chemical gettering" function of the Cu barrier. For I_2 test conditions, chemically assisted intermetallic interface delamination followed rupture of the residual Cu layer, and favored clad embrittlement. Copper-on-oxide barrier tubing exhibited little or no improvement in resistance to simulated PCI fracture with Cs/Cd. Good fracture resistance was observed for this barrier system, strained in the presence of I_2.

4.1.1.4 Irradiation Experiment on Specimens in EBR-II (R.P. Tucker, NTD)

The purpose of this portion of the work is to irradiate samples of barrier cladding of advanced design to a high fluence ($>5 \times 10^{21}$ n/cm^2, E >1 MeV) and subsequently to evaluate the susceptibility of these cladding types to PCI failures by use of expanding mandrel tests. The cladding materials (unfueled) to be evaluated are:

1. Reference Zircaloy-2
2. Zircaloy-2 lined with 10 μm thick electrolessly plated copper
3. Autoclaved Zircaloy-2 lined with 10 μm thick electrolessly plated copper, and
4. Zircaloy-2 lined with 0.076 mm thick low oxygen sponge zirconium.

In addition to the cladding specimens, two 1.27 mm thick sheets—one each of Zircaloy-2 and crystal bar zirconium—are being irradiated as thermal spacers to provide high fluence tensile sample material. The four tube specimens (1.234 m long) and two thermal spacers (1.140 m $\times$ 47.6 mm $\times$ 1.27 mm) are being irradiated in EBR-II along with a G.E. Fast Breeder Reactor Department Irradiation Creep Experiment. The experiment is designed to follow the EBR-II core coolant temperature which has a gradient from 700°F (371°C) at the core bottom inlet to approximately 900°F (482°C) at the core outlet. The actual irradiation temperature will be monitored by the use of thermal expansion difference (TED) monitors arrayed along the full length of the core. The external surfaces of the cladding specimens and thermal spacers are in contact with the sodium coolant; the specimens were internally filled at room temperature with 1 atmosphere reactor grade helium.

The cladding specimens and thermal spacers were inserted into EBR-II for Runs 97 and 98. Irradiation began September 24, 1978 and is scheduled to end January 6, 1979. The 34.3 cm in-core portions of the cladding specimens have a target fluence of $\sim 5 \times 10^{21}$ n/cm^2 (E $>$ 1 MeV).

Plans are being developed for the irradiation in EBR-II of a second set of cladding specimens and thermal spacers to a target fluence of 1×10^{22} n/cm^2 (E $>$ 1 MeV) during Runs 100 to 103 beginning in March 1979 and ending in October 1979. Specimen selection and fabrication have been initiated.

4.1.2 Subtask 1.2 Barrier Characterization and Stability (B.Cheng, W.L. Bell, J.E. Lewis and J.L. Lakner, NTD).

4.1.2.1 Objectives

1. Characterize the Cu-barrier and the Zr-liner.

2. Explore the stability of barrier tubing in steam and in steam-hydrogen environments.

4.1.2.2 Introduction

Characterization of the copper plated barrier cladding has included: (1) transmission electron microscopy (TEM) study of the grain size, grain shape and porosity; (2) SEM study of interface morphology; (3) secondary ion mass spectrometry (SIMS) study of elemental depth profile of the copper plating. In each study, specimens were prepared from both copper plated on etched Zircaloy (copper on Zircaloy) and copper plated on autoclave-oxidized Zircaloy (copper on oxide). The results of TEM and SEM studies were presented previously.[1] Additional TEM work on electrolytic copper plating was carried out in this reporting period, and its characteristics were compared with the electroless copper plating. The effects of 200°C and 400°C outgassing on the microstructure of the plating was also studied. The SIMS chemistry study was completed and is included in this report.

Besides the microstructural and chemical characterizations, the copper plating was tested for stability in wet hydrogen environments. Those experiments and other results were described in the two semiannual reports.[1,2] No further work on hydriding was carried out in this reporting period.

The texture of zirconium barrier layers co-extruded onto the inner surface of Zircaloy cladding was characterized using X-ray diffraction techniques. The results are included in this report.

4.1.2.3 SIMS Study of Copper Plating Chemistry

Secondary ion mass spectrometry (SIMS) by combining ion milling and mass spectrometry, is capable of performing elemental depth profile in the barrier materials. It thus allows a study of the chemistry of the copper plating as well as the copper-Zircaloy interface, where contamination by fluoride and other chemical species could possibly exist. An understanding of the plating chemistry can enhance the understanding of the time-delayed plating defects, i.e., blistering and staining, and can add insight into the response of the copper to irradiation. The effect of post-plating autoclave treatment (steam at 400°C) on the redistribution of impurities in the plating was also evaluated.

Experimental Procedures. Tubing samples analyzed included copper on Zircaloy (CZ) and copper on autoclave-oxidized Zircaloy (CA). In addition, a copper on Zircaloy sample was examined after receiving a post-plating autoclave treatment in 400°C, 10 psi steam (CZA). A copper standard (99.92% Cu) was also analyzed. The ion probe or SIMS uses certain primary ion beams which bombard the sample and generate secondary atoms from the sample surface to a depth of ~10 to 20 nm. The ion probe raster is a small rectangular area, producing secondary atoms from a tiny three-dimensional volume of the sample. Portions of the secondary atoms are ionized (secondary ions) and enter a mass spectrometer for analyses of elements and other chemical species by ratio of charge to mass of the secondary ions.

Since cations and anions are measured separately by changing the detector, the analysis of all ions in the same volume of material is impossible. An approach was taken to normalize for both metallic and nonmetallic elements by comparing one single element shown in both the anionic and metallic spectra.[6]

In the present study, the secondary ion (S.I.) mass spectra of positive ions were collected under 18.5 keV O_2^+ bombardment. The negative S.I. spectra were collected under primary bombardment with 18.5 keV N_2^+. Exposure time to the primary ion beam determines the depth over which secondary ions are sputtered. The sputtering rates could not be determined precisely because of lack of thin film standards. A rate of 2600Å/min/mA/cm² for copper was assumed. Analyses of the secondary ion spectra were carried out using a computer program, MAGCAL, which employs an empirical sensitivity factor method. Accuracy in trace or impurity analysis by this method or others could be within

factors of two or three. Thus, SIMS data should be treated as semi-quantitative, similar to most other newly developed surface technologies, *e.g.*, Auger electron spectrometry.[6]

Results and Discussion. Each sample was sputtered to approximately 10 different depths, and the mass spectra at each depth were obtained. To obtain the atomic concentrations of both metallic and nonmetallic elements, a comparison was made of the metallic and anionic mass spectra at approximately the same depth from the copper surface. This comparison was possible since fluorine appeared in both the metallic and nonmetallic spectra. Table 4.1-2 shows the normalized atomic concentrations of samples CZ, CA and CZA, respectively.

To determine the purity of the copper plating in samples CZ and CA, the data obtained at a depth of ~2.4 μm are chosen since these were obtained at a location where influence from the surface and the interface is minimum. It can be seen that both CZ (copper on Zircaloy) and CA (copper on oxide) contained carbon. Hydrogen and oxygen were also detected.

Estimation of elemental depth profile is complicated by the contributions of the secondary ions from the crater wall. This is indicated by the presence of Cu at crater depths ($> \sim 10$ μm) corresponding to location of Zircaloy-2. Nevertheless, a high fluorine peak was found near the Zircaloy-copper interface of sample CZ, which received an etch in ammonia bifluoride solution before being plated with copper. A depth profile of fluorine in sample CZ is shown in Figure 4.1-7. It can also be seen that the fluorine contents in samples CA and CZA (copper on Zircaloy, autoclaved) are relatively small. Hydrogen, at a relative concentration of 0.11 to 0.44 at.%, was found throughout the depth of the copper plating in samples CZ and CA. However, the sample, CZA, which had been heated in steam after plating has negligible hydrogen except at one location. The presence of an oxide layer at the interface was clearly identified for sample CA. Samples CZ and CZA showed slightly higher oxygen concentrations at the interface than in either copper or Zircaloy. The remaining trace impurities, *e.g.*, Fe, Na, Mg, Al, Si, and Ca are common to all copper samples. Occasionally, traces of Mn, V, Li, B, and Ba are found in some of the samples.

The copper plating after autoclaving was relatively free of impurities.

4.1.2.4 *TEM Studies of Unirradiated Copper Barriers*

Experimental Procedures

Additional copper platings were examined in this report period. Electrolessly plated copper on oxidized Zircaloy-2 cladding was outgassed in vacuum for 16 hours at both 200°C and 400°C, and the effects of both treatments were determined. In addition, a copper barrier electrolytically plated onto Zircaloy cladding was examined.

Specimen preparation procedures were essentially the same as reported previously.[1] However, the CA materials had a strongly adherent oxide film at the clad-barrier interface which defied most attempts to remove it. Abrasion, as before, with 400 grit SiC finishing paper was used, but the specimens were not glued to any surface. Instead the thin copper films were abraded between sheets of this finishing paper. This eliminated high spots due to varying glue thickness and prevented uneven removal of material.

Grain size measurements were made according to the single circle intercept method of the ASTM Standard E112-74.

Results and Discussion

Representative grain features for the plating materials are shown in Figure 4.1-8. The average grain sizes are quite small. The grain sizes or intercept distances for six barrier specimens are:

1. 4 μm Cu on etched Zircaloy: 0.14 ± 0.04 μm

2. 10 μm Cu on etched Zircaloy: 0.29 ± 0.09 μm

Table 4.1-2
RELATIVE CONCENTRATIONS OF COPPER-ON-ZIRCALOY SAMPLE (at. %)

Depth (μm)	Cu	Zr	Sn	Cr	Fe	Ni	O	C	F	H	Cl	$S^{**}_{(N)}$	Ca + Na Al + Si + Mg + Mn
(a) Copper on Zircaloy (CZ)													
0.03 to 0.05	87.4	—	—	—	0.021	—	1.99	4.45	0.048	4.45	0.49	0.093 (0.123)	0.83
2.3 to 2.5	90.1*	—	—	—	0.0009	—	1.98	6.85	0.0032	0.44	0.023	—	0.62
6.2	?	?	?	?	?	?	0.88	8.05	7.25	0.44	0.050	0.039	0.62
7.4 to 8.5	50.4	21.1	0.18	0.087	0.048	0.0087	1.81	5.82	19.5	0.33	0.093	0.098 (0.013)	0.52
10.4 to 14.0	49.8	45.6	0.29	0.18	0.079	0.029	0.58	1.80	0.97	0.18	0.032	— (0.040)	0.39
20.3	?	?	?	?	?	?	0.66	1.96	0.99	?	0.033	—	?

*97.96 wt%
99.72 wt% if only metallic elements are counted
**Numbers in parentheses indicate nitrogen; those without parentheses indicate sulfur

(b) Copper on Oxide (CA)

0.03 to 0.04	16.8	—	—	—	—	—	58.4	0.36	0.84	0.76	6.23	3.30	
2.3 to 2.6	79.8*	—	—	—	0.0032	—	0.45	19.0	0.0046	0.28	0.04	—	0.53
5.5 to 6.7	9.5	15.2	0.186	0.08	0.035	0.030	72.8	1.26	0.65	0.11	0.05	0.06	0.04
11.5 to 12.2	12.5	53.3	0.42	0.17	0.063	0.036	29.4	3.29	0.32	0.15	0.07	0.12	0.87
14.5	?	?	?	?	?	?	4.64	0.97	0.091	?	0.017	0.022	?
21.1	?	?	?	?	?	?	1.86	0.92	0.037	?	0.019	—	?

*95.30 wt%
99.73 wt% if only metallic elements are counted

(c) Copper on Zircaloy Receiving Post-Plating Autoclave Treatment (CZA)

0.03 to 0.05	84.1	0.096	0.085	0.008	0.13	—	10.1	0.26	0.011	1.7	0.35	0.51	1.95
2.3 to 2.5	99.4*	0.11	—	—	—	—	0.10	0.091	—	—	0.006	—	0.047
5.7 to 6.5	65.7	32.6	0.098	0.02	0.014	—	0.43	0.13	0.78	0.098	0.030	0.027	0.19
10.1 to 11.7	37.9	60.6	0.22	0.095	0.052	0.036	0.39	0.093	0.47	—	0.018	—	0.048
13.5 to 14	30.3	69.0	0.24	0.083	0.037	0.017	0.091	0.024	0.156	—	0.006	—	0.017
20.3 to 24.5	?	?	?	?	?	?	0.23	0.034	0.062	?	0.007	—	?

*99.78 wt%

—indicates concentration below limit of detection
? indicates either lack of data or spectrum was not computed

3. 10 μm Cu on oxidized Zircaloy: 0.38 ± 0.11 μm

4. Like 3 and outgassed at 200°C: 0.21 ± 0.02 μm

5. Like 3 and outgassed at 400°C: 0.46 ± 0.10 μm

6. 10 μm electrolytic Cu on etched Zircaloy: 0.40 ± 0.06 μm

The selected area electron diffraction patterns obtained from the areas in Figure 4.1-8 are shown in Figure 4.1-9. Consistent with the fine grain sizes, noticeable ring pattern effects are seen. The grain shapes are generally equiaxed.

Small pores or bubbles are present in the electroless copper plating even after outgassing at both 200°C and 400°C as shown in Figure 4.1-10. In the electrolytic copper no pores or bubbles were detected.

4.1.2.5 Crystallographic Texture of Zirconium Liner

Crystallographic texture measurements by x-ray diffraction were made at the mid-wall locations and at the inner surface locations (*i.e.*, the region of the zirconium liner). A combination of machining and chemical milling was used to prepare specimens comprising tubing sections only 0.1 mm thick oriented parallel to the tubing wall. The mid-wall specimens were prepared by machining and milling from both directions so the resulting specimen contained the mid-wall location of the initial tube. The specimens of the inner wall were machined and milled from the outside only, using the device in Figure 4.1-11 to mill from the outer surface without affecting the zirconium liner.

Such specimens were used to obtain inverse pole figures in the radial direction of the tubing by the method of Sturcken and Duke[7] and of Kearns.[8] Orientation parameters (f-factors in the radial direction of the tube) were computed from the inverse pole figure data.[8] Filtered Cu-Kα x-radiation was used for the inverse pole figures. The same specimens served for obtaining partial stereographic pole figures for the $\{0002\}$ poles viewed from the radial direction of the tubing. The back reflection technique of Shulz[9] was used with filtered Cr-Kα x-radiation to obtain the stereographic pole figures. One full stereographic figure was obtained (Figure 1.4-12) in which tubing sections normal to the longitudinal (axial) and tangential tubing directions had to be prepared. For the full pole figure the data acquisition and computation of orientation parameters was similar to the method used previously by Rosenbaum and Lewis.[10]

X-ray diffraction texture analyses of twelve zirconium liner tubes were performed. These samples cover a range of heat treatment and types of zirconium liner material. Both an inverse pole figure and a back reflection partial pole figure (along the radial direction) have been obtained for all of these samples at the midwall and at the alpha zirconium inner tube surface. In addition, a complete pole figure (three orthogonal directions, *i.e.*, radial, longitudinal, and tangential) was performed on the tubing with the low-oxygen sponge Zr-liner (annealed). The full midwall pole figure, the partial midwall pole figure and the partial alpha zirconium inner surface pole figure are shown in Figures 4.1-12 through 4.1-15, respectively. The inverse midwall pole figure compared with the inner surface one is shown in Figure 4.1-16. From these pole figures radial direction orientation parameters were calculated. A complete summary of these data is shown in Table 4.1-3.

4.1.3 Subtask 1.3—Effects of Irradiation on Zirconium of Various Purities (P.C. Kelly, D.S. Tomalin, CRD)

4.1.3.1 Objectives

Determine the effects of neutron irradiation on the simulated fission-product embrittlement of zirconium of various impurity levels, specifically:

1. Determine the susceptibility of irradiated zirconium to liquid metal embrittlement by cadmium in a cadmium-saturated cesium liquid.

Table 4.1-3
INVERSE POLE FIGURE ORIENTATION PARAMETERS

Zr Barrier Grade	Sample Condition	Sample Location	Inverse f-Factor (radial direction)	Full Pole Figure f-Factor (radial direction)
X.B	R	MW	0.63	
		ID	0.59	
X.B.	A	MW	0.61	
		ID	0.52	
L.O.	R	MW	0.62	
		ID	0.63	
L.O.	A	MW	0.64	0.67
		ID	0.59	
R.G.	R	MW	0.62	
		ID	0.63	
			0.64	
R.G.	A	MW	0.63	
		ID	0.58	
	R	MW	0.62	
		ID	—	
*	A	MW	0.63	
		ID	0.55	
*	A	MW	0.65	
			0.65	
			0.66	
		ID	0.54	
*	A	MW	0.60	
			0.58	
		ID	0.49	
			0.48	
+	A	MW	0.63	
		ID	0.57	
	A	MW	0.63	
		ID	0.64	

MW = Midwall
X.B. = Crystal bar, <100 ppm oxygen
L.O. = Low oxygen sponge, ~ 500 ppm oxygen
R.G. = Rector grade (high oxygen) sponge, ~ 1000 ppm oxygen
ID = Inner Surface
R = As rocked
A = Final anneal (577°C)
* = Crystal bar, oxygen level unknown
+ = Sponge, oxygen level unknown
630-1 is reference monolithic Zircaloy-2 tube fabricated along with the barrier materials

2. Compare irradiated crystal bar zirconium with irradiated sponge zirconium.

3. Compare characteristics at various strain rates and testing temperatures.

4.1.3.2 Summary

A liner of high purity crystal bar zirconium on the inner surface of Zircaloy fuel cladding has been shown to be effective in reducing the susceptibility of this cladding to PCI-type cladding failure. The aim of this subtask was to investigate the tensile properties of zirconium itself as affected by neutron irradiation and the presence of a potential liquid metal embrittling environment. Tensile tests of irradiated sheet material were conducted in inert environments, in cesium, or in a cadmium-saturated cesium liquid. Results reported in the semiannual reports[1,2] indicated that irradiated Zircaloy is in fact severely embrittled by the cadmium in a cadmium-saturated cesium liquid when tested near 350°C. In addition it was shown that crystal bar zirconium was not embrittled under similar test conditions (at strain rates of 0.001 and 0.01 min^{-1}). However, it was shown[2] that crystal bar zirconium was susceptible to liquid metal embrittlement in the cesium/cadmium environment when the strain rate was increased to 0.1 min^{-1} at test temperature of 350°C.

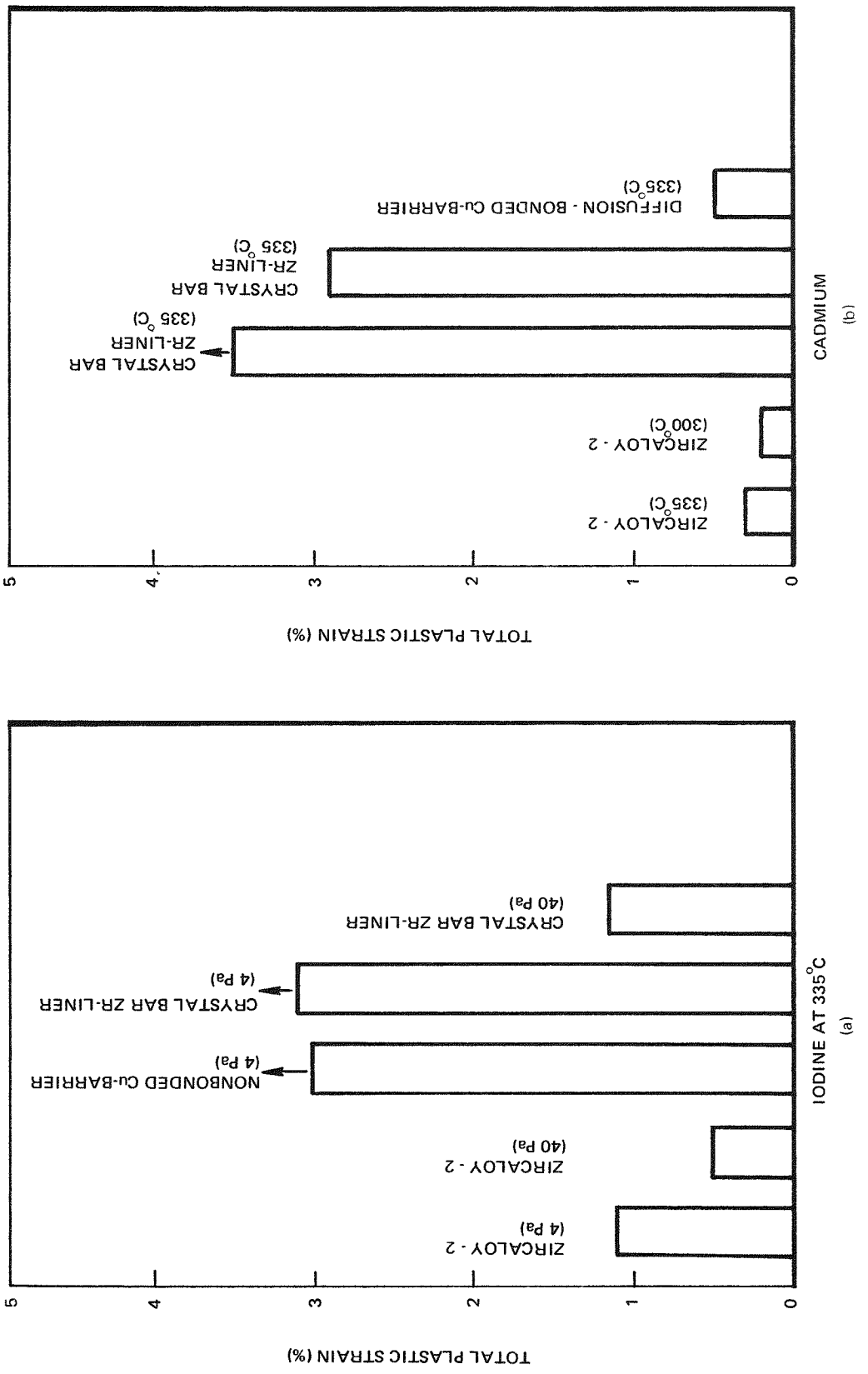

Figure 4 1-1 Comparison of Total Plastic Strain from Expanding Mandrel Tests on Irradiated Tubing Zircaloy-2, Nonbonded Copper Plated on Zircaloy-2, and Iodide Zirconium Bonded on Zircaloy-2 in Cadmium and Flowing Iodine, and Bonded Copper Plated on Zircaloy-2 in Cadmium

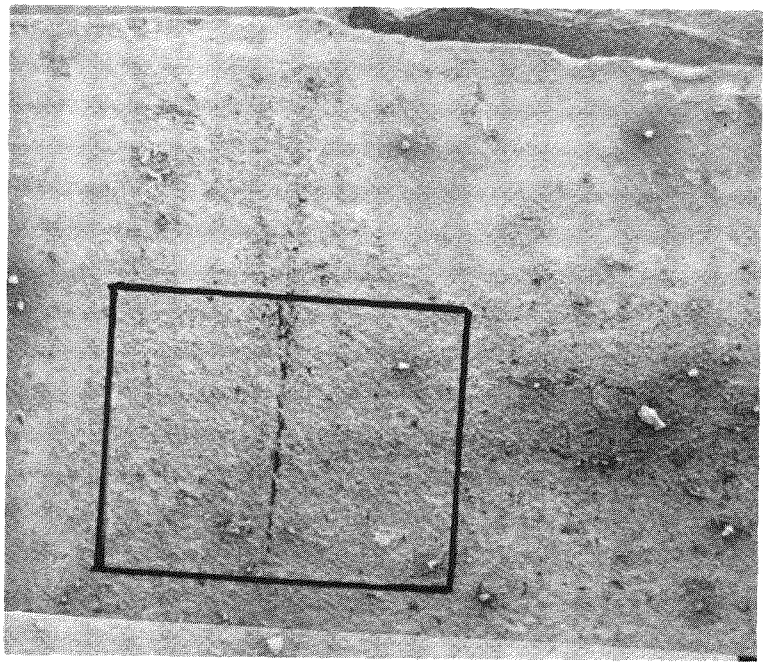

~40X

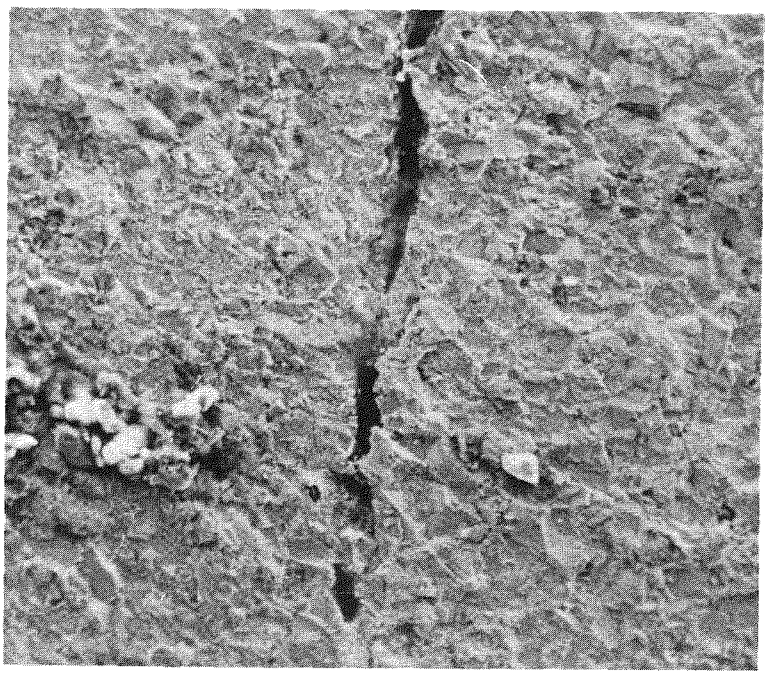

300X

Figure 4.1-2. Scanning Electron Micrographs (Secondary Electron Image) of the Inner Surface of SRP-3/15-1 (5 μm Electroplated and Nonbonded Copper Barrier on Zircaloy-2) Tested in 335°C Cadmium

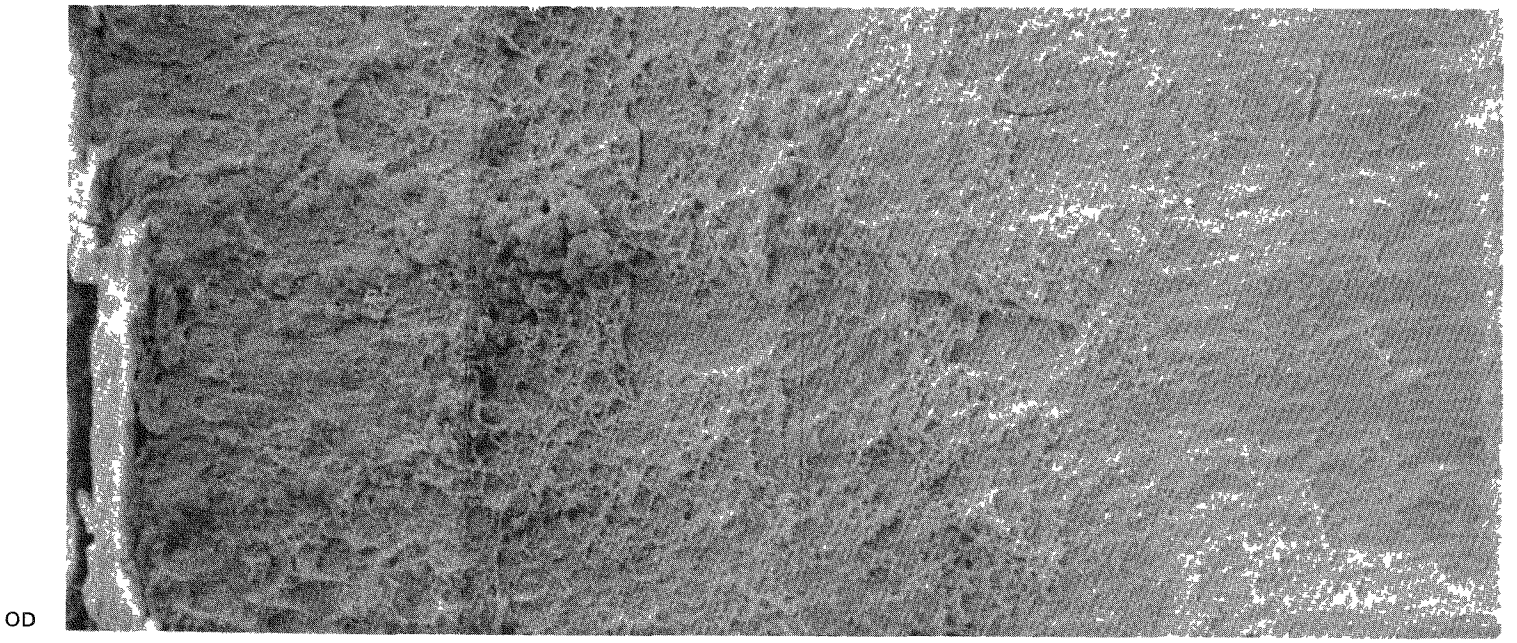

Figure 4 1-3 Scanning Electron Micrograph (Secondary Electron Image) of the Fracture Surface of SRP-3/17-1 (0 076 mm Iodide Zirconium Liner on Zircaloy-2) Showing Ductile Morphology Note the Shear Lip Region Near the Inner Surface Which Tilts Sharply Into the Plane of the Micrograph

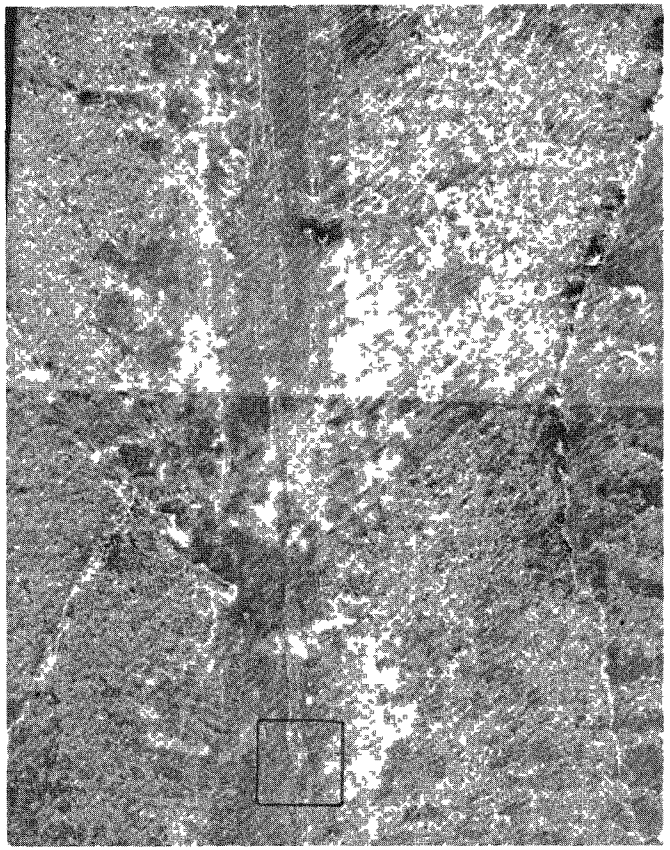

335°C CADMIUM 40X

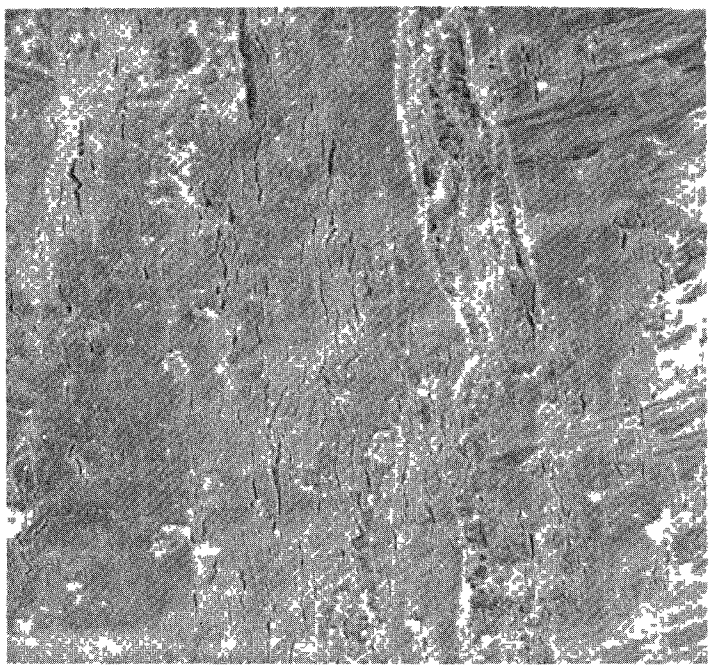

300X

Figure 4 1-4 Scanning Electron Micrographs (Secondary Electron Image) of the Inner Surface of the SRP-3/17-1 (0 076 mm Iodide Zirconium Liner on Zircaloy-2) Showing Superficial Cracks

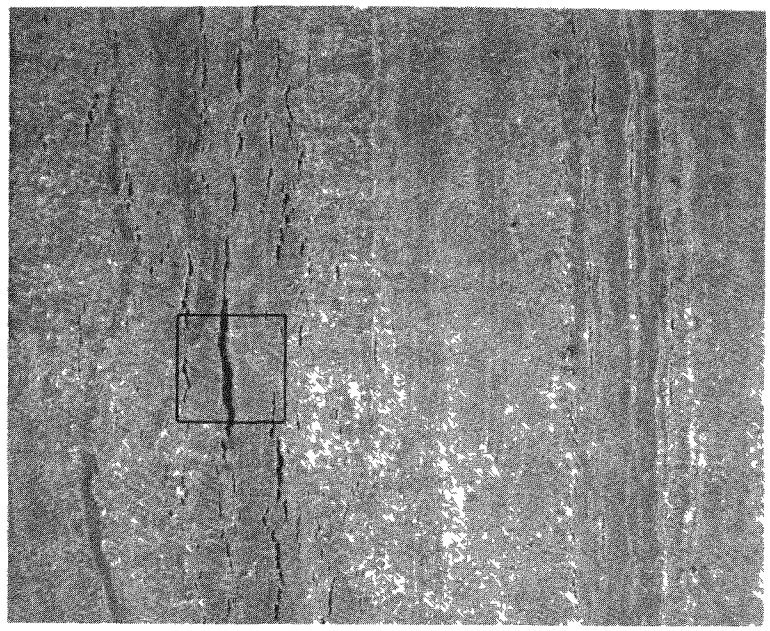

335°C 4 Pa IODINE 40X

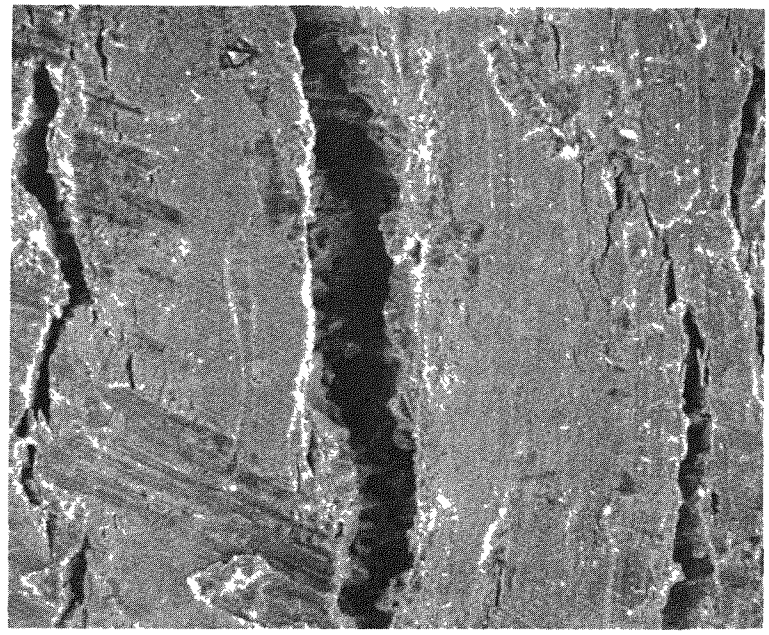

300X

Figure 4 1-5 Scanning Electron Micrographs (Secondary Electron Image) of the Inner Surface of SRP-3/17-2 (0 076 mm Iodide Zirconium Liner on Zircaloy-2) Showing Incipient Cracks

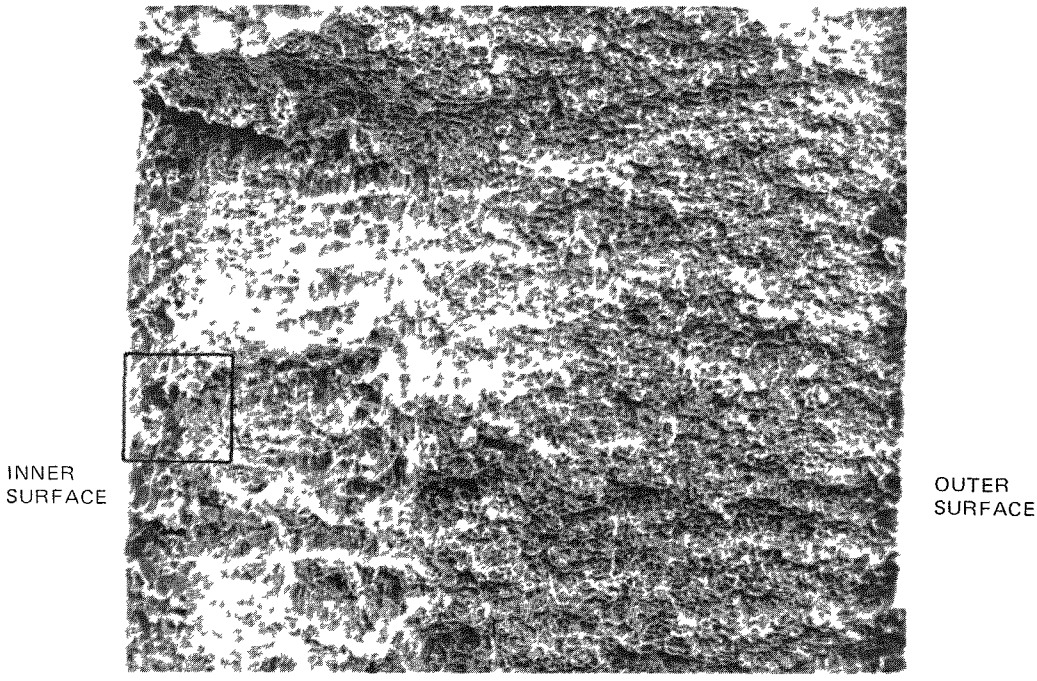

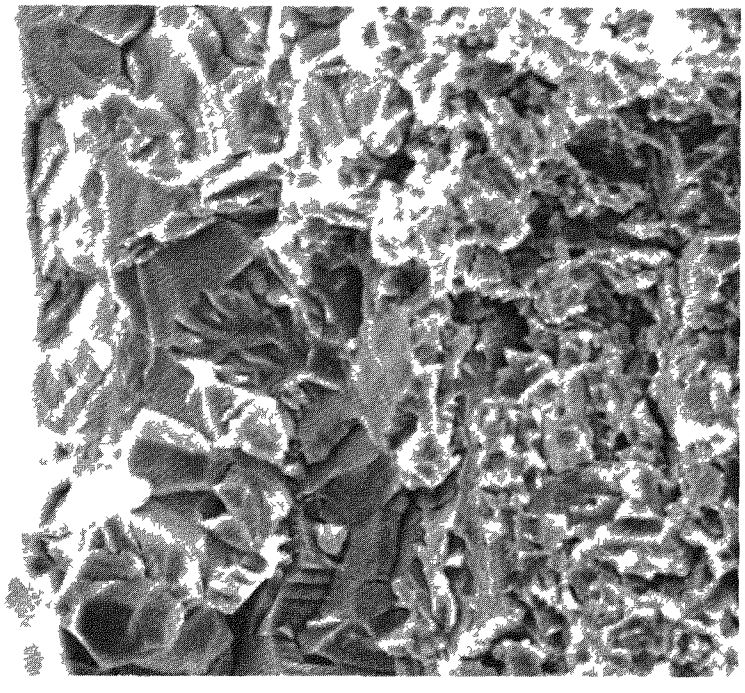

Figure 4 1-6 Scanning Electron Micrographs (Secondary Electron Image) Showing the Fracture Surface of SRP-3/19-1 (0 076 mm Iodide Zirconium Liner on Zircaloy-2) Tested at 335°C, 40 Pa Iodine

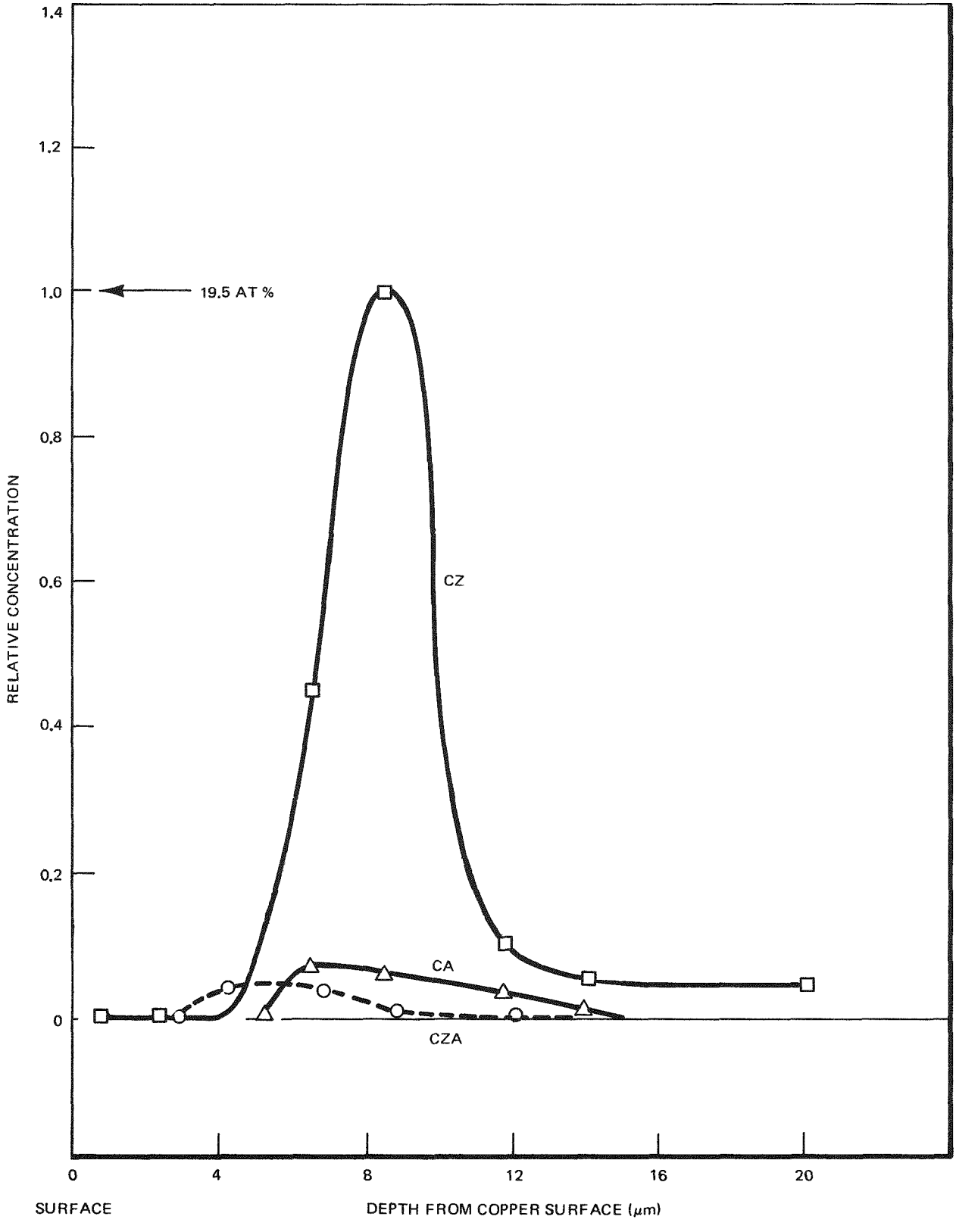

Figure 4.1-7. Relative Concentrations of Fluorine in Copper-On-Zircaloy (CZ), Copper-On-Oxide (CA), and Copper-On-Zircaloy Plus Post-Plating Autoclave Treatment (CZA) as a Function of Depth from the Copper Surface

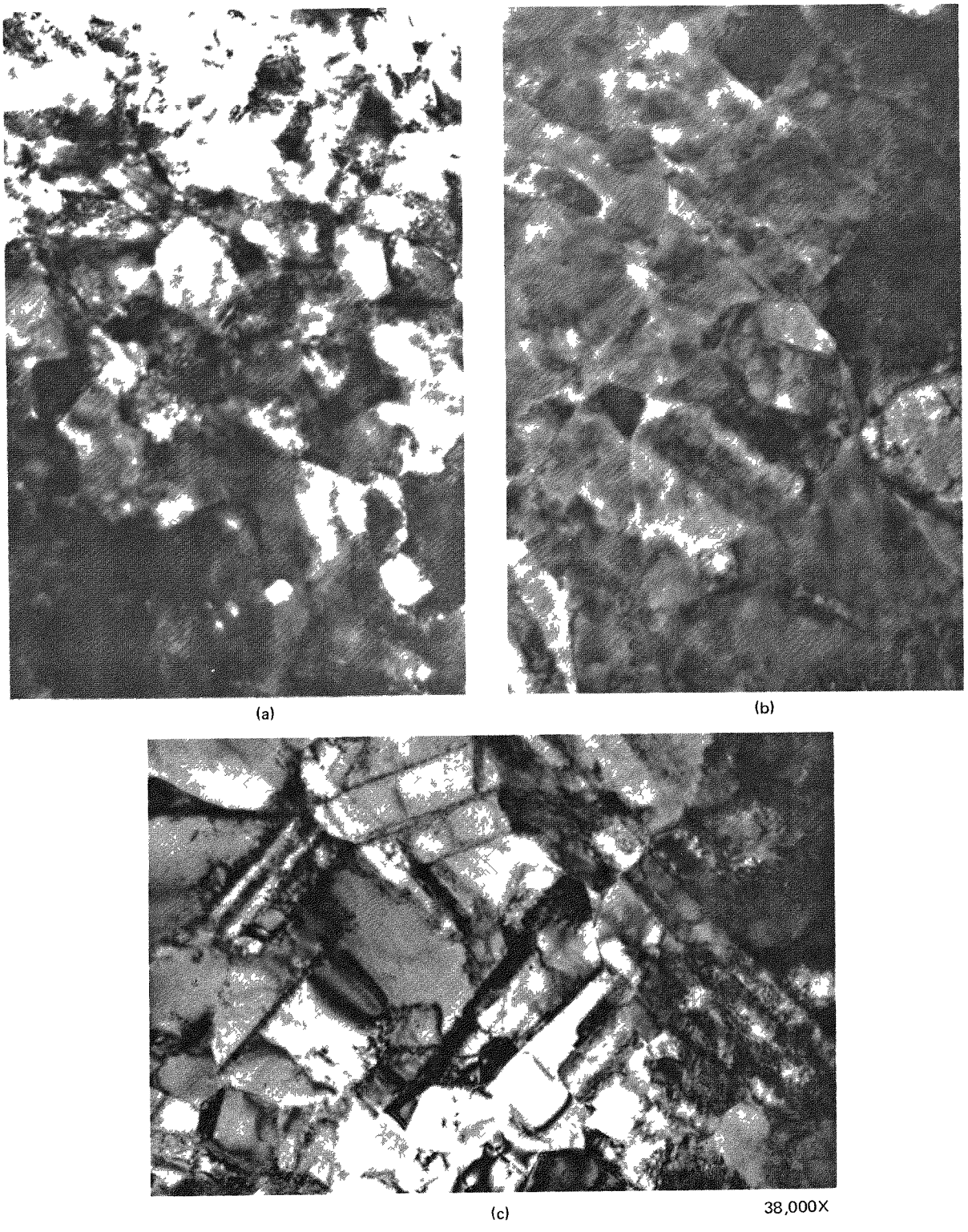

Figure 4.1-8. *Bright-Field Images of Grains in 10 μm Thick Polycrystalline Plated Copper Barriers:*
(a) Vacuum Outgassed at 200°C for 16 Hours
(b) Vacuum Outgassed at 400°C for 16 Hours
(c) Electrolytic (No Heat Treatment)
Magnification 38,000 X

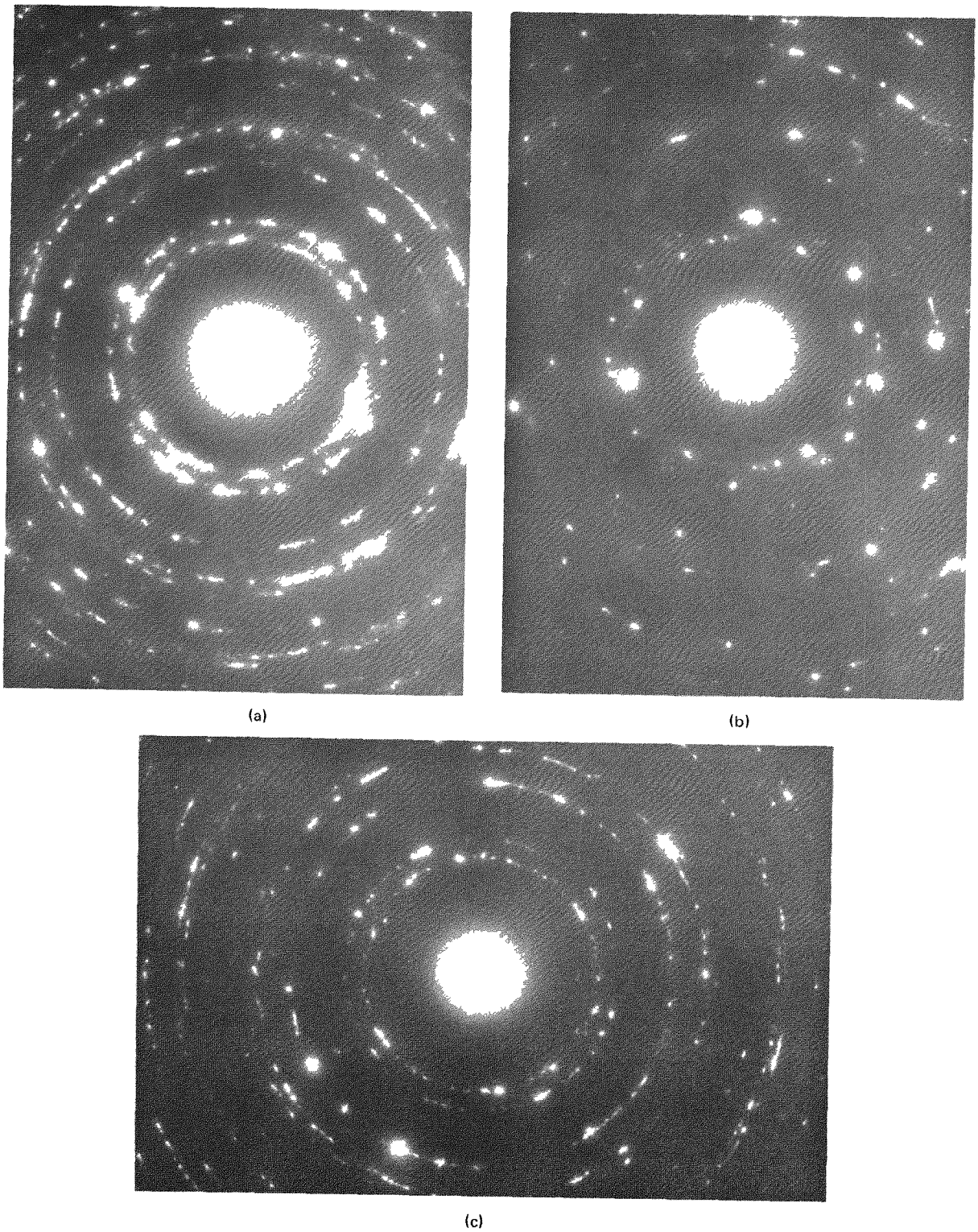

Figure 4.1-9. Selected Area Electron Diffraction Patterns from Thin Regions Illustrated in Figure 4.1-1 for Copper Barriers

(a) Vacuum Outgassed at 200°C for 16 Hours
(b) Vacuum Outgassed at 400°C for 16 Hours
(c) Electrolytic

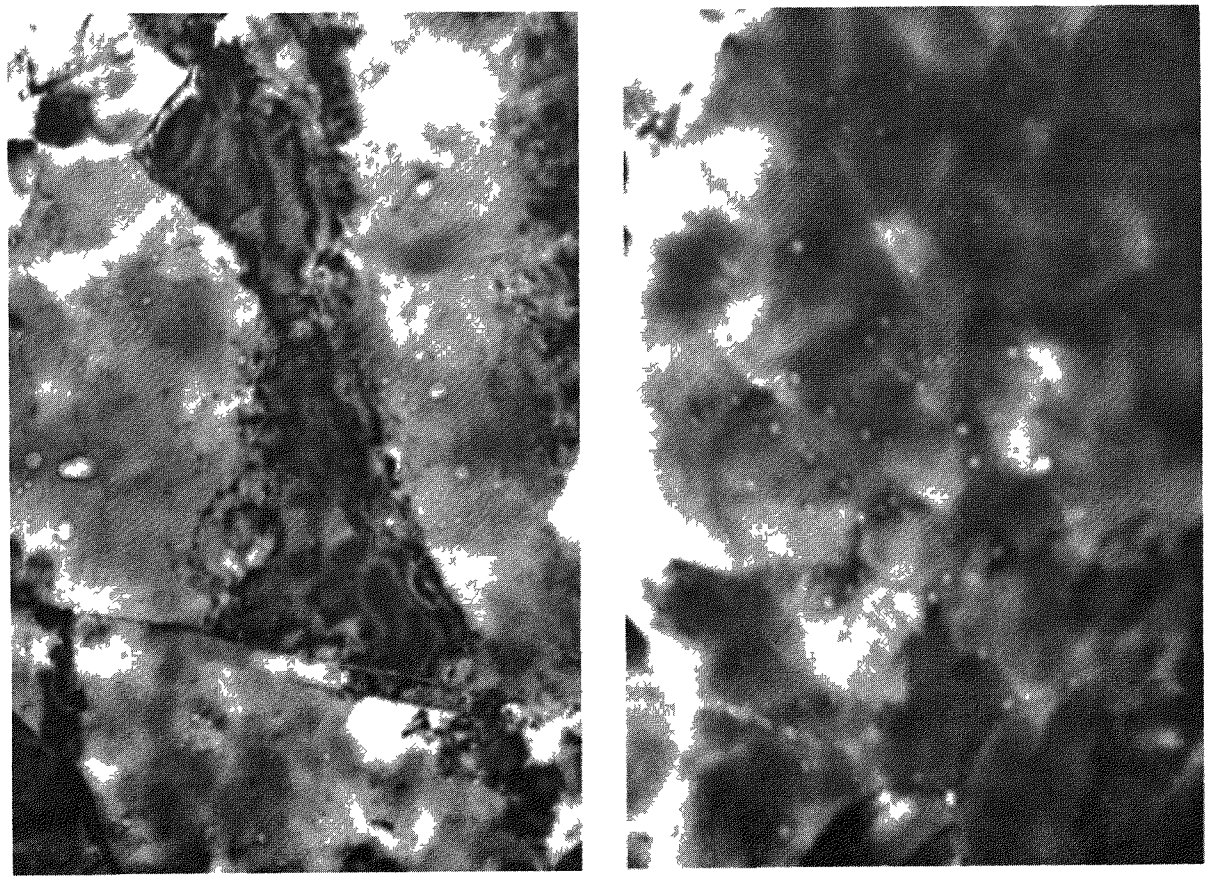

Figure 4.1-10. Bubbles in Copper Barriers Outgassed at (a) 200°C, (b) 400°C

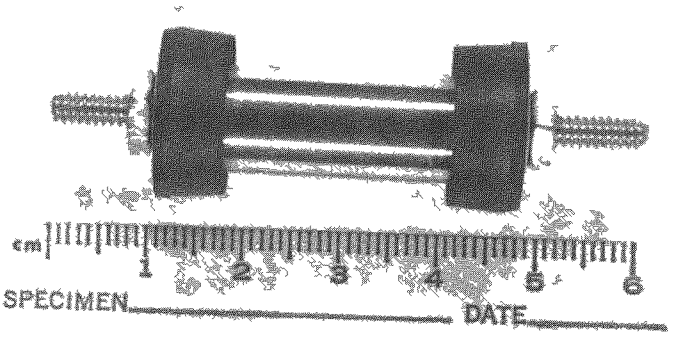

Figure 4 1-11 Apparatus for Protecting the Inner Barrier Material Surface During Chemical Milling Operation

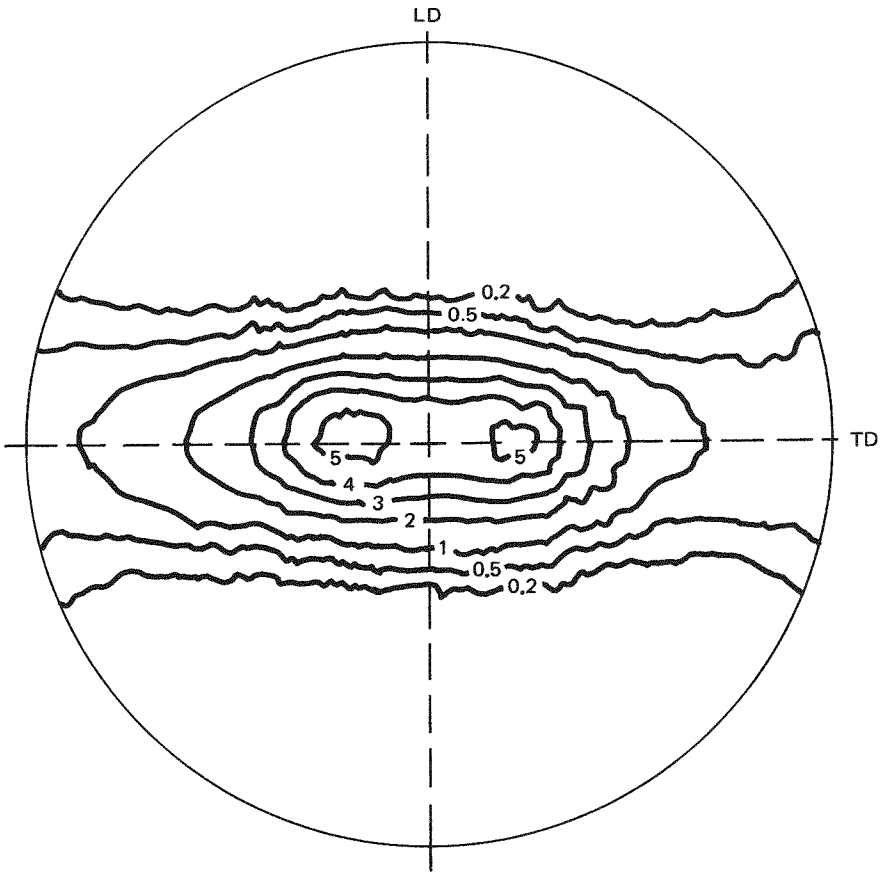

Figure 4.1-12. Radial Direction Pole Figure of the (0002) Plane of Tubing, Barrier-Low Oxygen Sponge Zirconium, Annealed 577°C. LD = longitudinal direction, TD = tangential direction

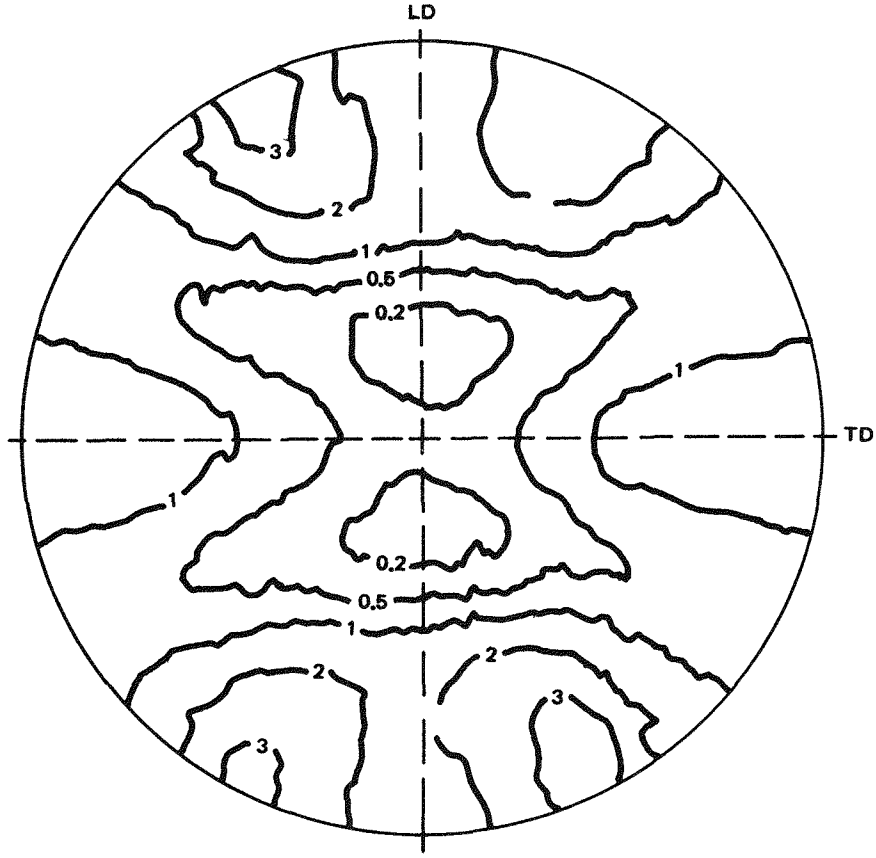

Figure 4.1-13. Radial Direction Pole Figure of the (10$\bar{1}$0) Plane of Tubing, Barrier-Low Oxygen Sponge Zirconium, Annealed 577°C

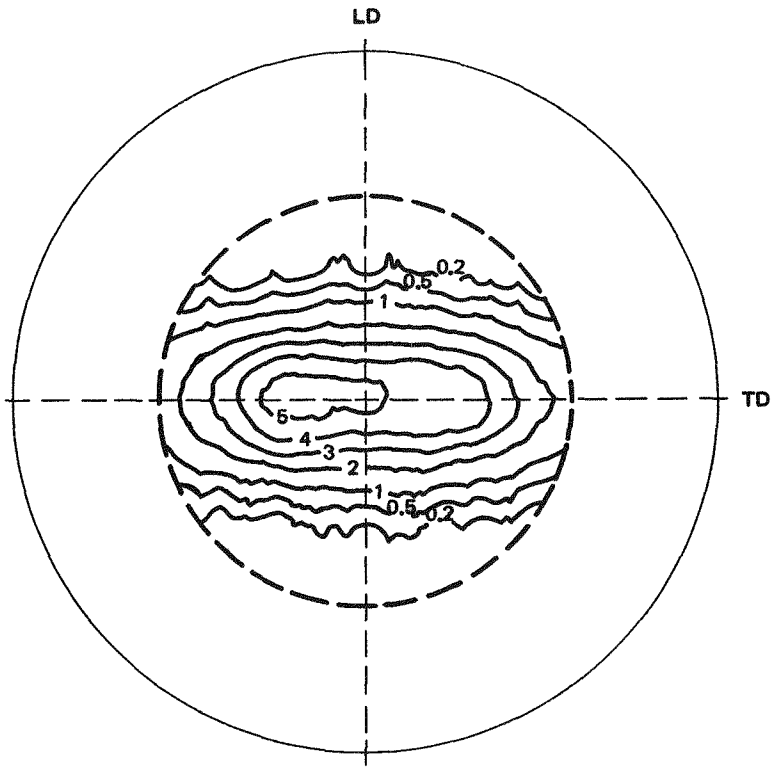

Figure 4.1-14. Radial Direction Pole Figure of the (0002) Plane of Tubing at Midwall, Barrier-Low Oxygen Sponge Zirconium, Annealed 577°C

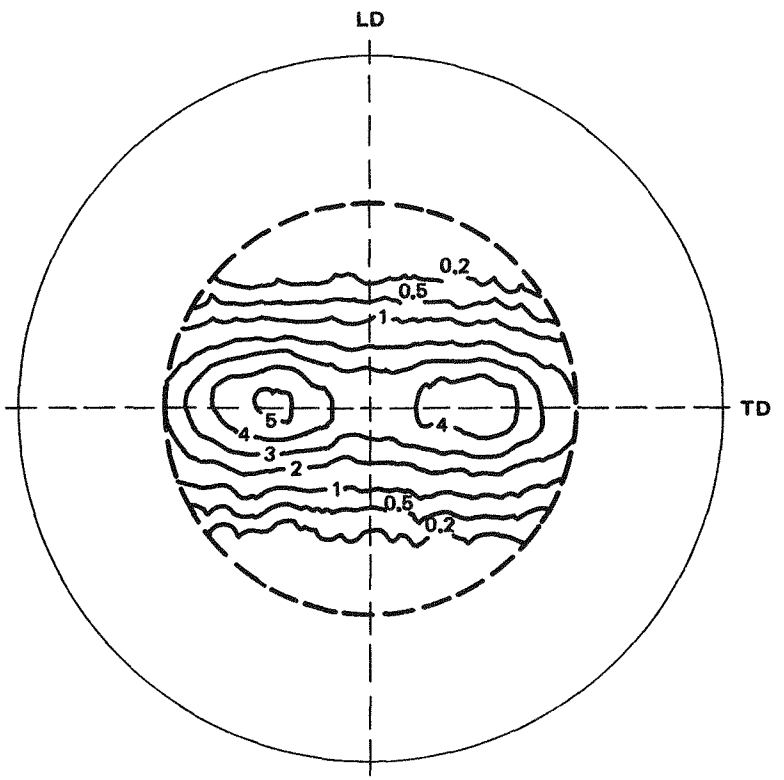

Figure 4.1-15. Radial Direction Pole Figure of the (0002) Plane of Tubing at Inner Surface, Barrier-Low Oxygen Sponge Zirconium, Annealed 577°C

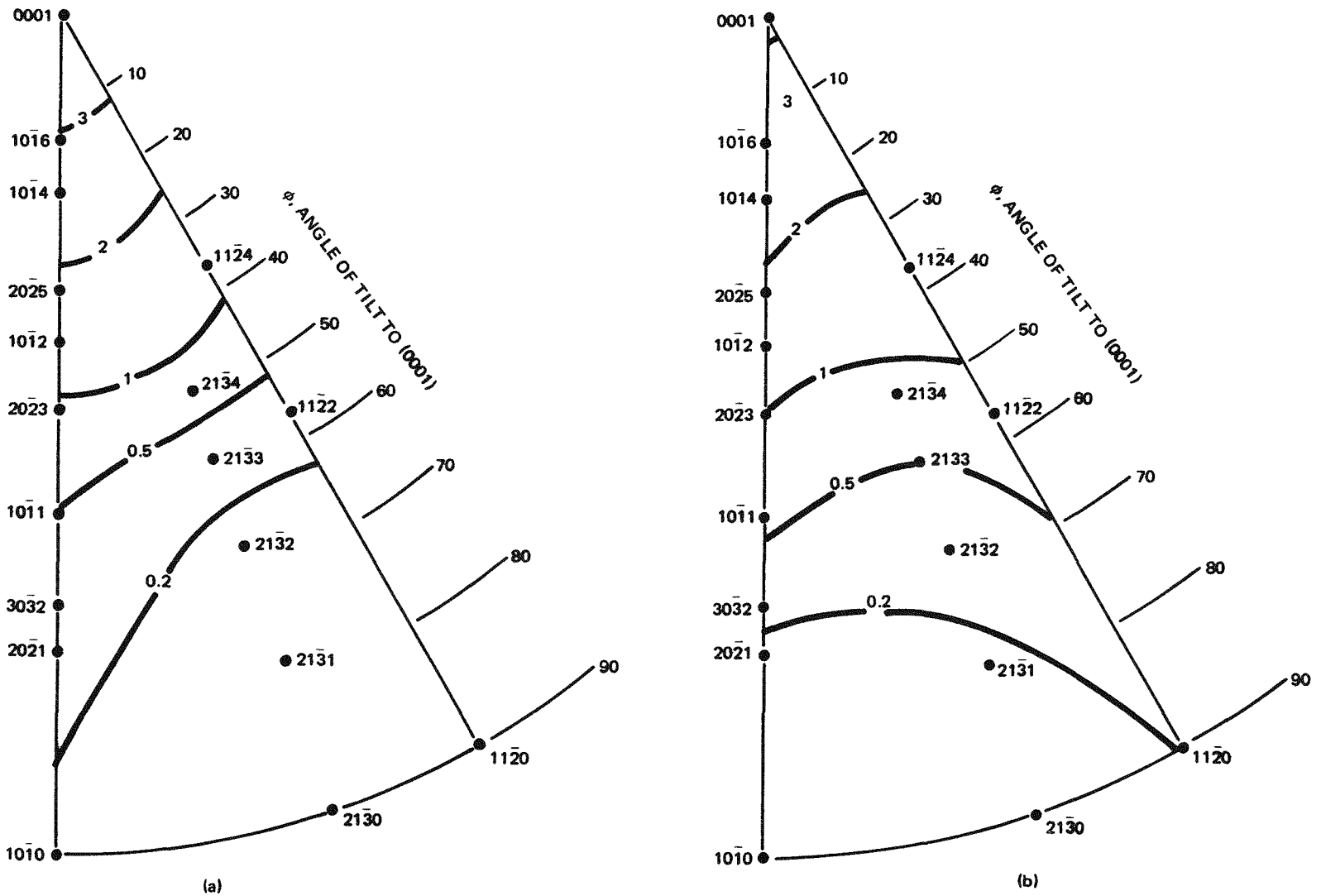

Figure 4.1-16. Inverse Pole Figure for Zr-lined Tubing, (a) Midwall of Zircaloy-2 Tubing, (b) Zirconium Barrier Surface of Low Oxygen Sponge, Annealed at 577°C

ACKNOWLEDGEMENTS

The contributing authors of Subsection 4.1 gratefully acknowledge the contributions to this work of their colleagues:

R. E. Blood, NTD, for assistance with the preparation of specimens for EBR-II irradiation.

R. D. Jones, NTD, for preparation of the temperature monitor capsule for the EBR-II experiment.

D. Pereyra, NTD, for help with optical metallography.

H. A. Storms of the Irradiation Processing Operation for performing the ion probe analyses and for help in interpreting the data.

R. W. Warner, NTD, for help with SEM metallography.

U. E. Wolff, NTD, for help in SEM and metallographic evaluations.

4.2 TASK 2.0 LICENSING TESTS

4.2.1 Subtask 2.1 Simulated Loss-of-Coolant-Accident Evaluations (R. P. Tucker, R. E. Blood, R. B. Adamson, NTD)

4.2.1.1 Objective

Compare the behavior of barrier cladding (both that with copper barrier and that with zirconium liner) under simulated loss-of-coolant-accident (LOCA) conditions to that of reference Zircaloy cladding.

4.2.1.2 Introduction

An experimental program to compare the performance of advanced Zircaloy-2 cladding lined with copper or zirconium (barrier fuel cladding) with that of reference Zircaloy-2 cladding has been conducted under transient pressure (stress) and temperature conditions which simulate a hypothetical LOCA. During the postulated LOCA, it is assumed that fission power generation would be reduced to zero and that liquid coolant would be lost, leaving the fuel segments surrounded by saturated steam at a pressure equal to or somewhat greater than atmospheric. Under this condition, the cladding temperature would rise as a result of residual and radioactive decay heat. If the heat source is sufficient, the cladding integrity could be lost as a result of oxidation, rupture from fission gas pressure, or a combination of the two.

In the LOCA event, the cladding is simultaneously deformed and degraded by the action of the steam environment as higher temperatures are reached. The typical LOCA experiment takes the following form: a segment of cladding, pressurized internally with an inert gas to a pressure corresponding to typical fission gas inventory, is heated in a saturated steam environment at a rate corresponding to an actual LOCA event. The mode of failure and deformation leading to failure are observed.

In the present report are summarized the results of LOCA tests on barrier and reference Zircaloy-2 cladding performed in PHASE 1. Data are presented on the cladding deformation under simulated LOCA conditions at internal pressures corresponding to hoop stresses of 3.44, 5.17, and 6.90 MPa (500, 750 and 1000 psi respectively) as well as metallographic and SEM X-ray spectroscopic evaluations of the barrier/cladding interactions following LOCA testing.

4.2.1.3 Experimental Details

Materials. In the current test series simulated LOCA evaluations have been conducted on BWR cladding (8x8 design) of the following types:

1. Reference (bright pickled) Zircaloy-2
2. Reference autoclaved (oxidized) Zircaloy-2
3. Zircaloy-2 with electroless Cu-barrier plated on etched inside surface
4. Zircaloy-2 with electroless Cu-barrier plated on an autoclave oxidized inside surface
5. Zircaloy-2 with crystal bar zirconium liner
6. Zircaloy-2 with sponge zirconium liner

The cladding had a nomimal o.d. of 12.52 mm (0.493 inches) and a wall thickness of 0.864 mm (0.034 inch), except for the crystal bar zirconium lined tube which had a nominal 12.29 mm o.d. The copper barrier was nominally 10 μm thick and the zirconium liners were nominally 0.076 mm in thickness.

Test Procedure. A schematic diagram of the LOCA testing apparatus was presented previously. Tests were performed on tubing segments internally pressurized with flowing argon at pressures of 0.55, 0.83, or 1.1 MPa (80, 120, or 160 psi respectively) to simulate fission gas pressure during a LOCA event. The hoop stresses produced in the thin-wall cladding were 3.45, 5.17, and 6.90 MPa (500, 750 and 1000 psi respectively). During the test the exterior surface of the cladding was exposed to circulating saturated steam at atmospheric pressure. The tubing was loaded with depleted uranium dioxide pellets to simulate the fuel in actual rods, Figure 4.2-1. A 25.4 cm tubing section was resistively heated utilizing an automatically programmed heating schedule that increased from 99°C (210°F) to 1204°C (2200°F) over a period of 430 seconds. (See Figure 4.2-2.) The temperature was measured at the midplane of the heated section by internal chromel/alumel thermocouples adjacent to the inside surface of the cladding and by an external infra-red pyrometer focused at the same location. In the simulation tests, the urania pellets acted as heat sinks resulting in a temperature lag for the cladding inner surface compared to the outer surface. Upon reaching 1204°C (2200°F), the electrical power was shut off, and the cladding cooled rapidly by the circulating steam. For specimens which ruptured during the heating cycle the power was shut off immediately upon failure.

Post-test metallographic examinations were made on selected test sections, particularly those originally with copper barriers, to evaluate the consequences of the high LOCA temperatures on the barrier. Interdiffusion of copper and zirconium was evaluated, to a limited extent, by SEM X-ray spectroscopy.

4.2.1.4 Results

LOCA Tests. The results of the simulated LOCA tests on all the types of cladding are summarized in Table 4.2-1.

Table 4.2-1
SIMULATED LOCA TEST RESULTS ON REFERENCE AND BARRIER ZIRCALOY-2 CLADDING

Test Number	Material	Hoop Stress, psi (MPa)	Average Final Temperature (°C)	Estimated Test Time (s)	Maximum % Diametral Strain
1	Zircaloy-2, bright etched	500 (3.45)	1204	430	3.6
2	Zircaloy-2, bright etched	750 (5.17)	1007	324	64 *
3	Zircaloy-2, bright etched	1000 (6.90)	939	252	127 *
4	Zircaloy-2, autoclave oxidized	500 (3.45)	1204	430	4.4
5	Zr-liner (low oxygen sponge)	500 (3.45)	1204	430	4.0
6	Zr-liner (crystal bar)	500 (3.45)	1204	430	3.7
7	Cu-barrier on etched Zircaloy-2	500 (3.45)	1204	430	5.5
8	Cu-barrier on etched Zircaloy-2	500 (3.45)	1204	430	5.1
9	Cu-barrier on etched Zircaloy-2	500 (3.45)	1204	430+180x	6.8
10	Cu-barrier on etched Zircaloy-2	500 (3.45)	1204	430	4.6
11	Cu-barrier on etched Zircaloy-2	1000 (6.90)	928	252	69 *
12	Cu-barrier on etched Zircaloy-2	750 (5.17)	987	294	46 *
13	Cu-barrier on autoclave-oxidized Zircaloy-2	500 (3.45)	1204	430	7.2
14	Cu-barrier on autoclave-oxidized Zircaloy-2	500 (3.45)	1204	430	7.8
15	Cu-barrier on autoclave-oxidized Zircaloy-2	500 (3.45)	1204	430	7.6
16	Cu-barrier on autoclave-oxidized Zircaloy-2	500 (3.45)	1204	430	6.1
17	Cu-barrier on autoclave-oxidized Zircaloy-2	1000 (6.90)	910	246	101 *
18	Cu-barrier on autoclave-oxidized Zircaloy-2	750 (5.17)	973	276	60 *

* Average maximum strain at failure location
† Tests at 500 psi (3.45 MPa) hoop stress were terminated without failure after 430 sec programmed heating schedule; for other tests the time to failure has been estimated.
x Specimen held 3 minutes at 1204°C

The specimens tested at 3.45 MPa (500 psi) hoop stress were heated to 1204°C (2200°F) in 430 seconds according to the programmed heating schedule (Figure 4.2-2); failure did not occur in any of the specimens under these conditions. From Table 4.2-1 it appears that the maximum diametral strain was greater for the copper barrier cladding than for the reference Zircaloy-2 or zirconium lined cladding. The cladding with copper plated on autoclave oxidized Zircaloy-2 exhibited the greatest strain, typically in excess of 7%, compared to about 4% strain for reference Zircaloy.

Tests at the higher hoop stresses of 5.17 and 6.90 MPa resulted in specimen ballooning and rupture prior to achieving the maximum temperature of 1204°C per the programmed heating schedule. The initial higher stress tests have been limited to single specimens of a given type at each stress level. Based on these data, it appears that the failure temperature of reference Zircaloy-2 is about 27 to 33°C greater than copper on autoclaved cladding at a given stress level and about 17°C greater than copper on bare Zircaloy-2.

The copper barrier on etched Zircaloy-2 showed, at both stress levels, the lowest diametral failure strain. At 5.17 MPa (750 psi) hoop stress, the reference and copper on autoclave oxidized Zircaloy-2 exhibited a failure strain of approximately 60% while for the copper on bare Zircaloy-2 the value was about 15% lower. At 6.90 MPa (1000 psi) hoop stress, the failure strain for the copper on bare Zircaloy-2 was about 30% less than for copper on autoclaved Zircaloy-2 and almost 60% less than for the reference cladding.

In copper barrier specimens that sustained temperatures above approximately 927°C, urania pellets were found to be stuck to the cladding; but in reference and zirconium lined tubing no pellet sticking occurred. Post-test longitudinal sectioning of copper-barrier specimens tested to 1204°C revealed a silvery layer at the pellet-cladding interface and at some locations between the pellets.

Metallographic Evaluation. Initial metallographic and SEM efforts have focused mainly on the copper-barrier cladding, since at LOCA temperatures a high rate of interdiffusion of copper and zirconium is expected with a eutectic reaction deemed likely. From the tests series at 3.45 MPa (500 psi) hoop stress in which the specimens reached 1204°C, metallographic examinations were conducted on specimens with electrolessly plated copper on both etched and oxidized Zircaloy-2 cladding. The autoclaved oxide layer appears not to have been an effective barrier to copper-zirconium interdiffusion under these high-temperature conditions. During the LOCA test, melting occurred at the inside surface of both types of cladding, and the copper was redistributed in several new microconstituents that formed as the molten layer solidified. In the lower section of the test pieces the wall thickness was observed to be increased up to approximately 1.27 mm (0.050 inch), compared to the nominal initial 0.864 mm (0.034-inch) wall. Substantial variation in wall thickness was observed circumferentially and axially. In a few locations, as illustrated in Figure 4.2-3, the post-test wall thickness was less than the initial value due to formation of molten material which flowed away. The minimum wall thickness observed was approximately 0.38 mm (0.015 inch) in the lower region of the copper on bare (unoxidized) Zircaloy specimen (Figure 4.2-3).

Based on the microstructures observed the following sequence is postulated to have occurred during the 1204°C LOCA test: during heating there was diffusion of copper into the Zircaloy, lowering its melting point. At some stage the remaining copper and a portion of the Zircaloy tube melted, flowed down the inner surface of the tube and entered into fuel cracks and pellet-pellet interfaces. Oxygen was absorbed by the melt. Upon cooling, oxygen-rich α-zirconium phase solidified first as a skin layer bonded to the cooler fuel pellets. Subsequently, β-zirconium (with Cu in solid solution) solidified dendritically as a primary microconstituent. Finally, a eutectic liquid solidified to form β-Zr and a Zr-Cu intermetallic (probably Zr_2Cu) in the remaining space. The microconstituents formed from the melt comprised a layer at the inner surface that typically was about 40% of the wall thickness at a given location. The cooling rate was rapid, apparently resulting in nonequilibrium conditions. This departure from equilibrium presumably accounts for the presence of a second primary phase containing more Cu than the β-Zr phase.

Figure 4.2-4 shows an example of the microstructure at the inside surface of a copper on oxide specimen which illustrates the features resulting from the sequence outlined above. The oxygen-rich α-phase layer at the interface with the pellet is marked "A" while the β-quenched Zircaloy structure is marked "B". Scanning electron microscope X-ray studies showed the α-phase layer contained little if any copper. Between these two microconstituents is a complex region associated with the eutectic reaction. Because of the nonequilibrium cooling experienced in these

tests there are numerous variations in the structures formed particularly at the cladding inner surface. A typical view of the cladding outer surface is shown in Figure 4.2-5, where the outermost ZrO_2 layer is marked "A", the oxygen stabilized α-phase layer is marked "B" and the β-quenched Zircaloy structure extending through much of the wall thickness is marked "C". (*N.B. The outermost layer is comprised of the oxidation products of Zircaloy-2. The* designation of this layer as "ZrO_2" is made for convenience.)

Metallographic examination of longitudinal sections from the crystal-bar and sponge zirconium lined specimens revealed that the liners could no longer be distinguished from the rest of the cladding wall following the high temperature LOCA. Except for the rather uniform layers of ZrO_2 and oxygen stabilized α-phase at the outer surface, the cladding showed a β-quenched structure.

From the specimens tested at higher hoop stresses, sections were cut for metallographic examination from above the ballooned region of the two copper on autoclave oxidized cladding specimens. Figure 4.2-6 shows a longitudinal section of the wall from the 5.17 MPa (750 psi) test specimen. The 10 μm copper layer originally plated on the inside surface has diffused into the Zircaloy to produce a 0.05 to 0.075 mm thick interaction layer which shows evidence of a eutectic reaction. The absence of an oxygen stabilized α-phase layer at the cladding inner surface should be noted. This observation, together with the uniform wall of approximately the initial thickness, suggests less extensive melting has occurred at the inner surface of this specimen. The specimen outer surface, as expected, was similar in appearance to that shown in Figure 4.2-5 with a layer of ZrO_2 over a layer of α-phase. The major portion of the wall appears to be a β-quenched Zircaloy structure.

The specimen tested at 6.90 MPa (1000 psi) exhibited an inner surface interaction layer of more uniform thickness in the range 0.046 to 0.051 mm. Figure 4.2-8 is a photomicrograph of the inner surface region of this cladding. The interaction layer is again complex but different in appearance from the previous case. Note in the micrograph the approximately equiaxed grains just beyond the interaction layer. In this specimen the major portion of the wall appears to be an $\alpha+\beta$ quenched structure.

SUMMARY

Simulated LOCA tests on reference, zirconium-lined and copper-barrier Zircaloy-2 cladding have demonstrated:

1. At a hoop stress of 3.45 MPa (500 psi) all cladding remained unbreached throughout the heating cycle. Cu-barrier cladding experienced greater diametral strain than other cladding types.

2. Zirconium-lined cladding exhibited LOCA behavior similar to reference Zircaloy-2.

3. Cu-barrier cladding experienced melting and flowing of the copper layer (3.45 MPa tests) and/or copper-zirconium interdiffusion resulting in a eutectic reaction and a complex interaction layer from about 6% up to ~40% of the wall thickness.

4. At high temperatures the autoclave oxide does not appear to prevent copper-zirconium interaction nor the formation of an intermetallic phase.

5. In higher stress LOCA tests the Cu-barrier seems to have lowered the rupture temperature by ~30°C on autoclave oxidized cladding and ~15°C on bare (unoxidized) Zircaloy-2.

6. In the saturated steam atmosphere, cladding outside surfaces formed an outermost layer of oxidized Zircaloy over a layer of oxygen stabilized α-phase.

4.2.2 Subtask 2.2 Reactivity Initiated Accident (L. D. Noble, NTD)

The objective of this task is to obtain experimental data on how the performance of fuel with a copper or zirconium barrier compared to that of nonbarrier fuel during a reactivity initiated accident (RIA).

For a BWR, the design basis RIA is a hypothetical case in which a control blade becomes decoupled from its control drive mechanism while in the inserted position. It is then postulated that the control drive is withdrawn, but the control blade remains in the reactor, to drop out, suddenly, at some later time. Analysis indicates that the most severe transients occur during ambient or hot standby conditions. The barrier tubing will be tested under both of these conditions.

The majority of the ambient and heated tests will be conducted in 1979 or 1980 at the NSRR in Japan through arrangements with Battelle, the Nuclear Regulatory Commission (NRC), and the Japan Atomic Energy Research Institute (JAERI).

Forty experimental fuel rods have been fabricated and shipped to the NSRR,[1,2] arriving in September. The shipment included 18 reference and 11 each of copper-barrier and zirconium-liner rods.

Thirty one tests are planned at the NSRR as summarized in Table 4.2-2. The low energy (140 cal/g) test on a reference rod which was performed in November is being destructively examined to confirm the energy deposition. Subsequent tests and post-irradiation exams through August 1979 will provide the comparative performance information on all rods over a range of energy depositions which produce slight cladding oxidation to fuel fragmentation.

Table 4.2-2
PLANNED RIA TESTS

Ambient Conditions		
8 reference	140 to 400 cal/g	
5 copper	170 to 400 cal/g	
5 zirconium	170 to 400 cal/g	
High Temperature and Pressure		
8 reference	140 to 400 cal/g	
5 barrier (to be specified)	170 to 400 cal/g	
Schedule		
1. 140 cal/g	November 1978	1 reference rod
2. 170 to 190 cal/g	April 1979	2 Cu, 2 Zr, 3 reference
3. 250 to 275 cal/g	June 1979	2 Cu, 2 Zr, 3 reference
4. 400 cal/g	August 1979	1 Cr, 1 Zr, 1 reference

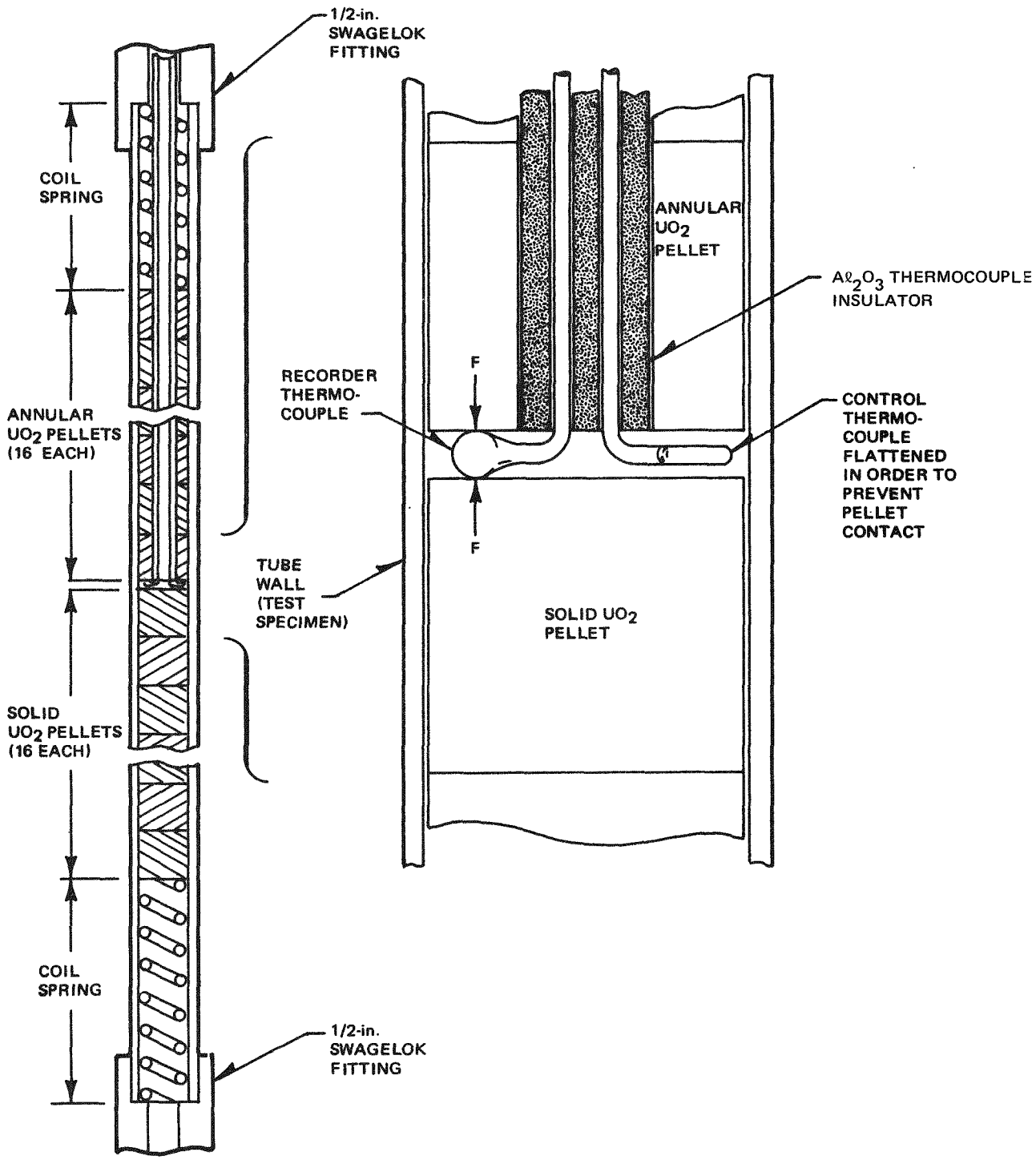

Figure 4.2-1. Schematic of LOCA Test Specimen

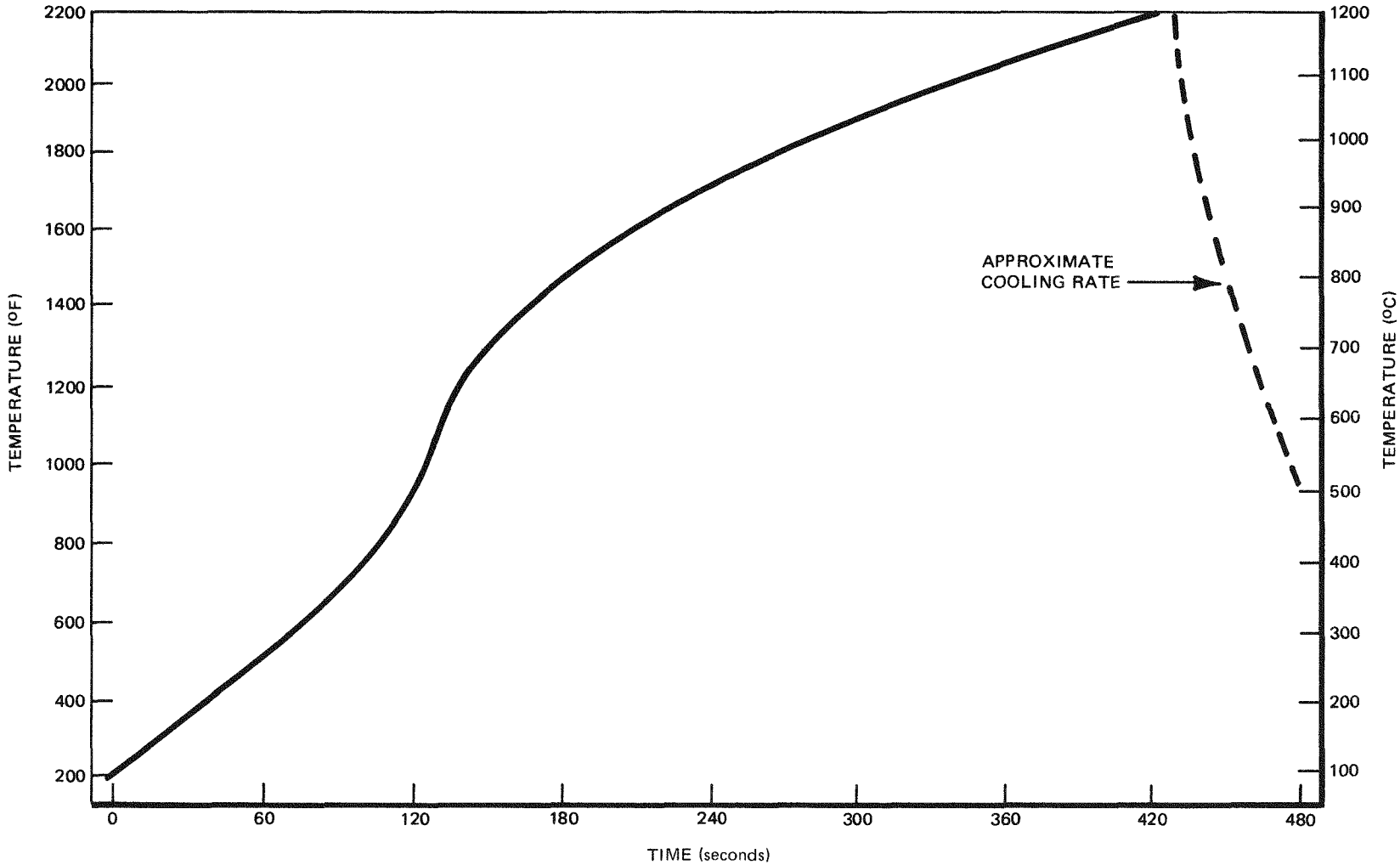

Figure 4.2-2. Temperature as a Function of Time for Simulated LOCA Testing

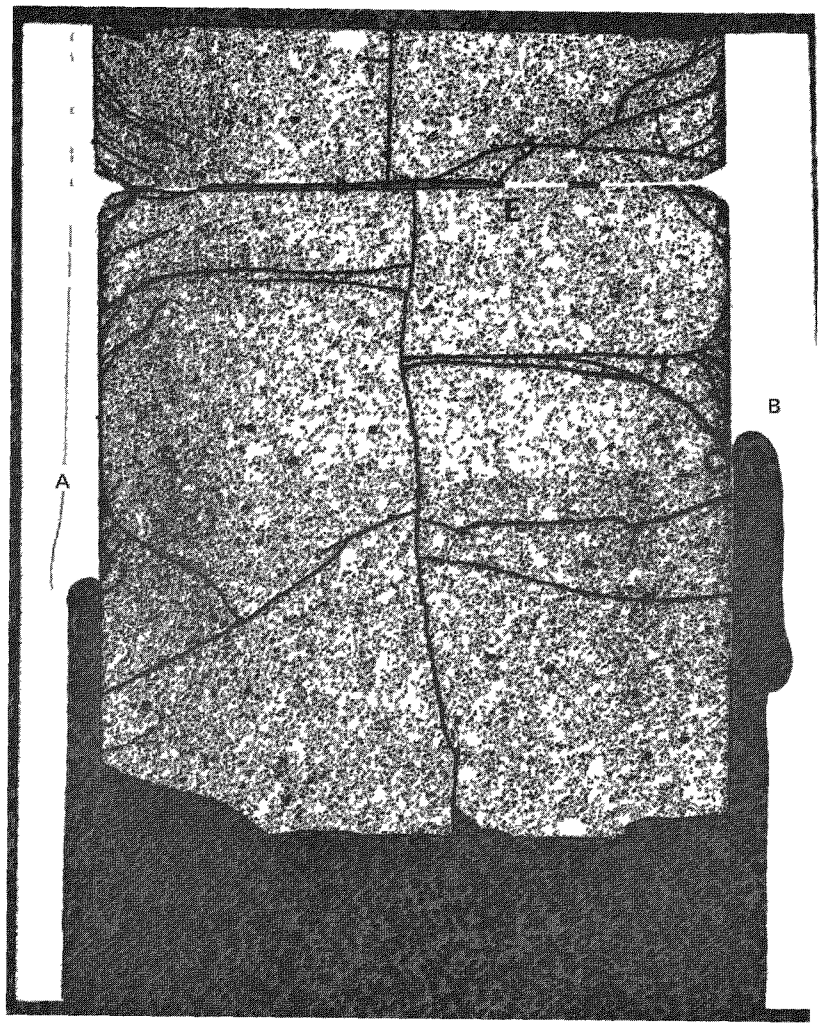

Figure 4 2-3 Longitudinal Section from Lower Portion of Cu on Unoxidized Zircaloy-2 Specimen Note Wall Thickness Buildup from Molten Metal at A and B, the Wall Thinning Below B, and Metal Between Urania Pellets at E Magnification 8X

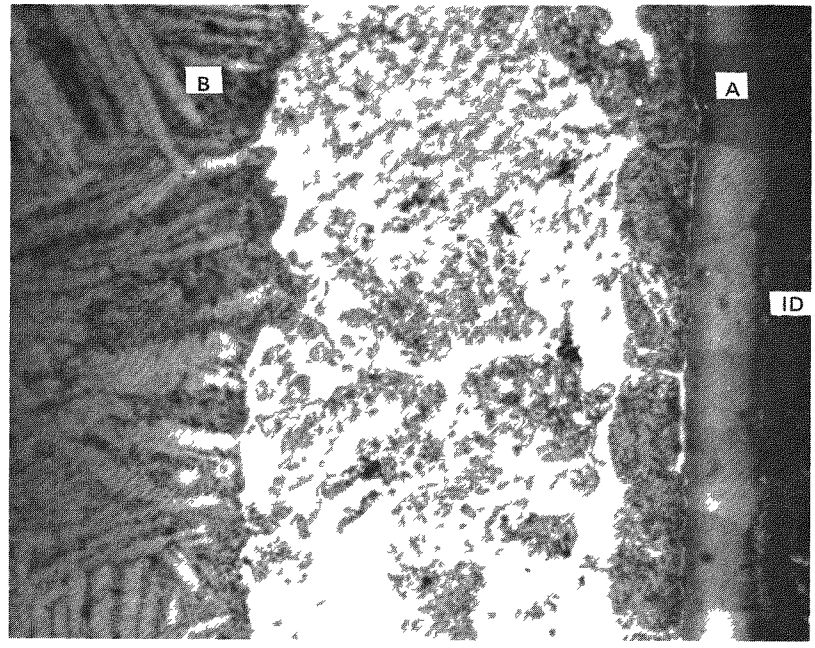

Figure 4 2-4 Post-Test Inner Surface (I D) Microstructure of Cu on Autoclaved Zircaloy-2 Specimen Note Oxygen Stabilized α-Zirconium Phase A, β-Quenched Structure B, and Complex Interaction Layer between A and B Regions Magnification 500X

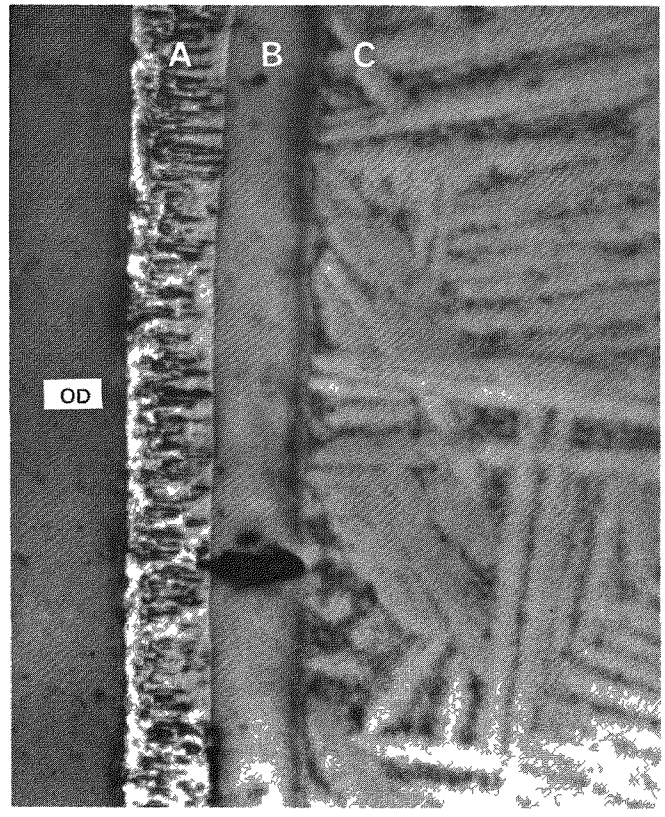

Figure 4 2-5 Typical Post-Test Outer Surface (O D) Microstructure of Zircaloy-2 Cladding After Heating to 1204°C in Saturated Steam Note ZrO_2 Layer A, Oxygen Stabilized α-Phase B, and β-Quenched Structure C Magnification 300X

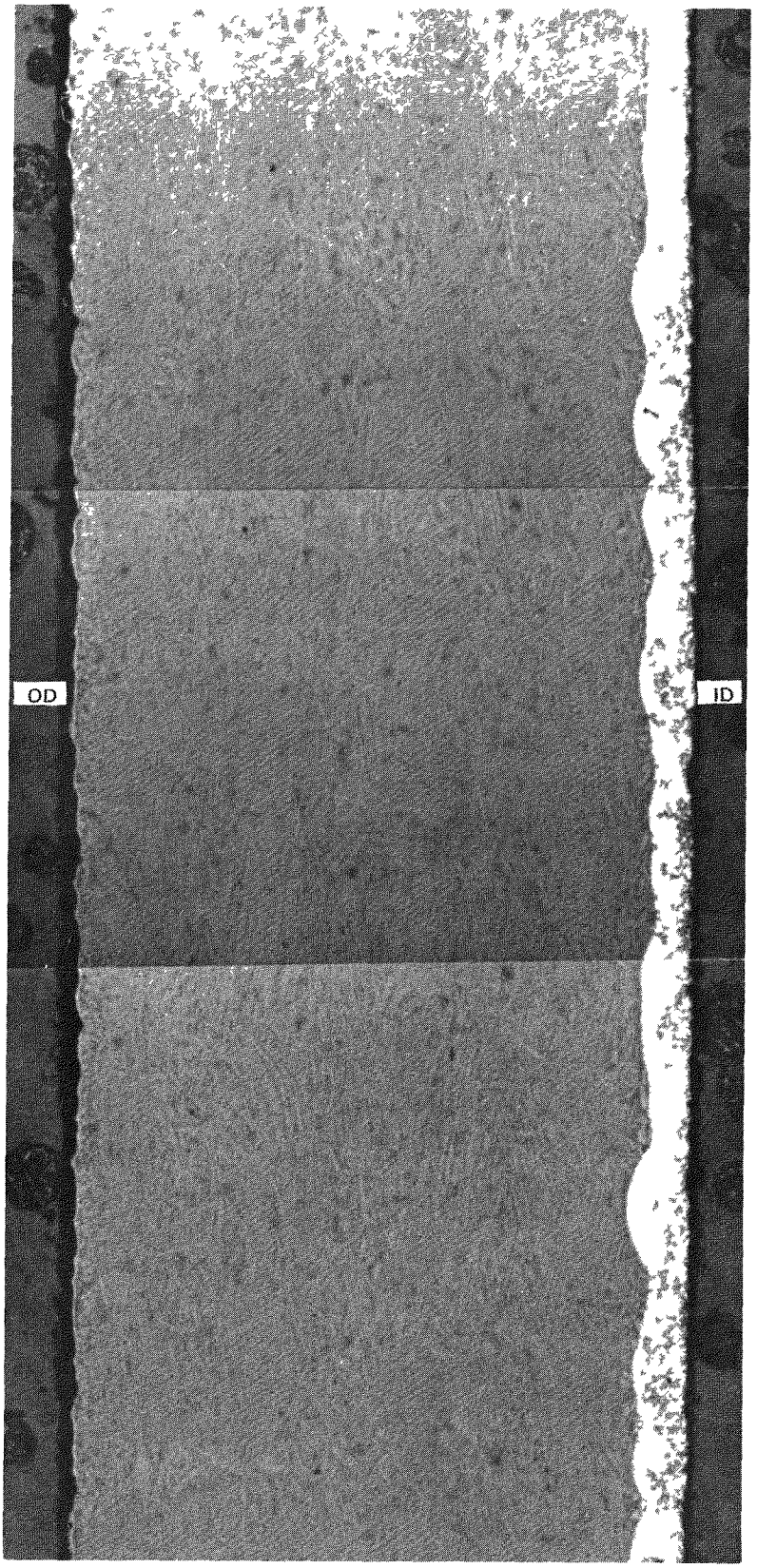

Figure 4 2-6 Longitudinal Section of Cu on Oxidized Cladding Showing Wall Thickness After 5 17 MPa (750 psi) Test Note Variation in Thickness of Inner Surface (I D) Cu-Zr Interaction Layer Magnification 100X

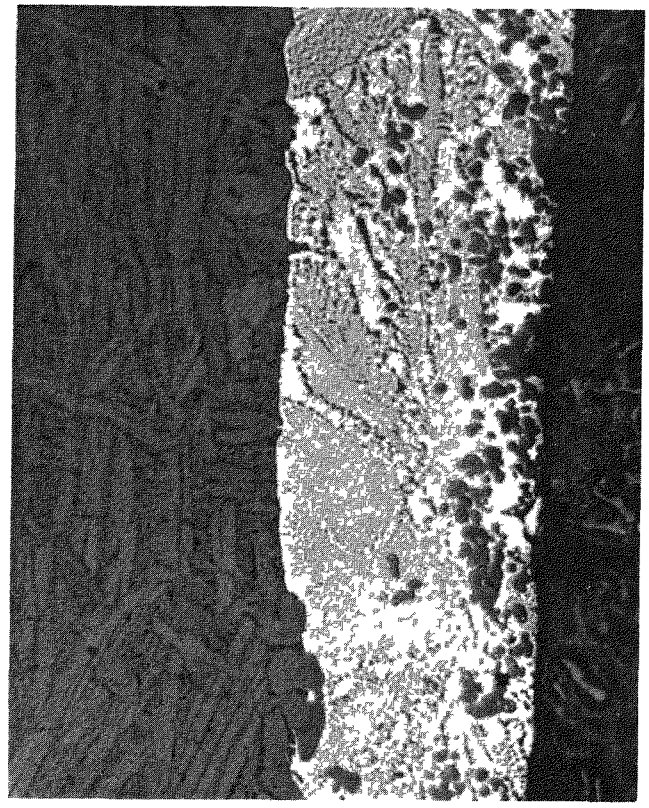

Figure 4 2-7 Post-Test Microstructure at Inner Surface of Cu on Autoclaved Zircaloy-2 Tested at 5 17 MPa (750 psi) Note Complex Eutectic Structure and Absence of Oxygen Stabilized α-Phase Layer Magnification 530X

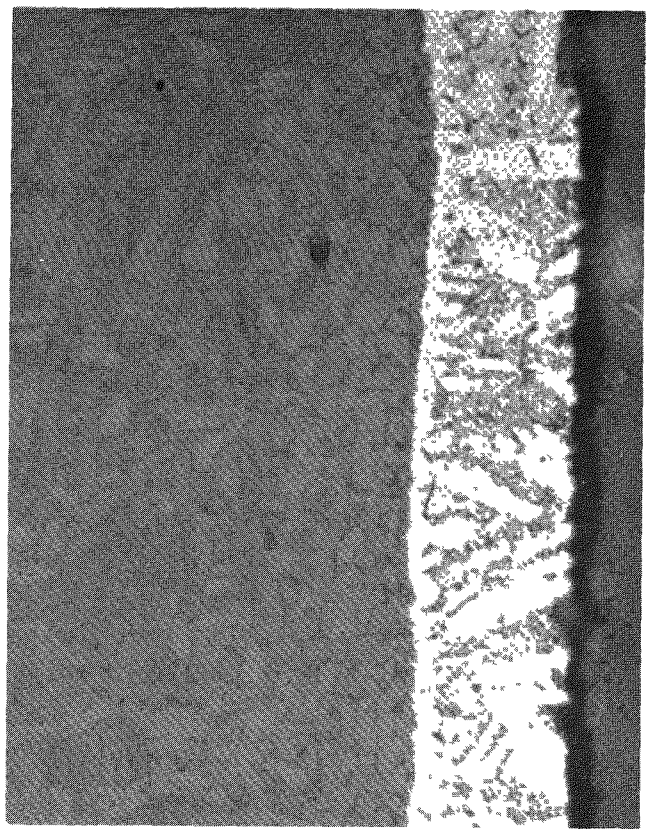

Figure 4.2-8. Post-Test Microstructure at Inner Surface of Cu on Autoclaved Zircaloy-2 Tested at 6.90 MPa (1000 psi). Magnification 530X

ACKNOWLEDGMENTS

The contributing authors of Subsection 4.2 gratefully acknowledge the invaluable assistance of:

E. L. Courtright of Battelle Pacific Northwest Laboratories for his diligent and systematic help in the fabrication of the RIA fuel specimens and in arranging for shipment to Japan.

M. L. Ishikawa of the Japan Atomic Energy Research Institute for his interest in the RIA work and for planning and implementing RIA tests.

G. F. Rieger, NTD, for getting the LOCA simulation tests started.

R. van Houten of the U.S. Nuclear Regulatory Commission for supporting the cooperative efforts required for implementation of the RIA tests.

4.3 TASK 3.0 — FUEL IRRADIATION TESTS (J. H. Davies, NTD)

4.3.1 Objectives

1. Evaluate the PCI-resistance of Cu-barrier and Zr-liner fuel using irradiated test fuel rods.

2. Provide data on the in-reactor behavior of Cu-barrier and Zr-liner fuel to form a basis for choosing which concept will ultimately be used in the large-scale demonstration.

4.3.2 Subtask 3.1 Accelerated PCI Tests (Collapsed Cladding) (J. H. Davies, E. L. Esch, NTD)

The GE Test Reactor (GETR) has remained shut down throughout the current reporting period. Thus the irradiation status of the collapsed cladding (CC) rods still on test remains the same as that described previously (see Table 6.3-4 of the First Semiannual Report[2]).

Post-Irradiation Examination

Nondestructive post-irradiation examination (PIE) was completed on CC-54A and B. These were Cu-barrier rods (10 μm electroless copper). The lower rod in the assembly, CC-54A, was ramp tested just prior to the GETR shutdown; it survived ramping to 66.3 kW/m (20.2 kW/ft) peak power at a burnup of ~5 MWd/kg-U. The upper rod, CC-54B, was not ramp tested, but experienced a peak power of 47.2 kW/m (14.4 kW/ft) during the ramping of the lower rod. The ramp test of CC-54A is the only one performed so far on an electroless Cu-barrier rod. The performance of the rod appears to match the good performance of electroplated Cu-barrier rods in the same exposure range.

Nondestructive PIE of both rods confirmed that they were sound. A summary of critical data for CC-54A is presented in Figure 4.3-1. Note that there were numerous pulsed eddy-current (PEC) indications of apparent flaws. This behavior does differ from previous Cu-barrier rods examined in this series and will have to be investigated by destructive examination. However, the PEC signals are believed to reflect the difficulties of collecting meaningful eddy-current data on Cu-barrier rods rather than being indicative of cladding flaws. Similar multiple signals were observed on CC-54B, which was not ramped.

A section of the inner surface of the Cu-barrier cladding of rod, CC-44A, has been examined using a scanning electron microscope with X-ray analysis capability. The results of this study are summarized along with similar results on SRP segments in a later section.

4.3.3 Subtask 3.2 Segmented Rod Irradiation Tests (J. H. Davies, E. Rosicky, U. E. Wolff, Y. Nivas, NTD)

4.3.3.1 Bundle Status

The irradiation status of the three segmented test rod assemblies is updated in Table 4.3-1. During the current report period the SRP-2 (Monticello) bundle was reconstituted as planned (Reconstitution No. 3). The designs of the replacement segments were described previously;[1] the retrieved segments, which are cooling at the site prior to shipping, are listed in Table 4.3-2.

4.3.3.2 Pre-Test Characterization

Precise length measurements are among the dimensional data collected in the course of characterizing the irradiated segments. These data have been evaluated, and an empirical relationship between irradiation growth and fast neutron fluence has been developed.The SRP-3 data are plotted in Figure 4.3-2. These rods were all fabricated from recrystallized tubing and were irradiated in the Millstone commercial power reactor to burnups in the range of 3.5 to 16.9 MWd/kg-U at peak powers not exceeding 23 kW/m (7 kW/ft). The SRP-2 data on recrystallized tubing fit the same relationship, which is used to project fuel rod growth to higher exposures.

Table 4.3-1
SRP IRRADIATION STATUS

STR Bundle	Segment Tier	Average Exposure (MWd/kg-U)	Highest SRP Segment Average Exposure (MWd/kg-U)	Date
	Top	9.7	11.5	October 1978
	Mid Top	14.1	16.9	
SRP-1	Mid Bottom	14.3	17.9	
	Bottom	12.3	15.7	
	Bundle Average	12.6		
	Top	11.8	14.5	October 1978
	Mid Top	17.2	21.8	(EOC-6)
SRP-2	Mid Bottom	19.2	24.3	
	Bottom	17.8	21.6	
	Bundle Average	16.5		
	Top	10.1	14.1	October 1978
	Mid Top	14.3	18.8	
SRP-3	Mid Bottom	16.0	20.9	
	Bottom	14.7	20.3	
	Bundle Average	13.8		

Table 4.3-2
SEGMENTS RETRIEVED DURING THIRD RECONSTITUTION OF BUNDLE SRP-2 (MONTICELLO)

Segment Serial No. [a]	Design Feature[b]	Cladding Wall Thickness (mm)	Diametral Gap (mm)	Estimated Average Burnup[c] (MWd/kg-U)
DTB-0143	10 μm Cu-Barrier (nonbonded)[d]	0.86	0.23	8.3
DTB-0142	10 μm Cu-Barrier (nonbonded)[d]	0.86	0.23	13.2
DTB-0141	10 μm Cu-Barrier (nonbonded)[d]	0.86	0.23	15.3
DTB-0137	10 μm Cu-Barrier (nonbonded)[d]	0.86	0.23	14.1
DTB-2315	10 μm Cu-Barrier (on oxide)[e]	0.86	0.23	4.5
DTB-2512	Zr-Liner (sponge)[e]	0.86	0.23	4.5
DTB-2406	Zr-Liner (crystal bar)[e]	0.86	0.23	5.3
8D15-1	Reference[f]	0.71	0.18	18.3
0D13-3	Reference[g]	0.71	0.18	18.6
0D13.4	Reference[g]	0.71	0.18	20.7
W5-1	Reference[f]	0.86	0.23	21.7
W5-3	Reference[f]	0.86	0.23	24.1
W5-4	Reference[f]	0.86	0.23	21.5

[a] Vallecitos identification number not yet assigned
[b] Cladding heat treatment, recrystallization anneal at 577°C; fuel density 95.5%
[c] Estimated segment burnups subject to revision following evaluation of ^{137}Cs gamma scan data.
[d] Replacement segment inserted in Recon 1 (1975); fill gas, 1 atm He
[e] Replacement segment inserted in Recon 2 (Oct 1977); fill gas, 3 atm He
[f] Original segment; fill gas, 1 atm He
[g] Original segment; fill gas, 22 atm He

4.3.3.3 Ramp Testing

Due to the prolonged shutdown of the GETR, ramp testing has been performed in the R-2 reactor in Studsvik, Sweden.

R-2 Test Facilities

The R-2 reactor is a 50 MW (thermal) materials testing reactor. The reactor is contained within an aluminum vessel at one end of a large open pool, which also serves as a storage area for spent fuel elements and irradiated samples. Light water is used as core coolant and moderator. Additional information about the reactor is provided in Table 4.3-3.

Table 4.3-3
R2 TECHNICAL DATA

Power	50 MWt
Moderator/coolant	H_2O
Reflector	Be and D_2O
Fuel material	U/Al alloy
enrichment	90% to 93%
loading	about 9 kg U-235
Control rods	6 Cd/U rods
Neutron flux in experiment position	
Thermal	1.8 to 5.0 · 10^{14} n/cm²/sec
Fast (>0.1 MeV)	2.5 to 4.5 · 10^{14} n/cm²/sec
Burnup	~50%
Primary flow	1200 kg/sec
temperature (inlet)	50°C
Secondary flow	1000 kg/sec
temperature (inlet)	<7°C

Fuel rod testing can be performed under realistic operating conditions in two pressurized light water loops. The in-pile part of each loop is of a U-tube design, taking up two core positions and thus providing two test positions, one with downward flow of coolant and one with upward flow. Pressurization is by a boiling surge tank with electrical heaters. Water is circulated through the in-pile parts of the loop by canned motor pumps and heated electrically by external heaters clamped on the pipes.

Provision is made for calorimetric power measurement in each tube, by means of precision resistance thermometers or thermocouples at several locations and the main flow meter. The U-tubes are isolated from the reactor primary coolant by a gas gap containing CO_2, which reduces heat losses facilitating accurate test rod power measurement.

Fission product monitoring (test rod failure detection) is performed by taking out a small bypass stream to a selective Cerenkov detector. A delay time of about 2-1/2 minutes has been determined between failure and detection in this system. If larger fuel defects occur, the resulting increase of activity level is detected virtually instantaneously by gamma detectors monitoring general radiation levels. Loop technical data are summarized in Table 4.3-4 and in-core loop instrumentation is listed in Table 4.3-5.

Controlled power ramping of fuel rods is performed using the ^3He neutron absorber technique. ^3He is contained in a stainless steel double minicoil screen around the fuel rod test section and rod power is regulated by varying the ^3He pressure. Power attenuation factors of ~2 can be obtained in this rig at constant reactor power. Figure 4.3-3 shows relative rod power attentuation as a function of ^3He pressure for a 2.6% enriched fuel rod.

Table 4.3-4
R2 LOOP 1 AND 2 TECHNICAL DATA SUMMARY

Technical Data	Loop 1	Loop 2
In-core test positions		
Number	2	2
Position in core	B8, C9	B3, C2
Flow direction	Up, Down	Up, Down
Inside diameter (mm)	45.5, 45.5	53.5, 45.5
In-core (useful) length (mm)	670	670
Coolant flow rate ($kg \cdot s^{-1}$)	3.5–6	3.5–6
Maximum pressure (MPa)	15.0	9.3
Maximum sample heat rating (kW)	150	~200
Neutron flux, unperturbed ($n \cdot cm^{-2} \cdot s^{-1}$)		
Peak thermal	$0.6–0.8 \times 10^{14}$	
Fast (>1 MeV)	$0.8–1.0 \times 10^{14}$	

Table 4.3-5
LOOP INSTRUMENTATION

Item	Function
Precision resistance thermometer	Measurement of coolant temperature at entrance into loop incore section
Thermocouples	Measurement of coolant temperature at inlet and outlet of the incore loop section.
Pressure meter	Measurement of loop coolant pressure.
Flowmeter	Loop flow rate measurement.
Conductivity meter	In-stream conductivity measurement of loop coolant water.
Fission product monitor	On-line monitoring of loop coolant water activity.
Flowmeter	Measurement of coolant flow rate in ramp test rig.
Thermocouples	Measurement of coolant temperature at inlet and outlet of ramp test rig.

Precise rod power monitoring during power ramps is provided by thermocouples and a flowmeter built into the ramp test rig. The outputs of these and the other instruments described are fed into a computer which manipulates and stores the data. Test status can be monitored in the control room and at a remote terminal by displaying key data on a video screen. Additionally, the test rod relative power and the loop activity are recorded in parallel on chart paper. Rod failure is usually indicated by a steep increase in the loop activity level.

Test Description

During the current period twelve segments were ramp tested in R-2, including four copper-barrier fuel rods and two Zr-liner fuel rods. The characteristic data for the fuel rod segments are provided in Table 4.3-6.

Figure 4.3-4, reproduced from the previous report,[1] summarizes the test specification. The standardization phase of the irradiation was performed on groups of four rods in Loop No. 2 during three consecutive reactor cycles: then all twelve rods were ramped in succession during the following cycle in Loop No. 1. Special rigs were designed and built to accommodate these rods, which were somewhat longer than those normally tested in R-2. Pre-ramp standardization phase irradiation summaries are given in Table 4.3-7.

Table 4.3-6
DESCRIPTION OF SEGMENTS RAMP TESTED IN R2

Segment Identification	Design Feature[a]	Cladding Wall (mm)	Diametral Gap (mm)	He Pressure (MPa)	Average Burnup[b] (MWd/kg-U)
SRP-2/10	Reference	0.86	0.23	0.1	16.4
SRP-2/11	Reference	0.86	0.23	0.1	15.4
SRP-2/13	Reference	0.86	0.23	0.1	15.4
SRP-2/14	Reference	0.86	0.23	0.1	14.6
SRP-2/19	Reference	0.71	0.18	2.2	14.6
SRP-2/20	Reference	0.71	0.18	2.2	13.8
SRP-2/1	10 μm Cu-Barrier (nonbonded)[c, d]	0.86	0.23	0.1	12.4
SRP-2/4	10 μm Cu-Barrier (bonded)[c]	0.86	0.23	0.1	14.4
SRP-3/33	5 μm Cu-Barrier (nonbonded)[c]	0.71	0.23	1.7	16.7
SRP-3/34	5 μm Cu-Barrier (nonbonded)[c]	0.71	0.23	1.7	16.1
SRP-3/35	Zr-Liner (crystal bar)	0.71	0.23	1.7	16.6
SRP-3/36	Zr-Liner (crystal bar)	0.71	0.23	1.7	15.3

[a] Cladding for all segments is Zircaloy-2 (recrystallization anneal); fuel density, 95.5%.
[b] Segment burnups calculated from ^{137}Cs gamma scans by comparison to known standard.
[c] Cu-Barrier designs are all electroplated. Bonded barrier means plated tubes subjected to diffusion anneal to form Cu-Zr intermetallic layer. This fabrication step is omitted in nonbonded designs.
[d] Cu-Barrier layer shot peened.

Table 4.3-7
PRE-RAMP STANDARDIZATION PHASE IRRADIATION SUMMARY[a]

Segment Identification	Peak Power Range[b] (kW/m)	Irradiation Time (h)
SRP-2/13	26.2 to 27.6	304
SRP-2/14	23.6 to 24.6	304
SRP-2/11	22.3 to 23.3	304
SRP-2/20	26.9 to 27.9	304
SRP-2/10	24.9 to 26.9	301
SRP-3/36	24.9 to 26.9	301
SRP-3/34	23.3 to 25.3	301
SRP-2/4	24.6 to 26.6	301
SRP-2/19	23.0 to 24.9	569[c]
SRP-3/35	25.6 to 27.9	569[c]
SRP-3/33	23.9 to 26.2	569[c]
SRP-2/1	23.0 to 24.9	569[c]

[a] Segments irradiated in sets of 4 (as shown) in Loop No. 2.
[b] Specified range was 21.3 to 29.5 kW/m (6.5 to 9.0 kW/ft). See Figure 4.3-3.
[c] Accumulated during two reactor cycles. See text.

The ramp test phase of the program was performed at the rate of one test per day. Reactor power was reduced during rod insertion, and the rods were brought up to pre-ramp power levels by raising the reactor power. Depending on the pre-ramp level, rod power was increased to 32.8 kW/m (10 kW/ft) in either one or two steps (individual ramp steps were not to exceed 6.6 kW/m or 2 kW/ft). These steps were performed by a combination of increasing reactor power and reducing ^3He pressure. All subsequent steps were performed at constant reactor power using only the ^3He coil with precise control. As mentioned earlier, the status of the test was followed by monitoring recorder chart outputs of rod power and loop activity. Rod failures were positively indicated by steep increases in the activity level. An example is shown in Figure 4.3-3. Note also the small peak or deflection on the power trace at the start of the ramp step. Similar thermal spikes were associated with other rod failures in this test series, but were not observed on the traces of sound rods. These features, which have not previously been detected in other Studsvik tests, are presently being evaluated. It is believed that they may represent an independent indication of rod failure time.

Following a certified rod failure, power was rapidly reduced by pressurizing the ^{3}He coil. Shortly thereafter the rod was withdrawn from the core location, and after an appropriate cooling period, it was removed from the rig.

All the rods have been visually examined in the Studsvik Hotcells and will be neutron radiographed prior to shipment back to the GE Vallecitos Nuclear Center for a more detailed examination.

4.3.3.4 Results

Preliminary results of the ramp tests are summarized in Table 4.3-8. All of the reference rods failed as expected.

Table 4.3-8
R2 RAMP TEST — RESULTS SUMMARY

Segment Identification	Design Feature	Average Burnup (MWd/kg-U)	Maximum Peak Power[a] (kW/m)	(kW/ft)	Time at Maximum Power[b]	Test Results
SRP-2/10	Reference	16.4	39.4	12	16 min	Failed
SRP-2/11	Reference	15.4	45.9	14	0[c]	Failed
SRP-2/13	Reference	15.4	52.5	16	30 s	Failed
SRP-2/14	Reference	14.6	45.9	14	30 s	Failed
SRP-2/19	Reference	14.6	52.5	16	29 min	Failed
SRP-2/20	Reference	13.8	45.9[d]	14[d]	59 min	Failed
SRP-2/1	10 μm Cu-Barrier (nonbonded)	12.4	59.1	18	12 h	Sound
SRP-2/4	10 μm Cu-Barrier (bonded)	14.4	59.1	18	100 min	Failed
SRP-3/33	5 μm Cu-Barrier (nonbonded)	16.7	52.5	16	39 min	Failed
SRP-3/34	5 μm Cu-Barrier (nonbonded)	16.1	59.1	18	0[c]	Failed
SRP-3/35	Zr-Liner (crystal bar)	16.6	59.1	18	12 h	Sound
SRP-3/36	Zr-Liner (crystal bar)	15.3	59.1	18	12 h	Sound

[a] Nominal value after last ramp step. See Figure 4.3-4.
[b] Failure times based on loop activity level. Actual failure times are in question (see discussion in paragraph 4.3.3.3).
[c] Failed during ramp step to peak power shown.
[d] Segment ramped to 54.5 kW/m (16 kW/ft) before failure indication recorded (2½ minute delay in loop activity monitor).

The presently proposed PCI remedy designs, crystal bar Zr-liner and 10 μm nonbonded Cu-barrier, both survived the test. However, the two 5 μm Cu-barrier rods failed after burnup >16 MWd/kg-U (three out of three similar segments survived the test at ~9 MWd/kg-U[1]. Full evaluation of these results must await the post-irradiation examinations scheduled to occur early in PHASE 2.

The failure of SRP-2/4, bonded Cu-barrier, was predictable on the basis of expanding mandrel test results[1,2], which showed that this design, in contrast to the nonbonded Cu-barrier, was embrittled by liquid cadmium.

4.3.3.5 Scanning Electron Microscopy of Barrier Cladding Inner Surface

Introduction

In October 1977 nine SRP fuel rod power ramps were tested in the GETR.[2] That group of nine consisted of three Cu-barrier rods, Zr-liner rods, and three reference rods. These rods had burnups ~9 MWd/kg-U; the barrier fuel rods all survived, while the reference rods failed the test.[1] Here the results of analyses by SEM of the sound barrier fuel rods are presented along with a similar analysis of a sound CC fuel pin, which also survived a ramp test. During the destructive examination of sound Cu-barrier and Zr-liner segments from previous ramp tests,[1] sections of the rods were slit longitudinally and the fuel was removed to examine the state of the barrier inner surfaces over substantial areas. Color photographs of these "clamshell" sections were taken at ~4× magnification. It was judged, in the case of Cu-barrier specimens, that the coverage and adherence of the copper layer in both SRP and CC rods were very good.

In addition, fuel and fission product deposits replicated pellet interfaces and cracks on the inner surfaces of both Cu-barrier and Zr-liner claddings. Small areas of these clamshell sections were selected and prepared for examination by Scanning Electron Microscopy (SEM). The purpose of the SEM examination, which included X-ray imaging, was to detect and document flaws or defects and to characterize the barrier surfaces as a function of rod nodal power and proximity to pellet interfaces. The samples selected for characterization are described briefly in Table 4.3-9.

Table 4.3-9
SEM SPECIMEN DETAILS

Design Feature	Sample Segment	Identification Section	Axial Location[d] (cm from bottom)	Maximum Nodal Power (kW/m)
Cu-Barrier[a]	SRP-3/15	Plenum[c]	—	—
Cu-Barrier[a]	SRP-3/15	B-5	19.6	44.3
Cu-Barrier[a]	SRP-3/15	B-2	26.2	52.8
Cu-Barrier[a]	SRP-3/15	G	39.1	59.7
Cu-Barrier[a]	SRP-3/14	L-2	74.4	44.9
Cu-Barrier[a]	SRP-3/13	H-2	46.5	58.4
Cu-Barrier[a]	CC-44A	G	26.7	62.7
Zr-Liner[b]	SRP-3/18	Plenum[c]	—	—
Zr-Liner[b]	SRP-3/18	H	41.7	58.1
Zr-Liner[b]	SRP-3/17	M-2	66.0	53.8

[a] SRP Segments: 5 μm electroplated, nonbonded Cu-Barrier; CC-44A: 10 μm electroplated, nonbonded, shot peened Cu-Barrier.
[b] Zr-Liner: 76 μm crystal bar Zr.
[c] Plenum sections selected as control samples.
[d] See Figures 5.3-3, 5.3-25 and 5.3-33 of previous report[1] for relative location of samples.

Experimental Procedures

After identifying areas of interest in macrophotographs of the clamshell sections, 10 mm square sections were cut out of the cladding wall with a dry cut-off wheel. The sections were cleaned only with a gas stream, mounted with silver conducting paint on SEM sample holders, and rephotographed. The selection and preparation steps for a particular sample are shown in Figure 4.3-6.

With the television display (rapidly formed secondary electron images viewed on a television monitor) of the scanning electron microscope the specimen surface was inspected thoroughly for defects and special surface features. A low magnification composite SEM micrograph was taken of those areas containing significant features (Figure 4.3-7). In the present context the term "SEM micrograph" implies a secondary electron image. Representative areas, their location marked on the survey composite, were imaged at appropriate higher magnifications. Since the specimens were highly radioactive (2 to 3 R/h gamma and 17 to 60 R/h beta at contact), the energy dispersive X-ray analyzer could not be used. Qualitative elemental analyses were made by scanning the wavelength dispersive X-ray (WDX) spectrometer through the appropriate diffraction angles. X-ray maps of elements known or found to be present were also taken with the WDX analyzer. Trace elements were recorded with high beam currents and very slow scan rates. Elements present in higher concentrations (*e.g.*, the matrix metal) were recorded with lower beam currents and/or faster scan speed. The absolute density of the (white) X-ray pulse dots on any given X-ray map is, therefore, of little significance, *i.e.*, there is no quantitative relationship among different X-ray maps of a particular area. However, within any one map, the density differences indicate relative concentration differences, and the X-ray images thereby give a good qualitative picture of the spatial distribution of the element in question.

Results

Cu-Barrier

The appearance of the Cu-barrier in the plenum section (Figure 4.3-8) is representative of the as-plated condition. The nodular appearance is typical. Random pores of 1 to 2 μm diameter are visible; in addition, very fine porosity (0.1 to 0.3 μm) is visible at higher magnifications. The nodular appearance of the Cu surface is preserved in fueled sections at locations removed from deposits and fuel pellet imaging effects. A typical example is shown in Figure 4.3-9, which also displays the Cu and U X-ray maps. Note that besides the obvious large fuel particle, there are numerous smaller particles sticking to the Cu-barrier.

The nodular, as-plated appearance of the copper surface can be obscured by deposits and modified by pellet-cladding mechanical interaction effects. An example of the former is shown in Figure 4.3-10. These micrographs were taken at the intersection of the pellet interface and the major longitudinal crack in Figure 4.3-6 (see also Figure 4.3-7). The intersection is marked by an accumulation of small UO_2 particles, which appear to be cemented to the cladding by a glassy layer. This material, which has formed a "mudcrack" pattern of hairline cracks on cooling, is sufficiently thick not only to obscure the appearance of the copper surface, but to prevent excitation of the Cu characteristic radiation from the underlying barrier layer (Figure 4.3-11). Figure 4.3-12 illustrates that this material is rich in Cs and I with only traces of Te. The relatively small amount of Te is a general observation in these Cu-barrier samples and its distribution does not generally match that of I. The Te is usually associated with some Cs. An interesting feature is the apparent handling scratch in the upper right quadrant of Figure 4.3-10a (see also Figure 4.3-7). By referring to Figures 4.3-11 and 4.3-12, it can be seen that the scratch has smeared, but not removed, the material which is rich in Cs and I. A similar observation was made on the CC-44A sample.

The region of the apparent second pellet interface visible in Figure 4.3-6 has a clean Cu surface with only a small amount of Cs deposited rather uniformly. However, the bumpy Cu surface appears to have been smeared or flattened (Figure 4.3-13), apparently by hard mechanical interaction with the fuel. A demarcation line between smeared and bumpy Cu in another sample is shown in Figure 4.3-14; the Cu X-ray map shows that the smearing effect is quite superficial, *i.e.*, the Cu layer has not been penetrated. This is consistent with the results of fuel loading tests performed on as-plated Cu-barrier tubes. The barrier is remarkably resistant to loading damage.

An apparent defect in the Cu layer was observed in only one (SRP-3/15, B-2) of the seven SEM samples. A small break is shown in Figure 4.3-15. The depth of penetration of this feature was not ascertained. The Cu X-ray map in the vicinity of the break (Figure 4.3-16) appears continuous, except for UO_2 overlays. The Zr X-ray map of the same area does not definitively show if the break in the barrier penetrates down to the base metal. There is a concentration of Zr in the vicinity, but it has more the appearance of an accumulation of small particles, possibly cutting debris, than exposed cladding. Zr X-ray maps of other areas were somewhat similar, *i.e.*, a random distribution of one or two small Zr particles. No evidence was noted of a Zr-rich area that could be interpreted as exposed cladding surface.

In general the heaviest deposits occurred at the highest nodal powers, but there was also an indication that the nature of the deposited material changed as a function of power. Figure 4.3-17 shows a heavy pellet interface deposit on the highest rated sample, CC-44A(a). Corresponding X-ray maps are presented in Figures 4.3-18 and 4.3-19. Note the rough correspondence of the distributions of U and Cs (remembering that the relative intensities of two X-ray maps are not a measure of the relative concentrations of the respective elements). The heavy deposit appears to be both Cs- and U-rich and to cover another material, which is rich in Cs and I. Contrast this deposit with a pellet interface deposit on the SRP-3/15 (B-5) sample (Figure 4.3-20). Here the X-ray maps (Figure 4.3-21) of the Cs and U distributions do not correspond. The U-rich particles are clearly UO_2 fuel particles either embedded in the Cu layer or cemented to it by the Cs-rich material. These UO_2 particles are faceted and crystalline in appearance in contrast to the material shown in Figure 4.3-17, which looks and analyzes differently. The latter may be a co-deposit of Cs and U oxides or a ternary compound. Alternatively, it may be a large particle of UO_2 in the process of being consumed by vapor deposited Cs_2O, as suggested by Cubicciotti and Sanecki[12] to explain UO_2 bonding to Zircaloy.

There is a partial correspondence in Figures 4.3-18 and 19 between the distributions of I and Cu, which may argue for the formation of CuI. Note, however, that these regions are also Cs-rich and a more probable explanation of the X-ray maps is a thin layer of CsI (probably with excess Cs) deposited on the Cu followed by a thick overlayer of Cs, U compounds. Note also the noncorrespondence of the Te and I distributions.

Zr-Liner

The superficial appearance of the Zr-liner in the sample from the plenum section of SRP-3/18 is shown in Figure 4.3-22. The wavy longitudinal grooves are a normal feature of pickled Zr-lined tubing. The grooves are shallow and well-rounded. The grooves are still visible in fueled samples (Figure 4.3-23), but are partially obscured by surface oxidation and fuel debris. There are UO_2 particles in the grooves, which are probably identical with the "indents" described in the metallographic report on the Zr-liner rods.[1]

Fuel and fission product deposits further obscure the Zr-liner surface features at pellet interface locations (Figures 4.3-24 and 4.3-25). It is of interest to note that the fission product phase here is rich in Cs and Te with only traces of I, in contrast to the Cu-barrier samples, where there appeared to be more I than Te. There have been too few observations on Zr-liner samples to say that this observation is a general one, but, if this apparent difference between Cu-barrier and Zr-liner samples were confirmed, it might imply that the Cu-barrier exerted some chemical influence on the internal fuel rod environment.

SEM Results Summary

In terms of the objectives of this phase of the post-irradiation examination:

1. The Cu-barrier appeared to be smeared or flattened, but not breached, by hard interaction with the fuel pellets.

2. One small break in the Cu layer was observed and documented. It was not in an area where the Cu surface had been deformed by interaction with the fuel and it was not in an area of heavy deposits.

3. The surface appearance of the Zr-liner was somewhat modified by oxidation and by accumulations of fuel debris, but as-fabricated features were still recognizable and there was no evidence of in-service defects.

4. Besides obvious large particles of bonded or embedded fuel, the surfaces of both kinds of cladding were covered with numerous small particles.

5. Fuel and fission product deposits were much heavier at fuel crack and pellet interface locations, usually obscuring the underlying material. In general the heavier deposits were observed at the higher powers.

6. The fission products in the Cu-barrier samples are distributed as follows:

    a. Cesium is found everywhere. However, generally more Cs is present near bonded UO_2 than on the bare Cu surface and Cs is concentrated at pellet interfaces and cracks.

    b. Iodine is noted almost exclusively at pellet interfaces and cracks.

    c. Very little Te was found. The Te distribution does not correspond to the I distribution.

7. The fission products in the Zr-liner samples are distributed as follows:

    a. Cesium and Te are found in conjunction, mostly at cracks and pellet interfaces.

    b. Iodine was noted only in a few isolated particles.

4.3.3.6 Fission Gas Release Measurements

The fission gas contents from seven SRP segments, which survived ramp testing in GETR have been measured and evaluated These segments were irradiated in the SRP-3 bundle (Millstone) at peak powers of less than 22.0 kW/m (6 7 kW/ft) to exposures in the range of 5 to 10 MWd/kg-U prior to ramping to a peak power level of 59.1 kW/m (18 kW ft). The accuracy of the power monitoring system has been shown to be ±10%, but one early segment, SRP-3/2, was overpowered due to a deficiency in the irradiation capsule design.[2]

The results are presented in Table 4 3-10. Release fractions ranged from 11 5 to 18.7% for those segments tested after correction of the capsule design problem. The differences are generally due to differences in actual peak power values within the range of accuracy of the power monitoring system.

The peak power values were also calculated from grain growth data obtained from fuel sections. The inferred peak power values are sensitive to small differences in the assumed temperatures and measured radii of columnar and equiaxed grain growth, but are generally within the spread of power measurement accuracy. As expected, fission gas release fraction correlates well with grain growth radii.

Table 4.3-10
SUMMARY OF FISSION GAS RELEASE FOR SRP-3 RODS RAMP TESTED IN GETR

Segment Identification	Burnup[a] (MWd/kg-U)	Peak[b] Power (kW/m)	Time at Peak Power (h)	Total Xe+Kr Released (cm³ at STP)	Fission Gas (Xe+Kr) Release Fraction	UO_2 Grain Growth in Peak Power Region[c] r_c/r_o	r/r_o
SRP-3/2	4 83	62 0[d]	24	22.5	0.254	0.66[e]	0.74[e]
SRP-3/13	9 15	59 1	24	28.6	0.170	0 48	0.62
SRP-3/14	10.81	59.1	6	37.2	0.187	0.52	0.65
SRP-3/15	10 53	59.7	24	30.2	0.157	0.37	0.57
SRP-3/17	8 95	59.1	6	18.9	0.115	0	0.45
SRP-3/18	11 18	59.1	24	34.5	0.168	0.44	0.60
SRP-3/19	10.16	59.4	6	33.6	0.180	0.50	0.63

[a] Burnup is based on Nd measurement and preGETR gross gamma scan profile
[b] Power values are from Rod Power Monitoring System (RPMS) (accuracy ±10%)
[c] r_c = radius of columnar grain growth in peak power region
r = radius of equiaxed grain growth in peak power region
r_o = radius of pellets before irradiation
[d] Nominal value Segment overpowered [2]
[e] No metallographic sample was taken at peak power location This data was obtained by extrapolating three other data points from the same rod

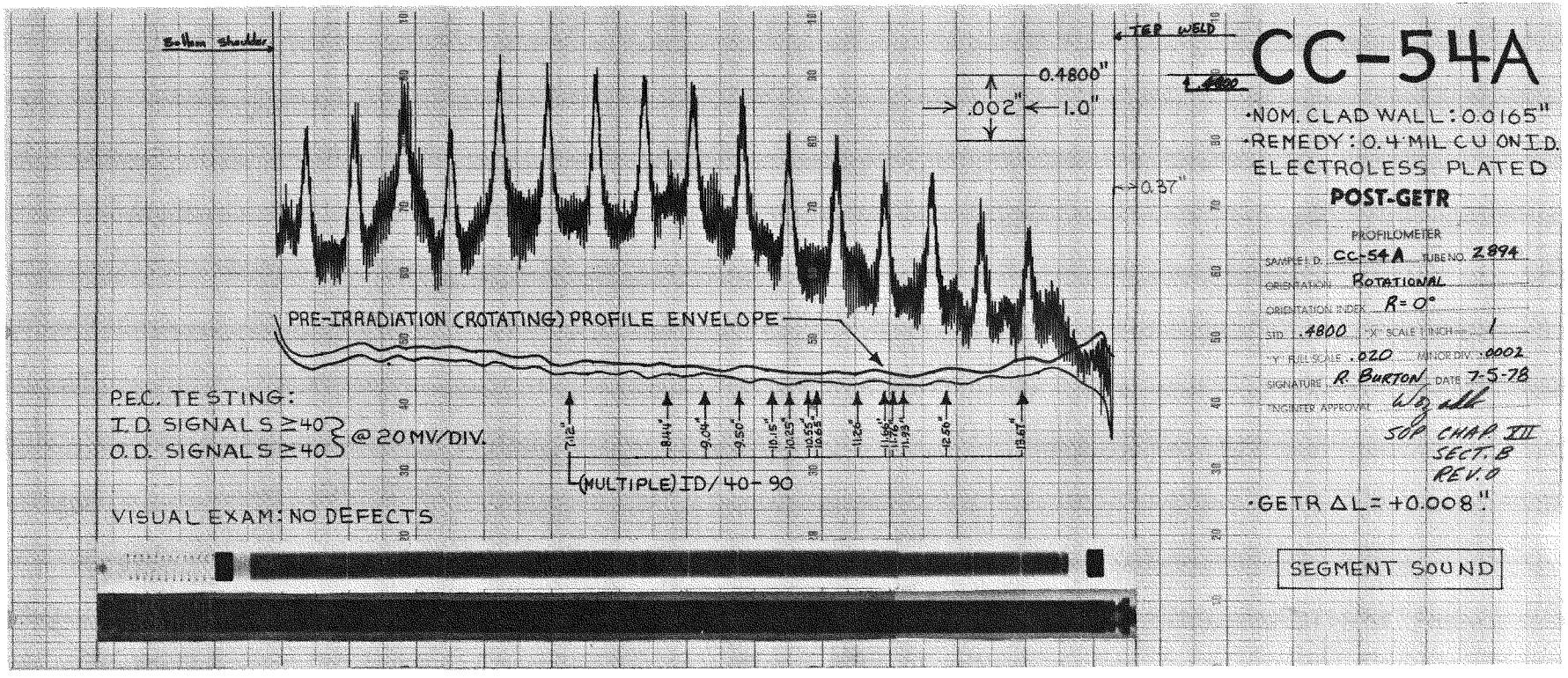

Figure 4.3-1. Nondestructive Test Summary – Sound Electroless Cu-Barrier Rod CC-54A

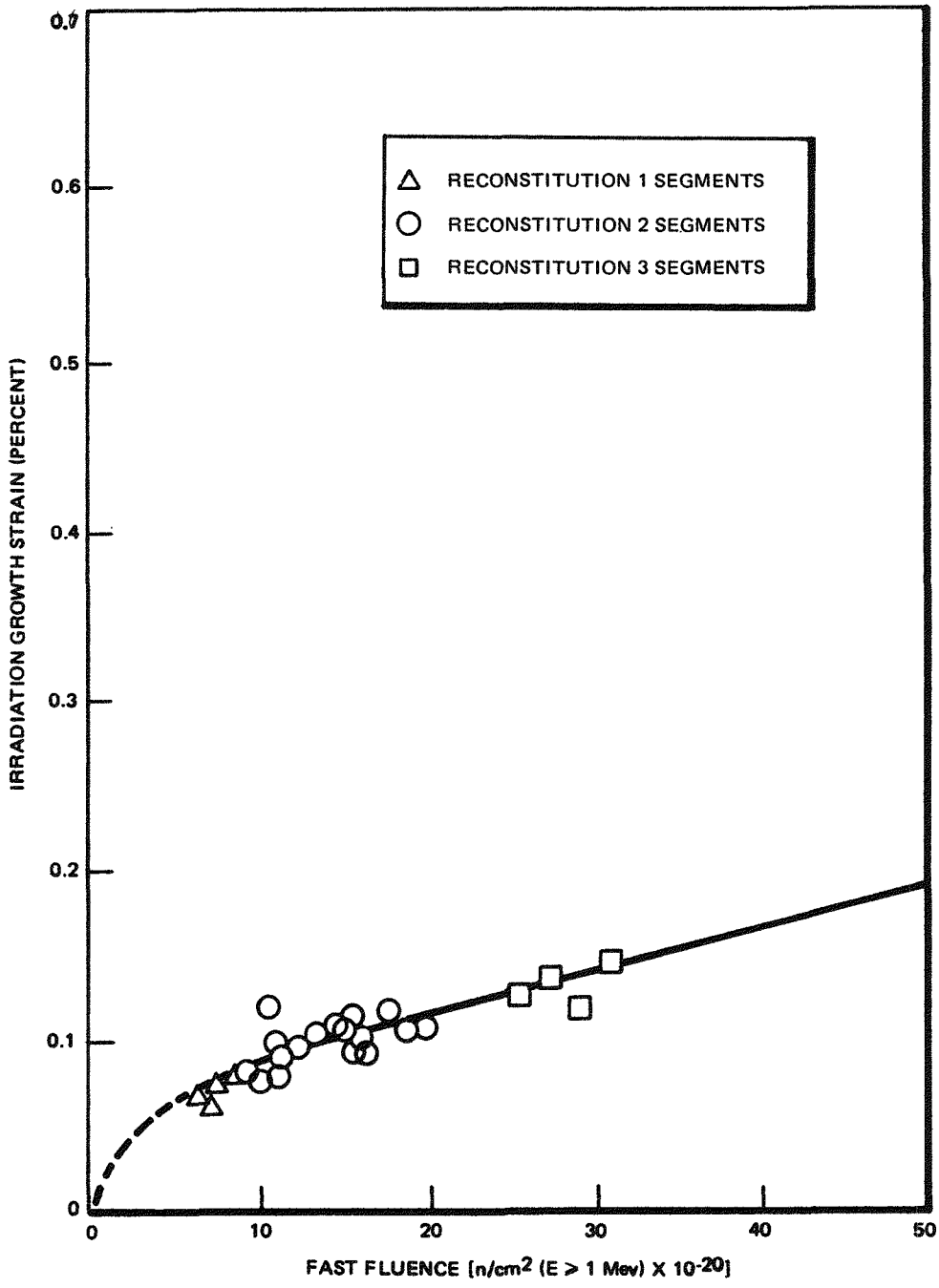

Figure 4.3-2. Irradiation Growth of SRP-3 Fuel Rod Segments

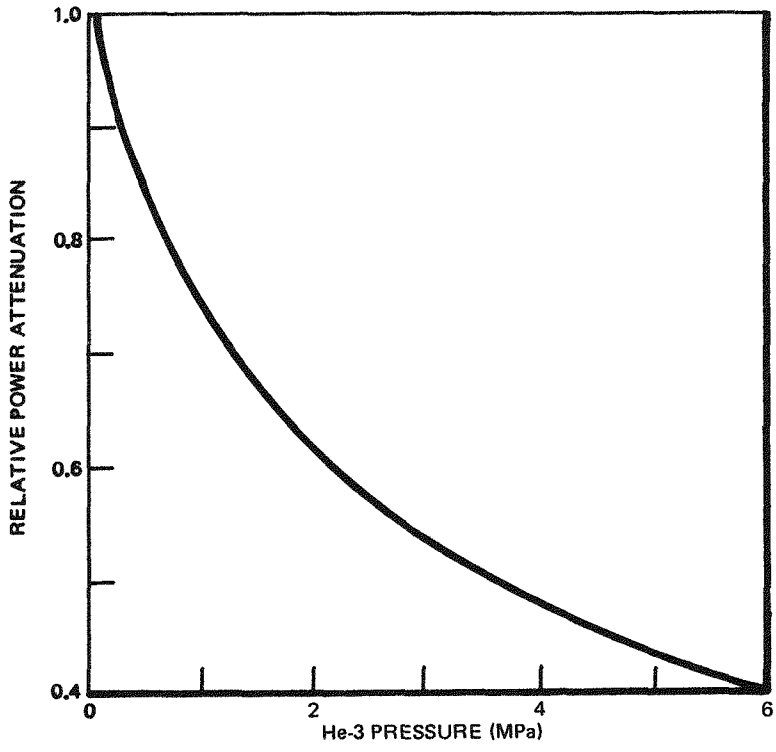

Figure 4.3-3. Relative Power Attenuation Versus ^{3}He Pressure (for ~2.6% ^{235}U Enriched Fuel Rod)

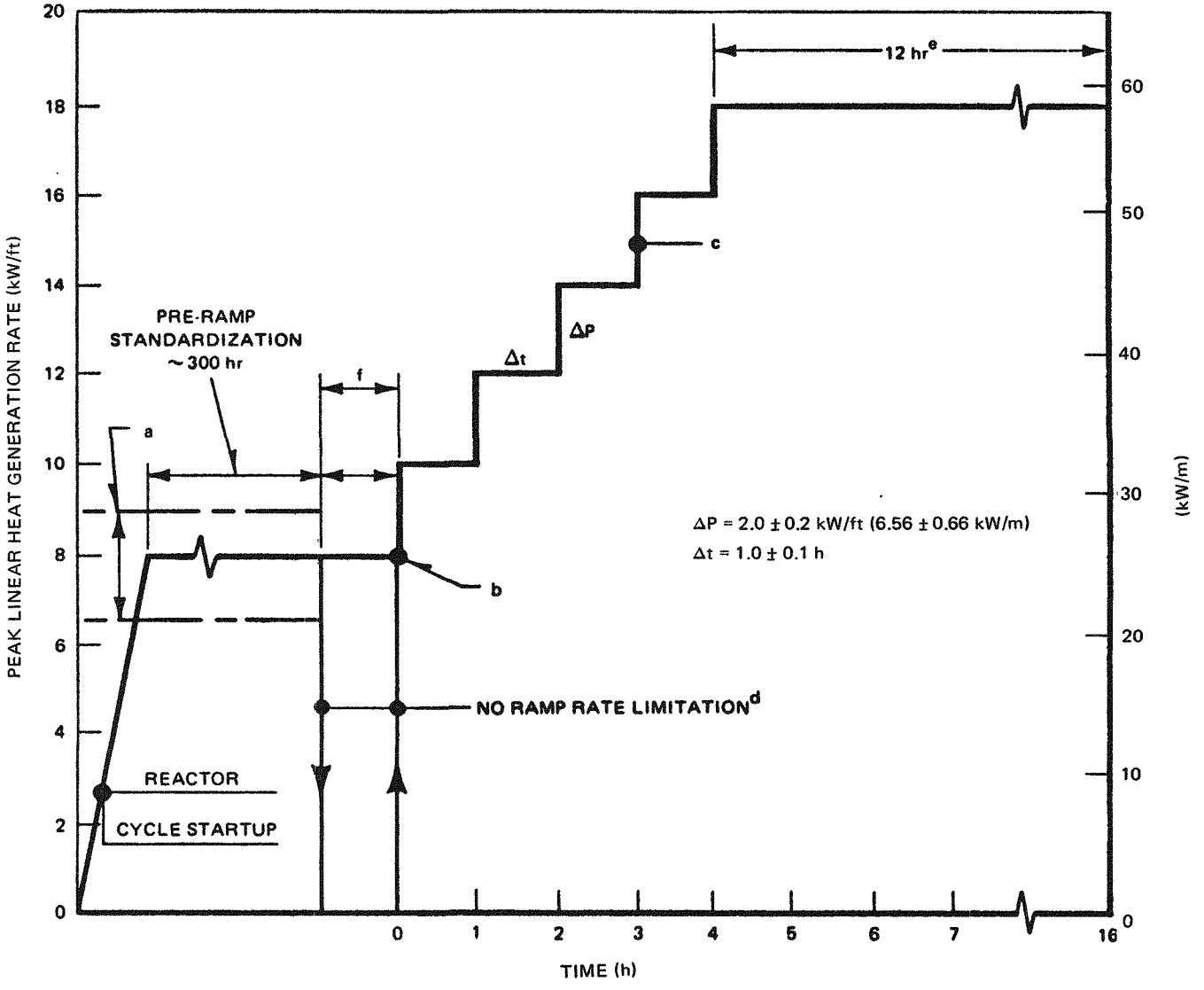

a. PEAK POWER DURING STANDARDIZATION, 21.3 to 29.5 kW/m

b. INITIAL PEAK POWER FOR RAMP TEST TO BE THE SAME (WITHIN ± 1.6 kW/m) AS DURING STANDARDIZATION FOR EACH INDIVIDUAL ROD

c. ALL UP-RAMPS DURING RAMP TEST AT A RATE OF ~ 6.6 kW · m^{-1} · min^{-1}

d. NO RATE RESTRICTIONS ON DOWN RAMPS OR POWER INCREASE RATES DURING INSERTION OF ROD FOR RAMP TESTING

e. MAXIMUM PEAK POWER 59.1 ± 3.3 kW/m. DO NOT FINE-TUNE DURING HOLD PERIOD

f. PRE-RAMP STANDARDIZATION CAN BE PERFORMED SIMULTANEOUSLY ON FOUR RODS DURING THREE CONSECUTIVE REACTOR CYCLES. UP TO 6 WEEKS' PAUSE BETWEEN THE END OF THE STANDARDIZATION PHASE AND RAMP TEST IS PERMISSIBLE

NOTES:

OPERATIONAL FAILURE DETECTION SYSTEM REQUIRED

POWER DEFINITION/CONTROL BY RELIABLE ROD POWER MONITORING INSTRUMENTATION

A FEW SHORT TERM POWER REDUCTIONS DURING THE PRE-RAMP STANDARDIZATION PHASE ARE ACCEPTABLE

Figure 4.3-4. Specified Ramp Test Sequence for Tests at the R-2 Test Reactor

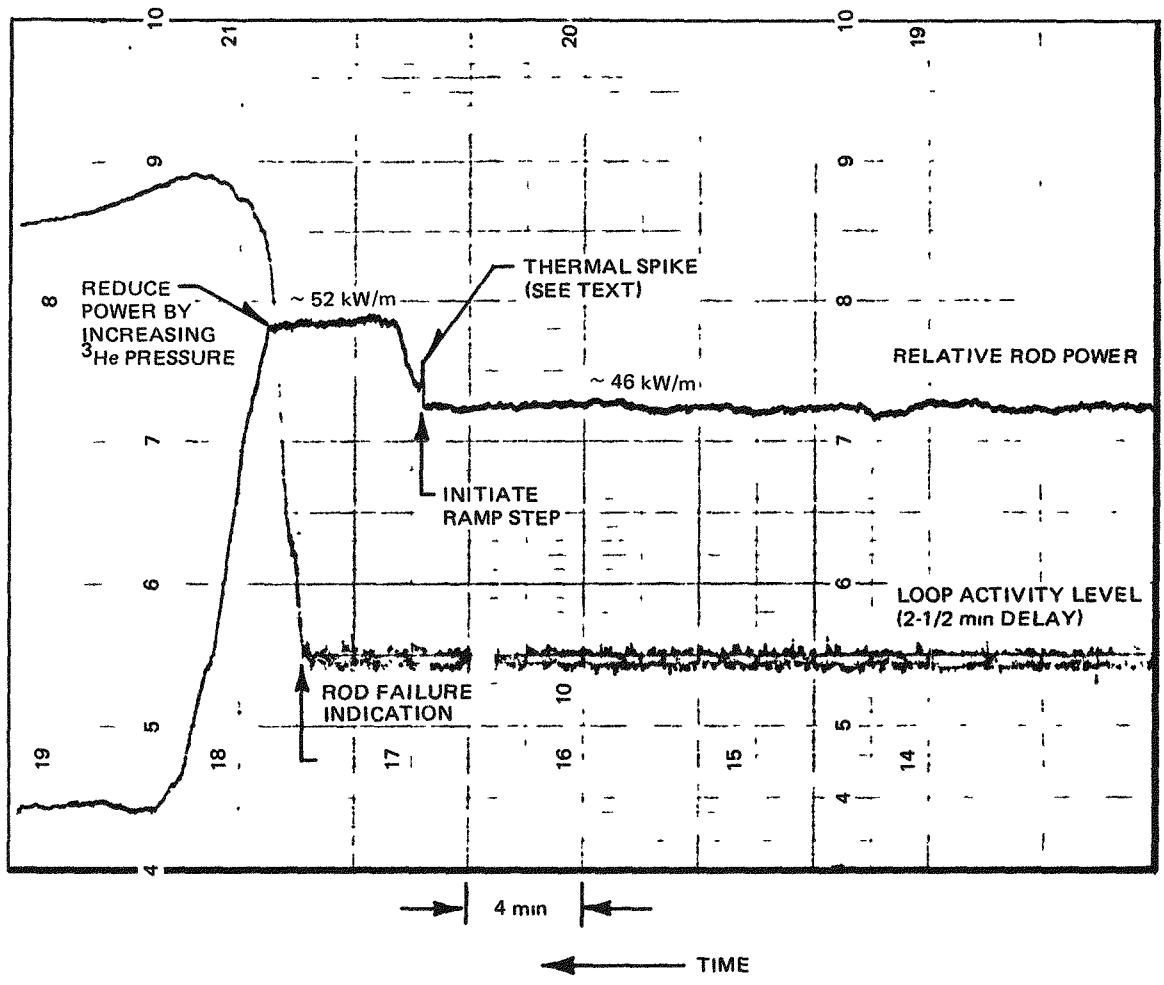

Figure 4.3-5. Recorder Chart Output of Relative Rod Power and Loop Activity Level Indicating Failure of SRP-2/13

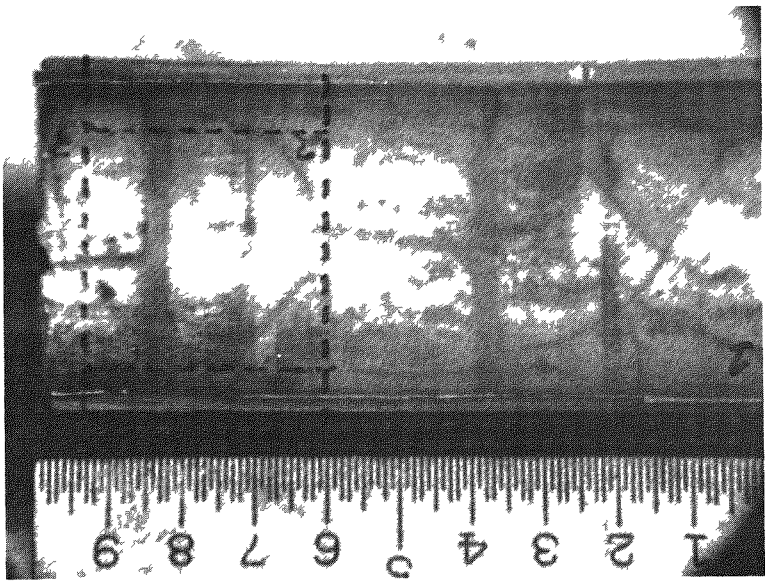

79169 (a) CLAMSHELL SECTION

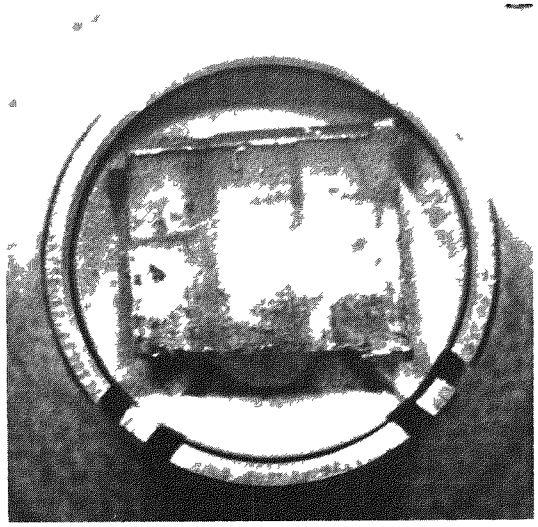

79177 (c) SEM SAMPLE

TOP ◄——————————————————► BOTTOM

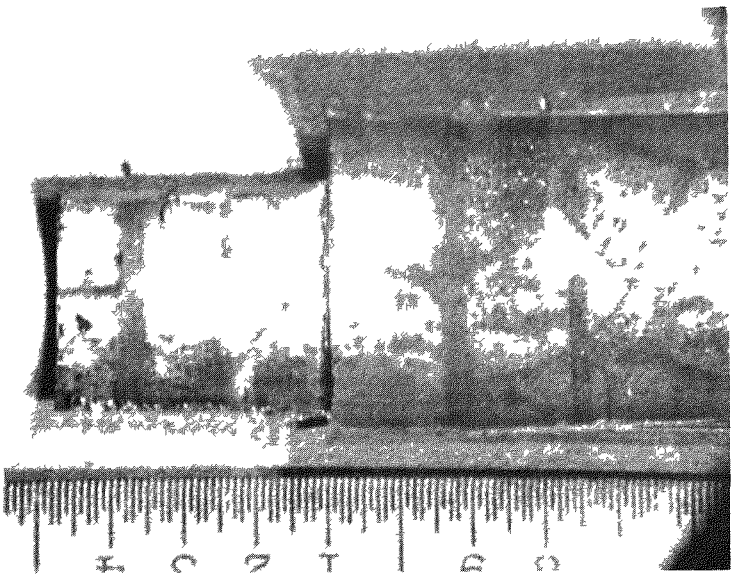

79173 (b) SEM SAMPLE CUTOUT

Figure 4 3-6 Preparation of SEM Sample (SRP-3/14, L-2)

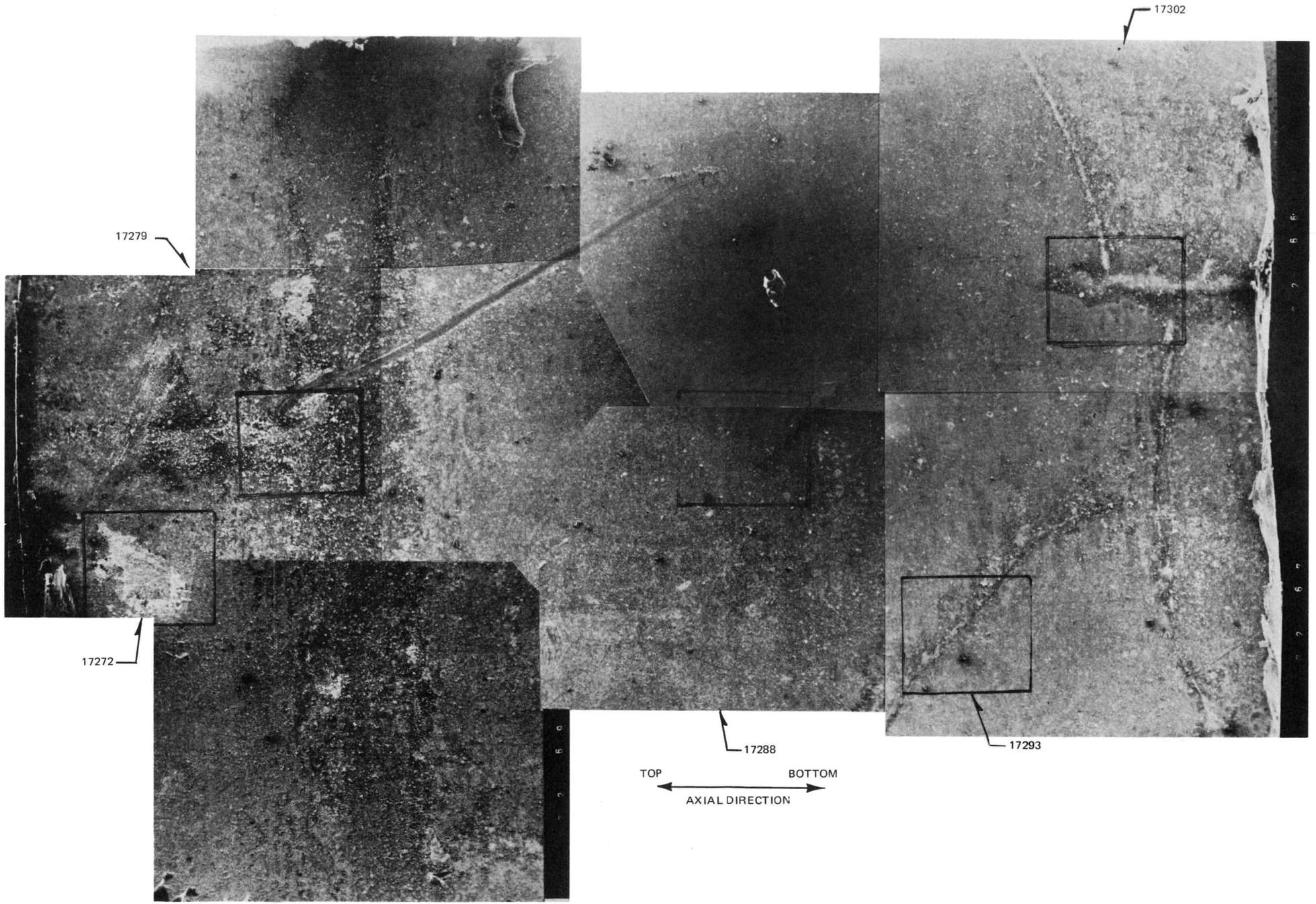

Figure 4.3-7. Low Magnification (~30X) Composite SEM Micrograph (secondary electron image), (SRP-3/14, L-2) Showing Areas for More Detailed Study

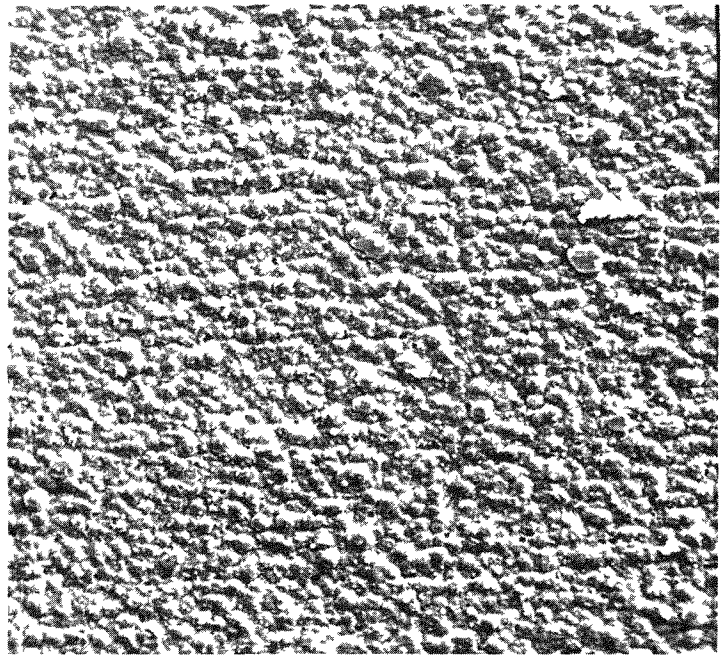

17517

(a) 300X

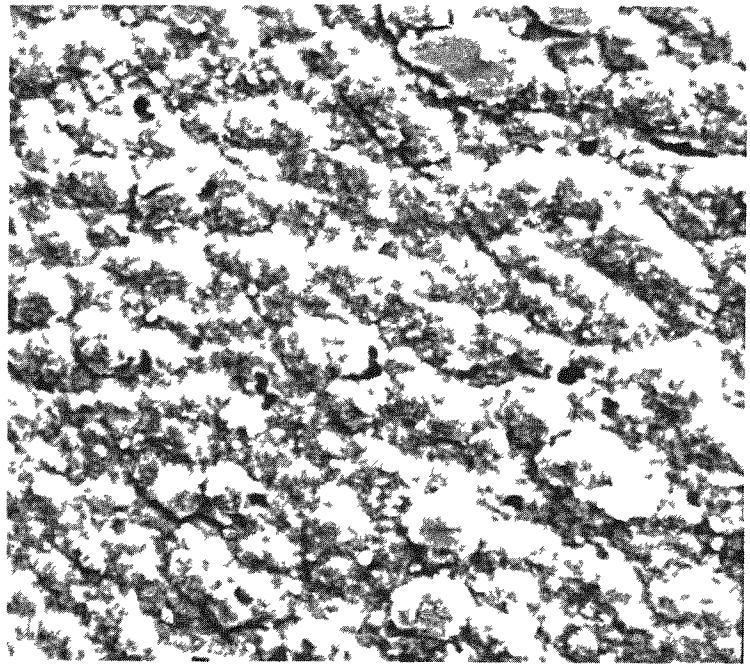

17518

(b) 1000X

Figure 4 3-8 SEM Micrographs (secondary electron images) of Cu-Barrier in Plenum Section (SRP-3/15)

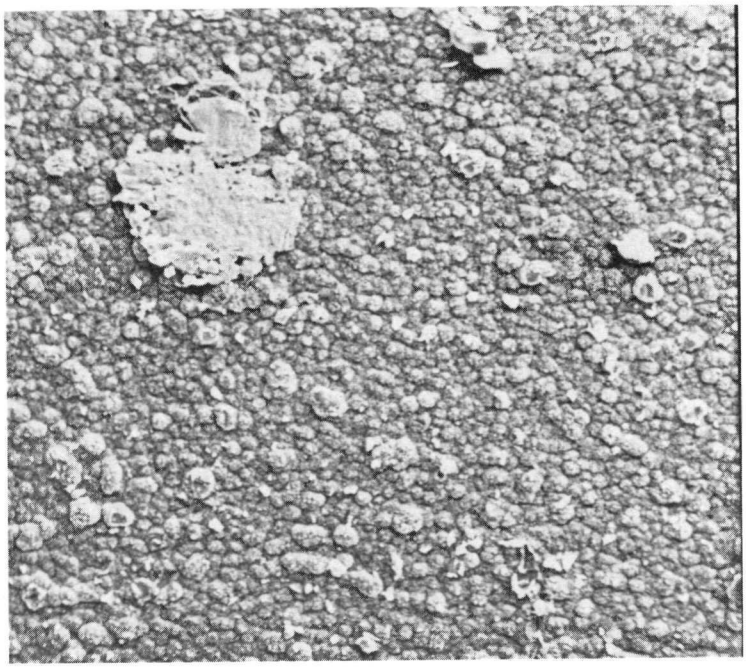

16925 (a) SECONDARY ELECTRON IMAGE (300X)

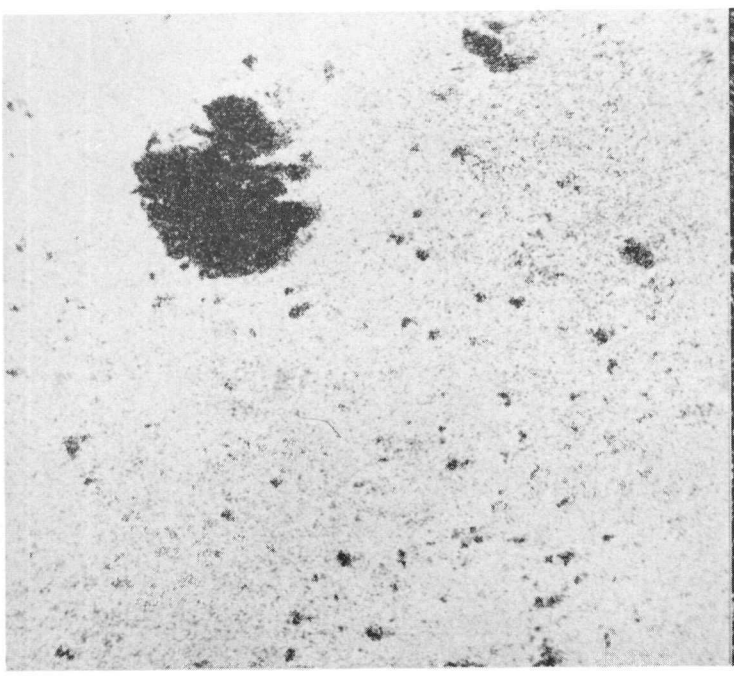

16928 (b) Cu Kα X-RAY MAP

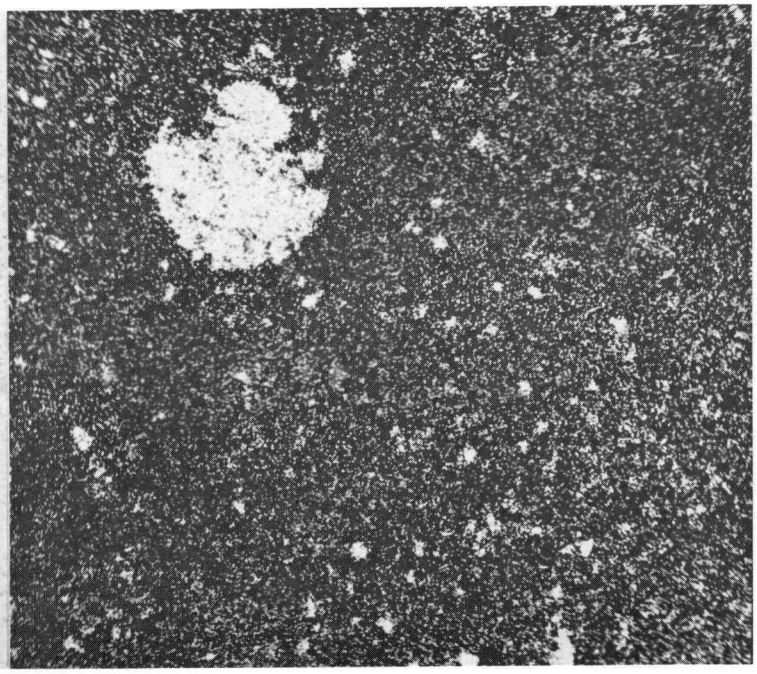

16929 (c) U M_β X-RAY MAP

Figure 4.3-9. Cu-Barrier in Fueled Section (SRP-3/15, B-5)

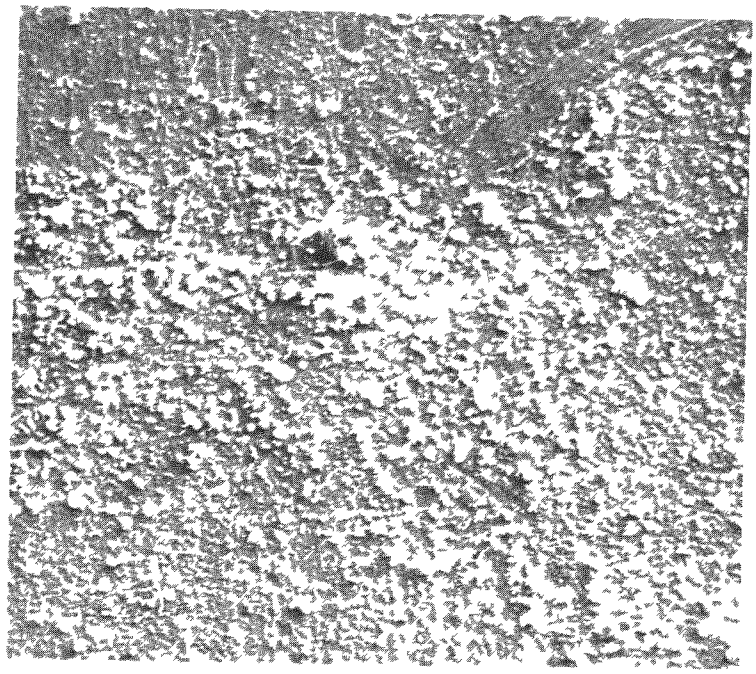

17279

(a) 100X

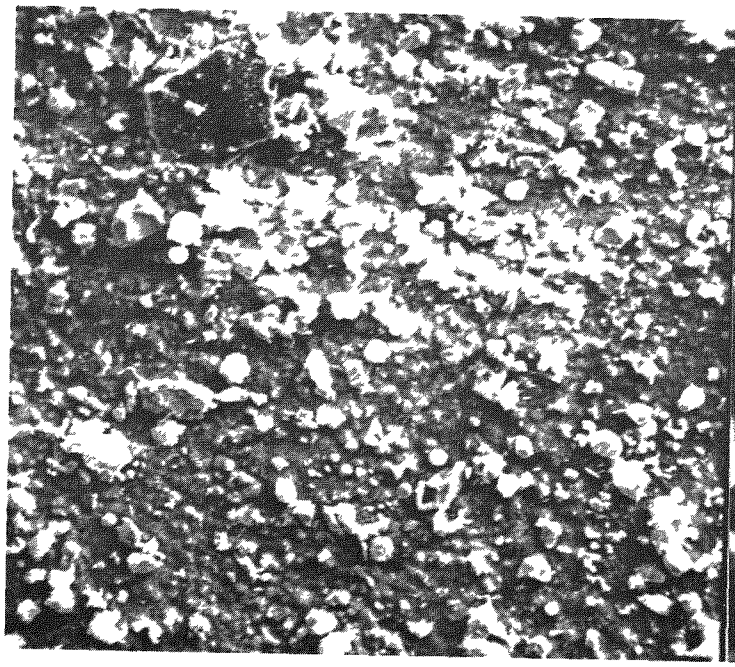

17280

(b) 300X

17281

(c) 1000X

Figure 4 3-10 SEM Micrograph Fuel and Fission Product Deposits on Cu-Barrier at Pellet Interface Location (SRP-3/14, L-2)

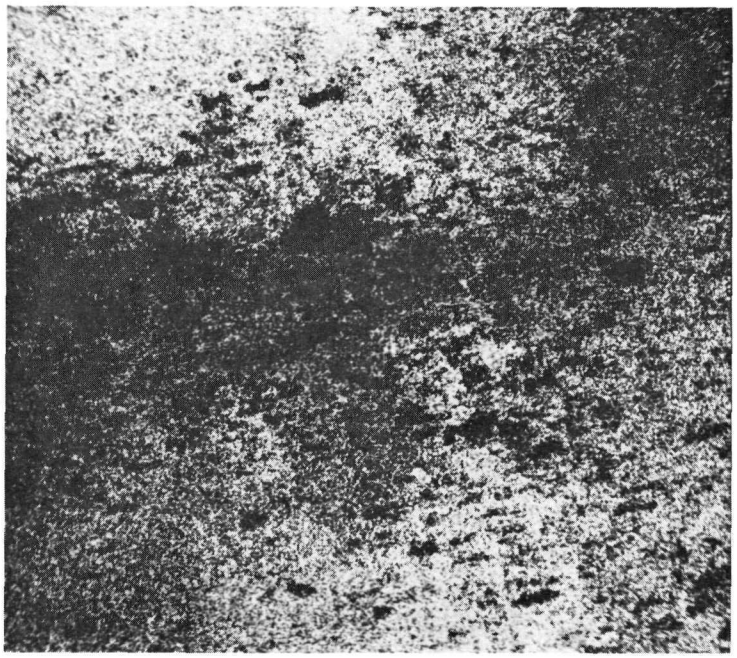

17285

(a) Cu K_{α}, 100X

17286

(b) U M_{β}, 100X

Figure 4.3-11. X-ray Maps of Area Shown in Figure 4.3-10(a)

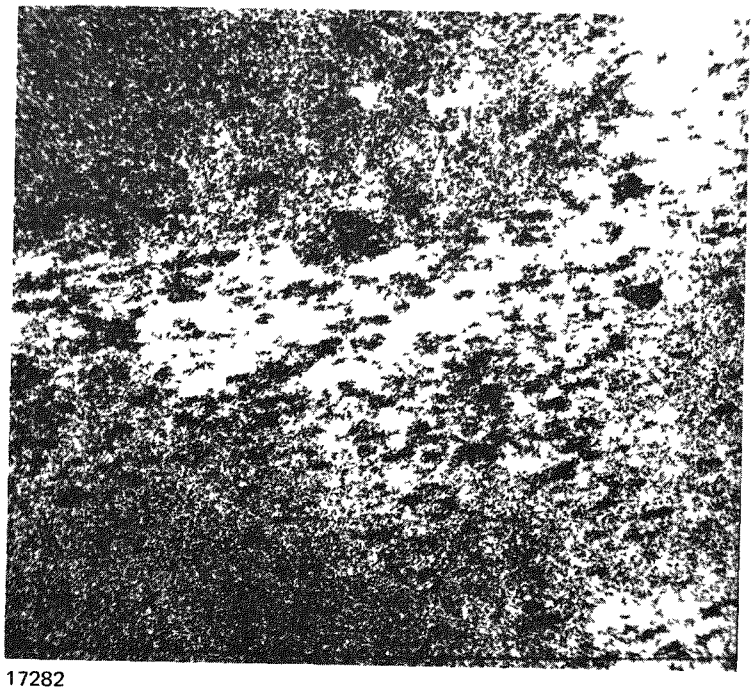

17282

(a) Cs L_α, 100X

17283

(b) I L_α 100X

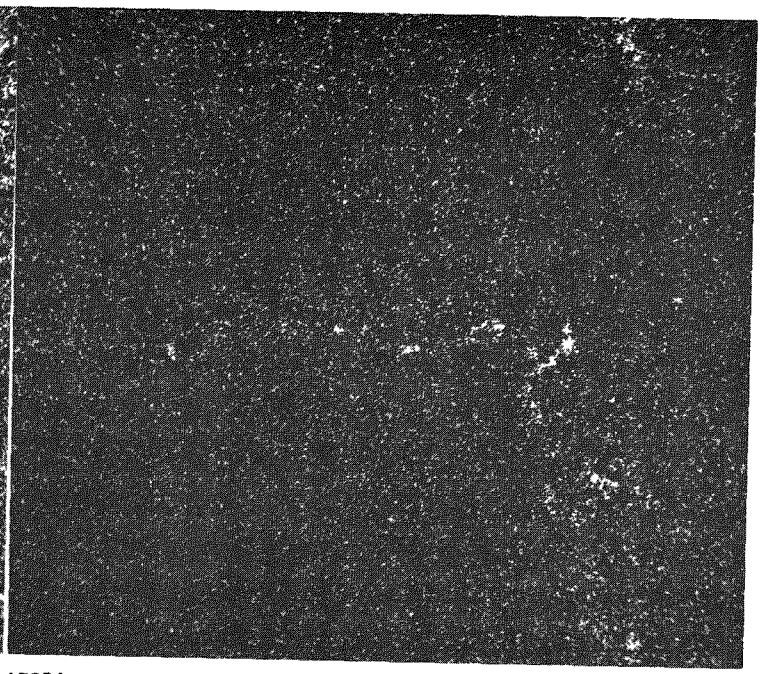

17284

(c) Te L_α 100X

Figure 4 3-12 Fission Product X-ray Maps of Area Shown in Figure 4 3-10(a)

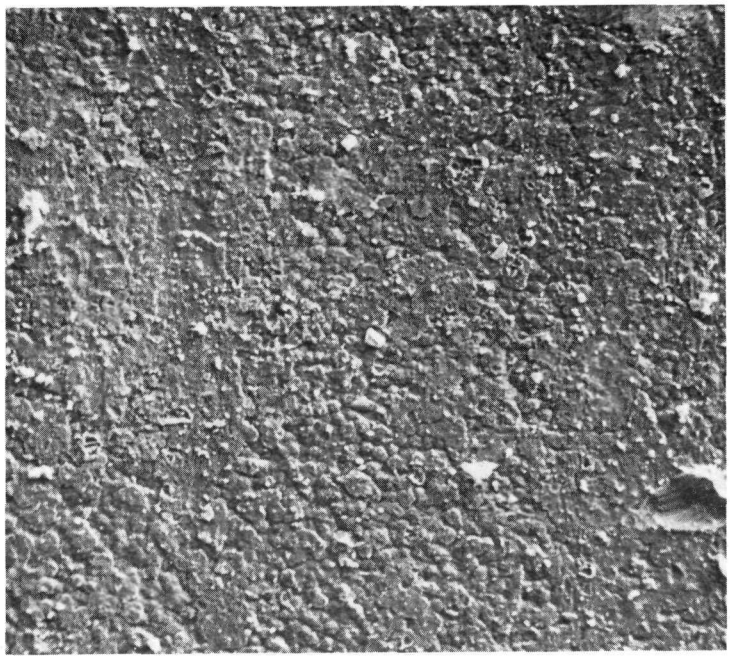

17289

(a) 300X

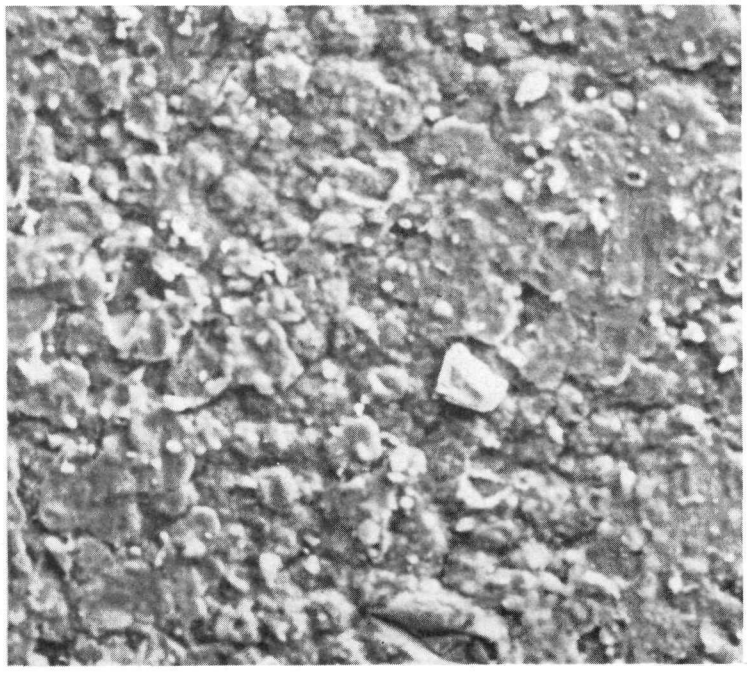

17290

(b) 1000X

Figure 4.3-13. Cu-Barrier Surface Apparently Smeared or Flattened by Hard Interaction with Fuel Pellet (SRP-3/14, L-2)

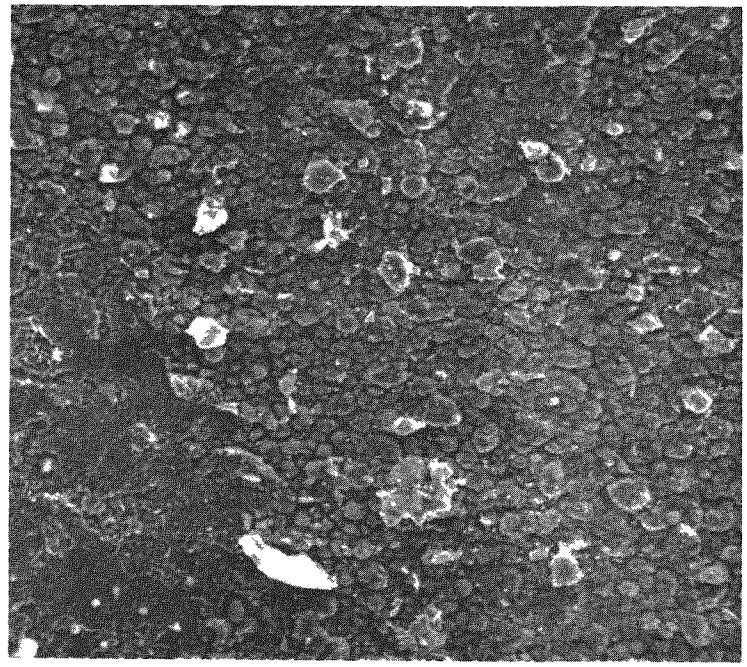

16439

(a) SECONDARY ELECTRON IMAGE (300X)

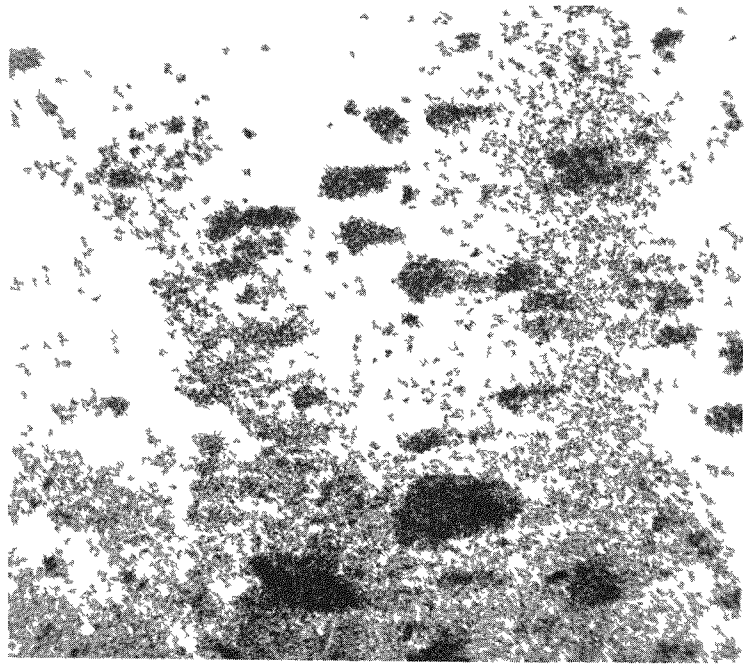

16441

(b) Cu K_α X RAY MAP

Figure 4 3-14 Cu-Barrier Surface in Fueled Section Showing Flattened Area (SRP-3/15, G-2)

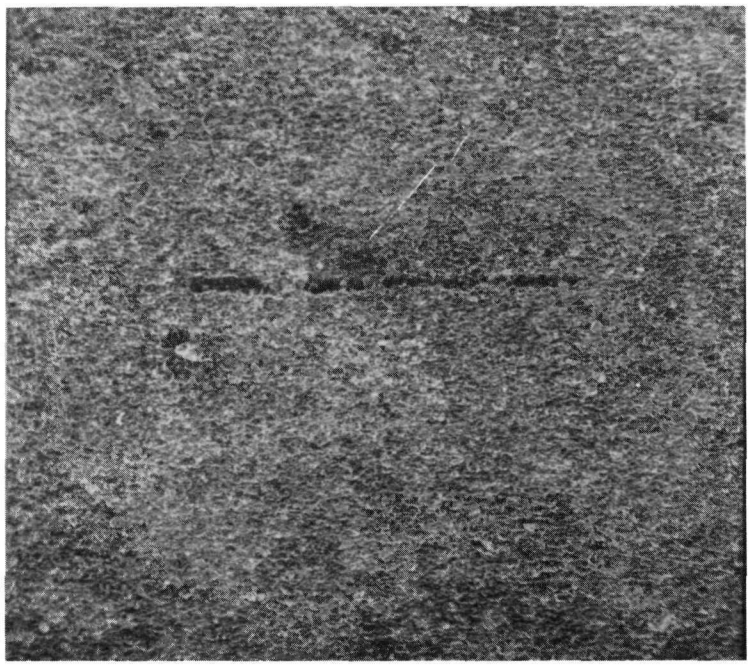

16789

(a) 100X

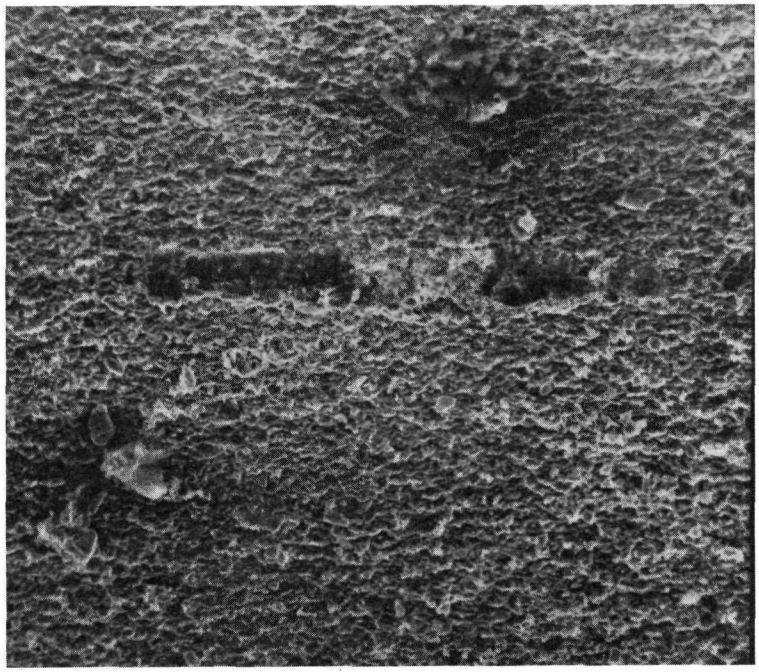

16790

(b) 300X

Figure 4.3-15. Break in Cu Layer (SRP-3/15, B-2) (Secondary Electron Image).

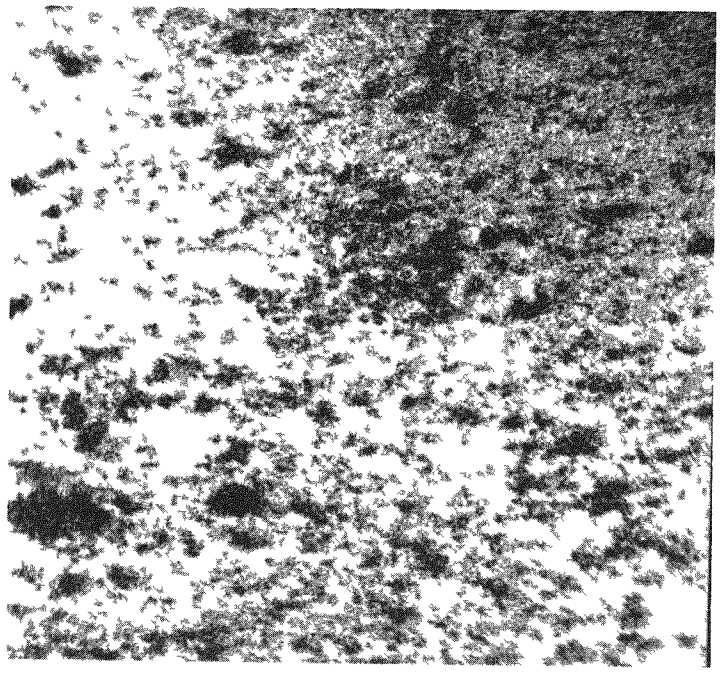

16964

(a) Cu K_α 300X

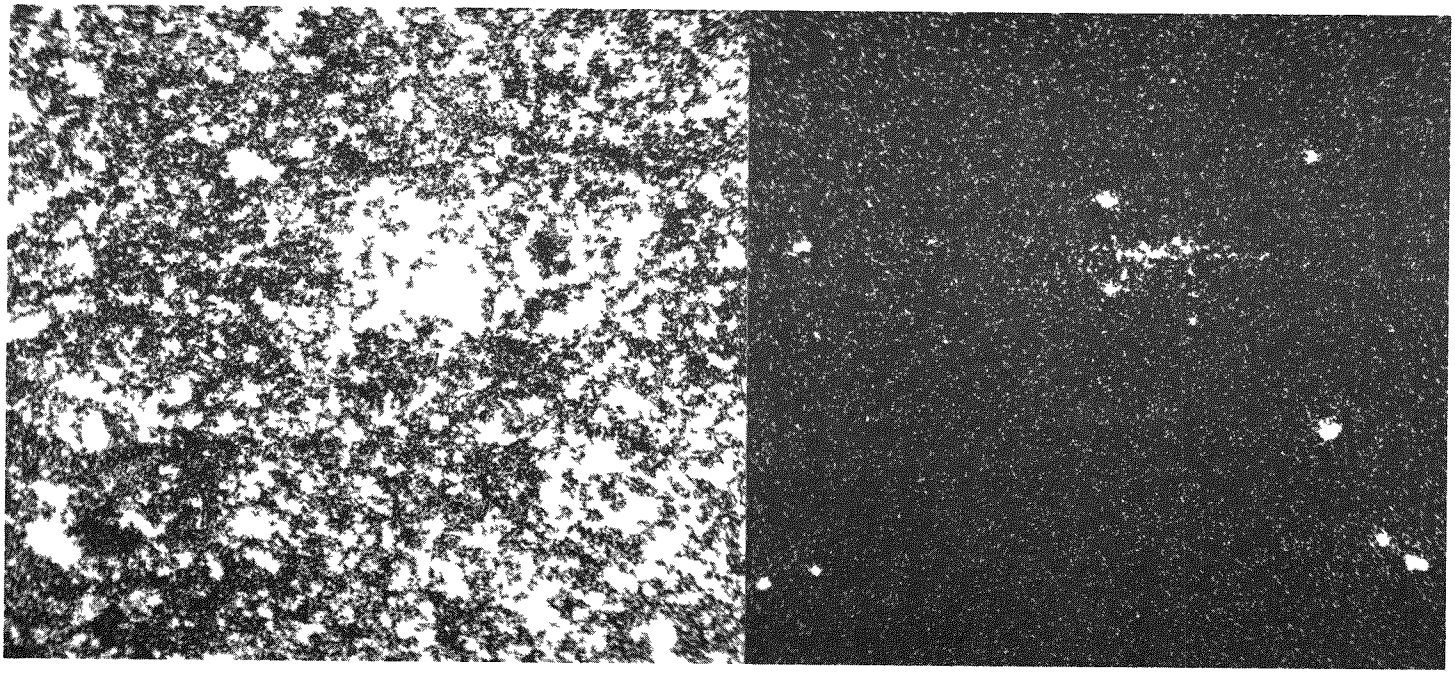

16962

(b) U M_β 300X

16963

(c) Zr L_α 300X

Figure 4 3-16 X-ray Maps of Area Shown in Figure 4 3-15(b)

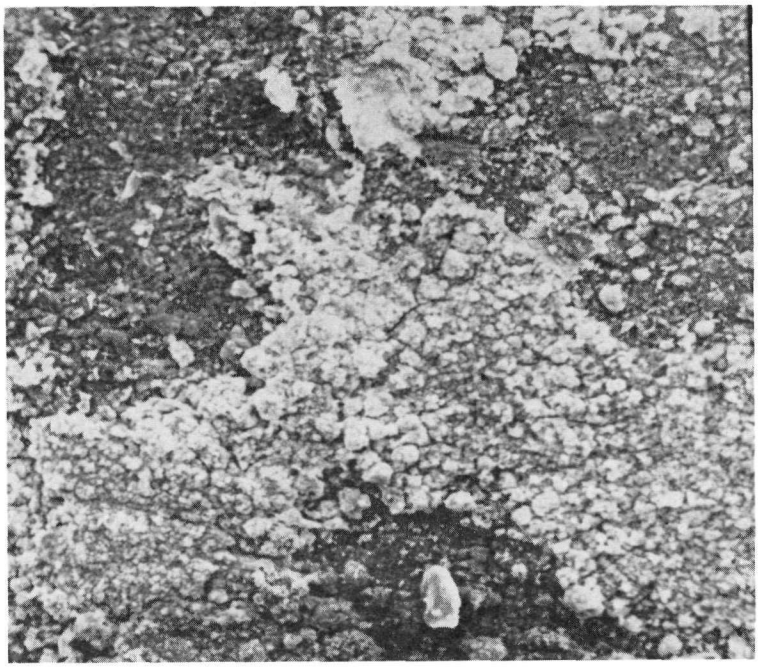

16558 (a) 300x

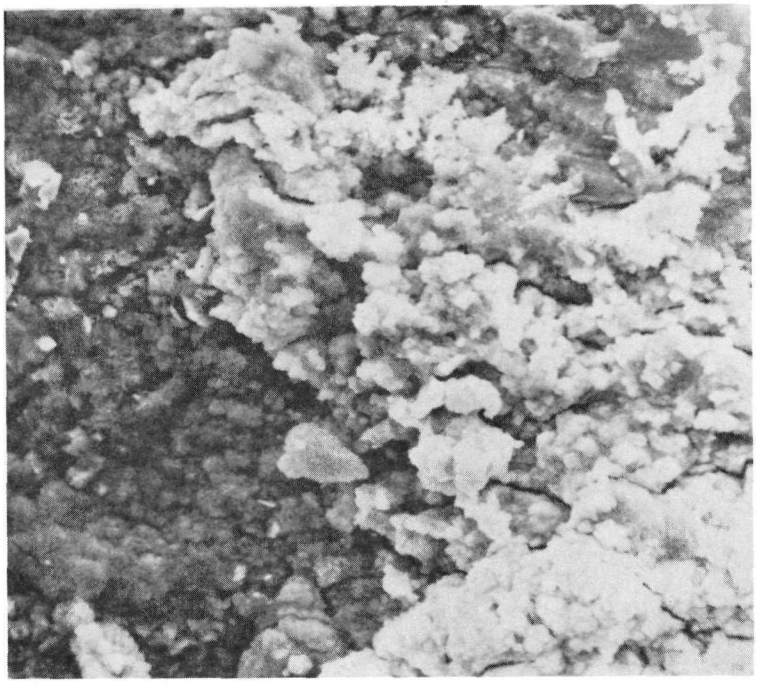

16559 (b) 1000X

Figure 4.3-17. Heavy Deposits on Cu-Barrier Surface at Pellet Interface Location (CC-44A, G)

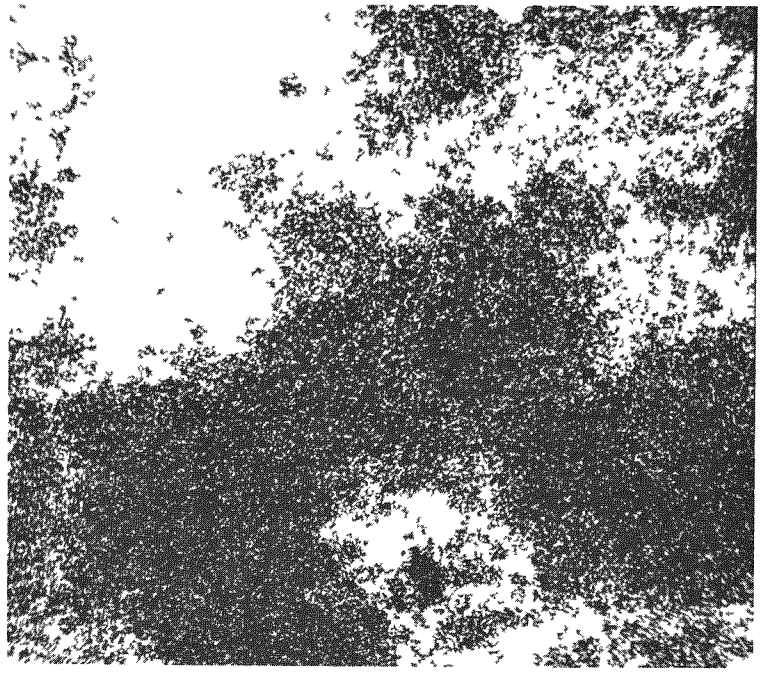

16561

(a) Cu Kα (300X)

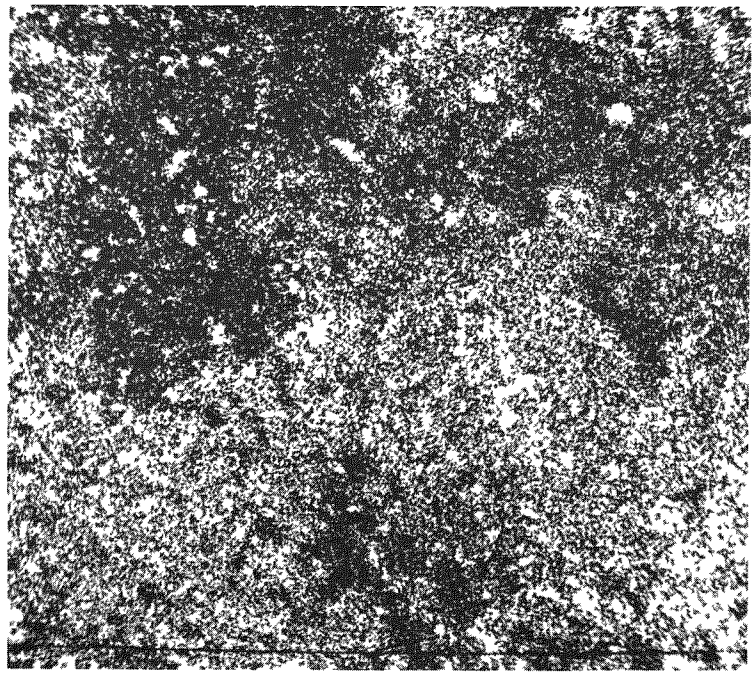

16560

(b) U M$_\beta$ (300X)

Figure 4 3-18 X-ray Maps of Area Shown in Figure 4 3-17(a)

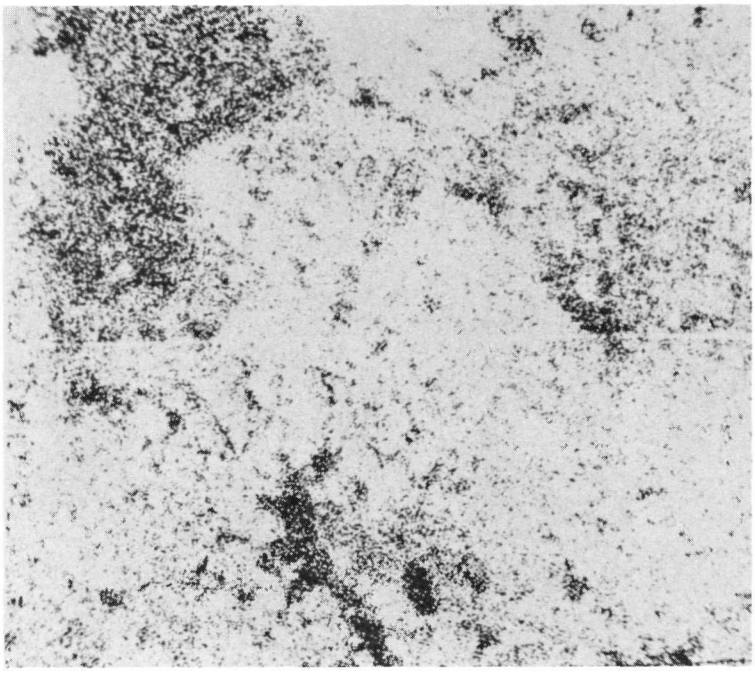

16562

(a) Cs L_α (300X)

16563

(b) I L_α (300X)

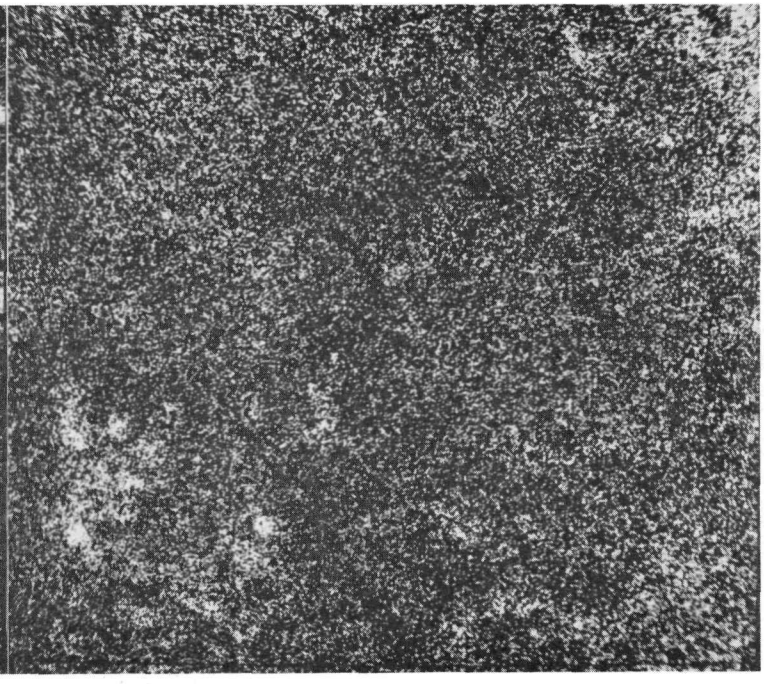

16564

(c) Te L_α (300X)

Figure 4.3-19. Fission Product X-ray Maps of Area Shown in Figure 4.3-17(a)

16822

(a) SECONDARY ELECTRON IMAGE (300X)

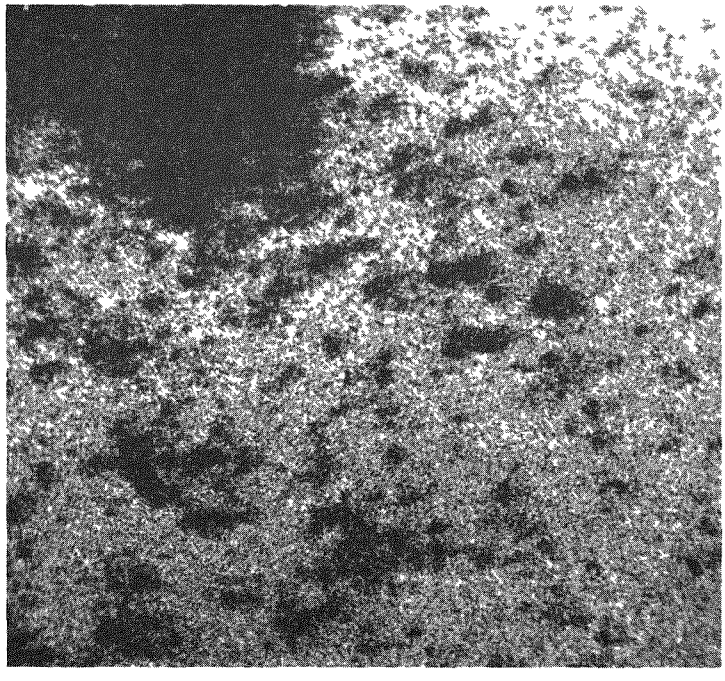

16823

(b) Cu K_α X-RAY MAP (300X)

Figure 4 3-20 Deposit on Cu-Barrier Surface at Pellet Interface Location (SRP-3/15, B-5)

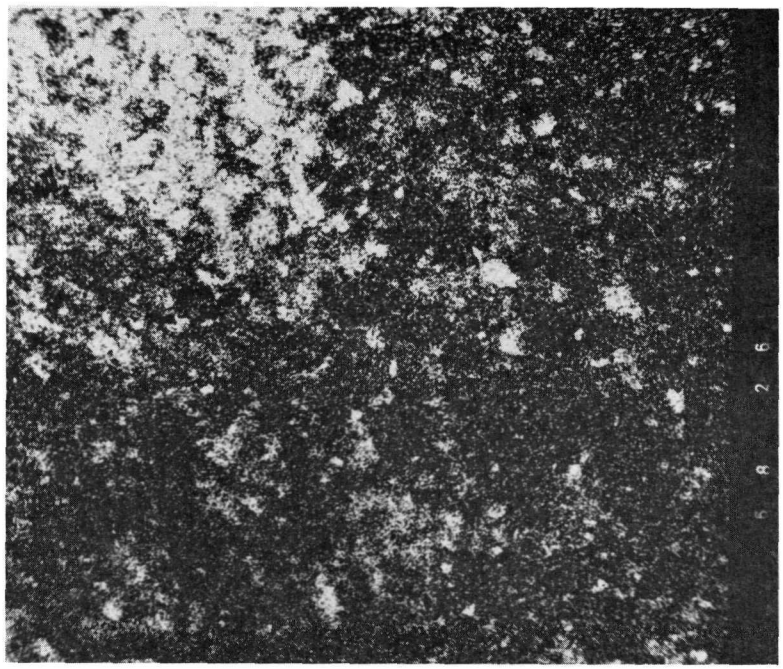

16826

(a) U M_β (300X)

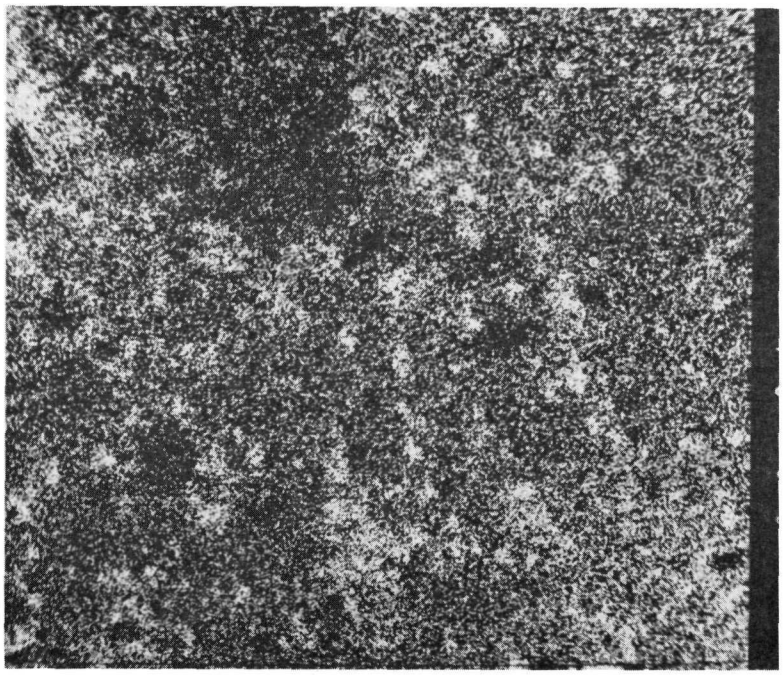

16824

(b) Cs L_α (300X)

Figure 4.3-21. X-ray Maps of Area Shown in Figure 4.3-20(a)

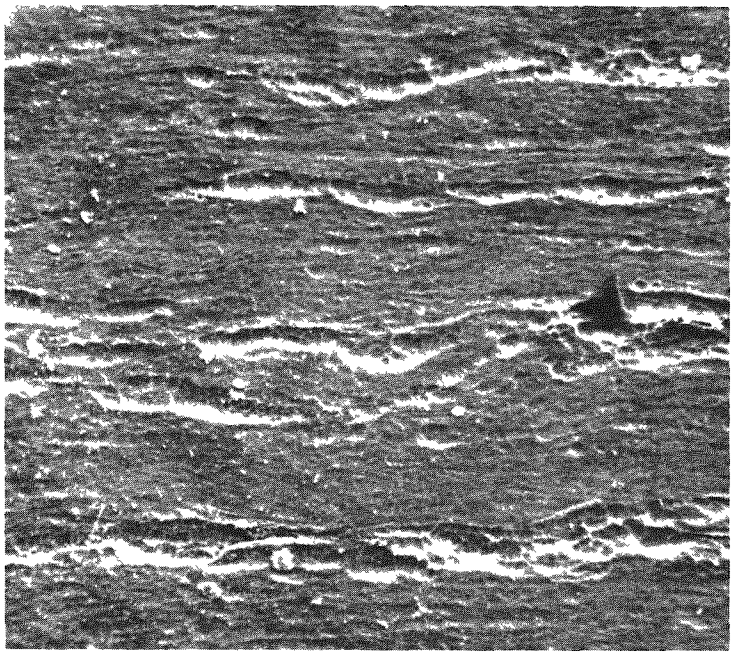

Figure 4 3-22 Zr-Liner Surface in Plenum Section (SRP-3/18)

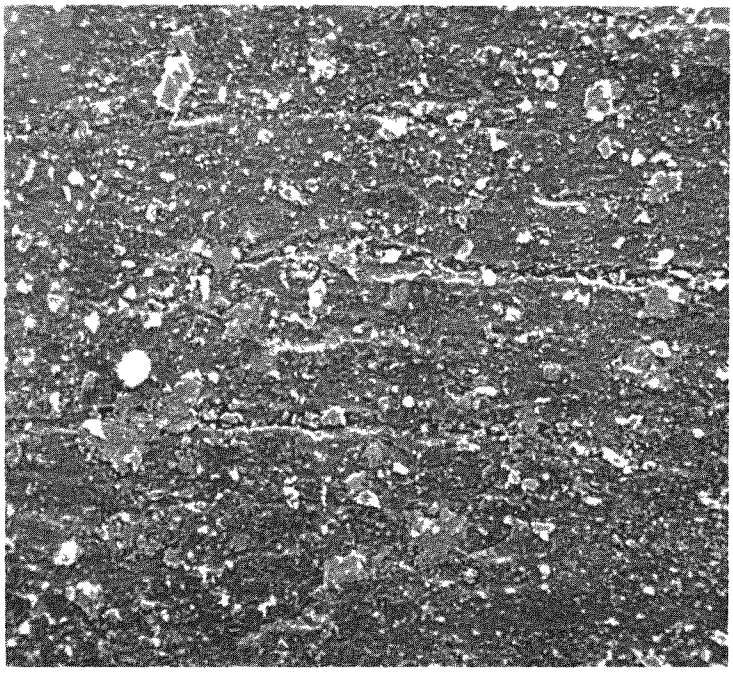

Figure 4 3-23 Zr-Liner in Fueled Section (SRP-3/18, H-2)

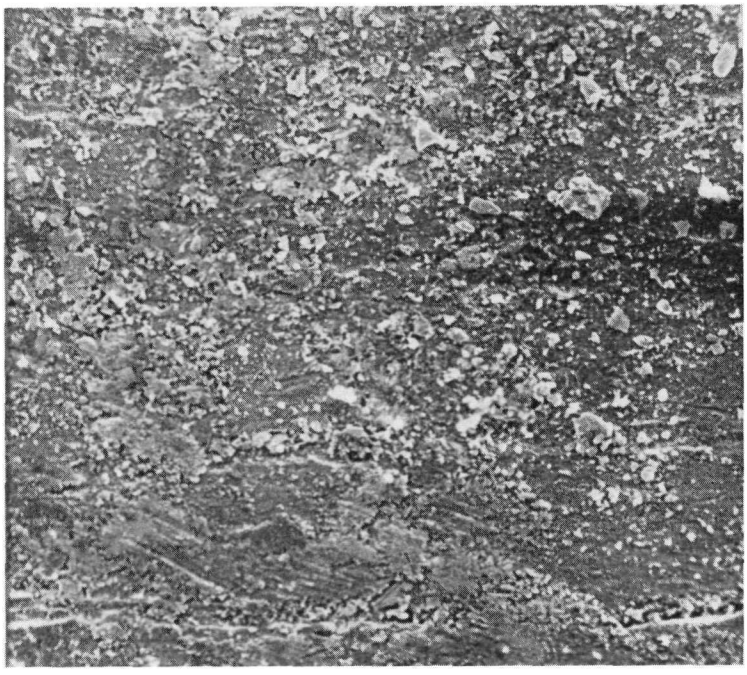

16469 (a) SECONDARY ELECTRON IMAGE (300X)

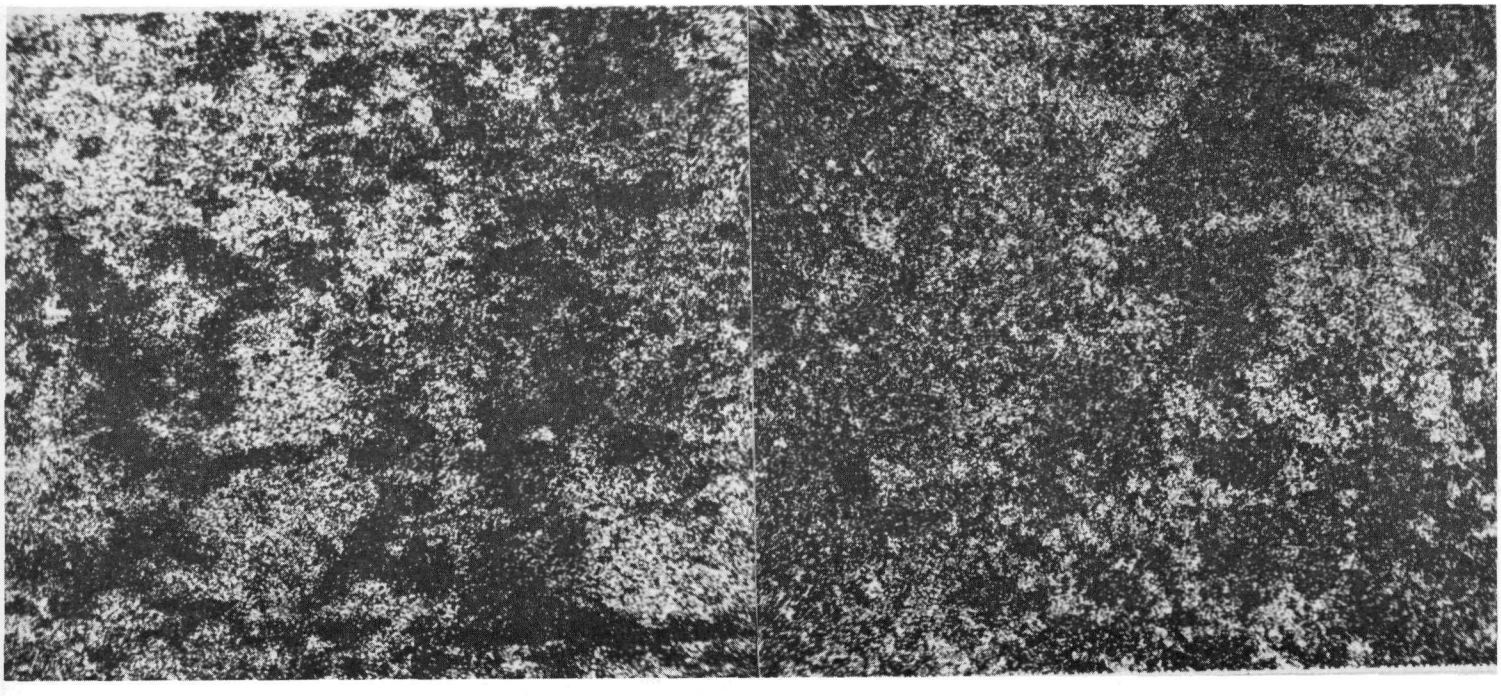

16472 (b) Zr L_{α} X-RAY MAP

16471 (c) U M_{β} X-RAY MAP

Figure 4.3-24. Deposit on Zr-Liner Surface at Pellet Interface Location (SRP-3/18, H-2)

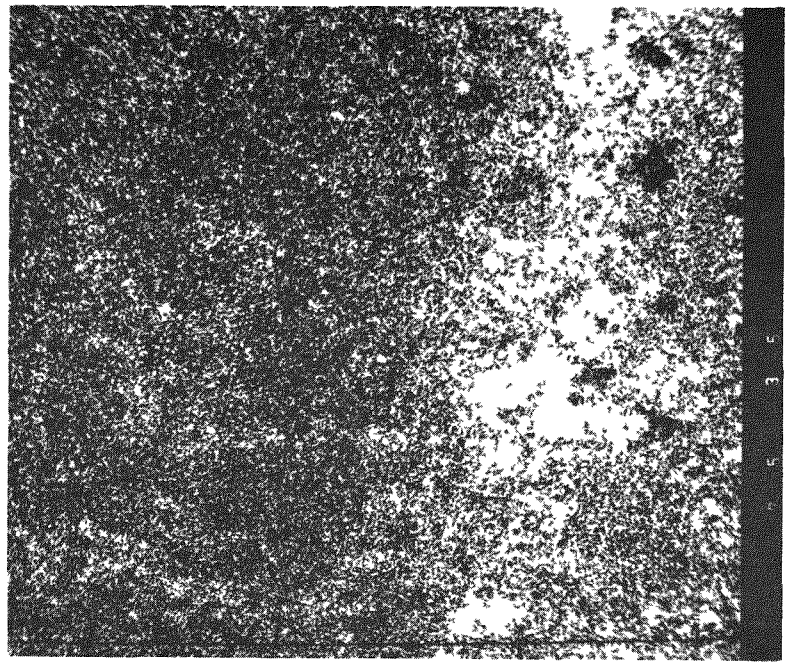

17535

(a) C_S L_α (300X)

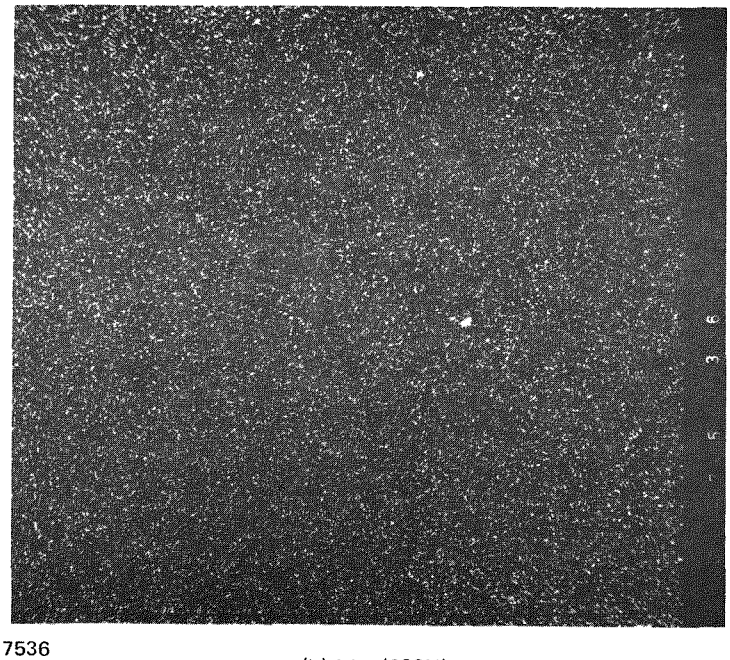

17536

(b) I L_α (300X)

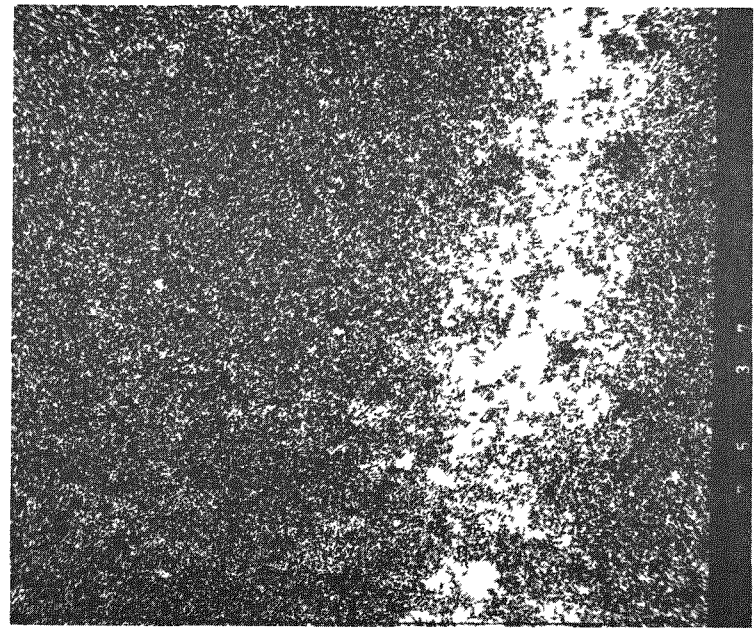

17537

(c) Te L_α (300X)

Figure 4 3-25 Fission Product X-ray Maps of Area Shown in Figure 4 3-24(a)

ACKNOWLEDGEMENTS

The contributing authors of Subsection 4.3 gratefully acknowledge the help of their colleagues:

K. Saltvedt and his staff at the R2 reactor in Sweden for their support and cooperation leading to the successful ramp tests of the GE segments in R2.

G. P. Wozadlo of the Irradiation Processing Operation for performance of hot cell activities in support of post-irradiation examination and shipping of segments.

J. M. Isaacson of NTD for coordination of destructive examinations of fuel specimens.

R. E. Smith and D. L. Orten of the Irradiation Processing Operation for hot cell metallography.

M. Alper, M. M. Csicsery, R. D. Reager, and D. E. Rey of NTD for providing chemical analyses of fuel and cladding samples.

T. C. Rowland of NTD for assistance in the performance and evaluation of the R2 irradiation tests.

5. PART 3. LEAD TEST ASSEMBLIES

5.1 OBJECTIVES

1. Design, license and fabricate four lead test assemblies (LTA's) of barrier fuel:

   —Copper barrier on etched Zircaloy

   —Copper barrier on autoclave-oxidized Zircaloy

   —Zirconium-liner (crystal bar zirconium) coreduced with Zircaloy

   —Zirconium-liner (low-oxygen sponge zirconium) coreduced with Zircaloy

2. Characterize selected fuel rods from each LTA to enable subsequent evaluations of irradiation-induced changes.

3. Establish the capability for documenting power histories of the LTA's to facilitate subsequent performance evaluations.

5.2 TASK 1.0 DESIGN AND LICENSING (J. A. Baumgartner, BWRSED)

Final Task 1.0 activities in Part 3 have been directed toward engineering support of the barrier lead test assembly fabrication and characterization, and completion of the licensing documentation.

Barrier Lead Test Assembly Design

The design characteristics of the lead test assemblies which were presented in the First Semiannual Report[2] have been incorporated as required in the completed assemblies. Figures 5.1-1 to 5.1-4 show the fuel rod matrices for each of the four lead test assemblies. Bundle serial numbers, individual rod serial numbers, and locations of fully characterized rods are identified. Figure 5.1-5 illustrates the rod types by enrichment which applies to all of the barrier LTAs.

The following is a summary description of the pre-irradiation characterization performed, per engineering instructions, on the lead test assembly components.

Fuel Pellets

Samples were taken from each enrichment and records of density measurements, microstructure, and chemical analyses were maintained.

Tubing

Ultrasonic testing (U/T) for flaws was performed and strip chart records made for all tubes used in the barrier LTA fuel rods. Destructive examination of some Zr-liner tubes was done to determine and document characteristics of the U/T indications. This also provides a high level of confidence that none of the subrejectable flaws recorded in the Zr-liner tubing exceed the thickness of the liner. Ultrasonic testing flaw detection on the Cu-barrier tubes was performed prior to plating.

Dimensional measurements (inside diameter, wall thickness, and ovality) were made on all tubes. Chart recordings as a function of axial position have been maintained.

Eddy-current traces on all Cu-barrier tubes were made both before and after plating to measure and document plating thickness. A third set of eddy-current traces was run on completed Cu-barrier rods after it was found that indications of potential damage to the copper during fuel loading could be detected.

Mechanical and metallurgical test data were obtained on samples of the copper-barrier and zirconium-liner tubes. Data include tensile properties, burst pressure, liner bonding, grain size, hydride orientation, surface finish, and chemical analysis (oxygen, hydrogen, nitrogen).

Fuel Rods

Rod length measurements were obtained on all fuel rods. Water rod lengths and spacer positioning tab locations were also measured.

Rod diameter profilometry was performed on the fully characterized rods indicated in Figures 5.1-1 through 5.1-4. Fuel rods were measured in a single helical pass. Data was recorded digitally on magnetic tape and simultaneously plotted on 4 linear traces (0°, 45°, 90°, 135°) and one helical trace derived from one single helical pass.

Eddy-current traces, utilizing equipment like that which is planned for use at reactor site examinations, also were obtained for all of the fuel rods. These additional eddy-current measurements are particularly important in providing a pre-irradiation signature on the Cu-barrier rods because of the high eddy-current sensitivity to Cu-plating anomalies.

X-ray radiographs were taken of the entire plenum region on all fully characterized rods.

Licensing

A supplemental licensing document for application of the four barrier LTA's to Reload 4 (Cycle 5) at Quad Cities Unit 1 was prepared and given to Commonwealth Edison Co. for submittal to the U.S. Nuclear Regulatory Commission. The licensing supplement presents a description of the barrier LTA's and gives the results of design and safety analyses performed to support their operation in Quad Cities 1.

5.3 TASKS 2.0 AND 3.0 FABRICATION, CHARACTERIZATION AND QUALITY ASSURANCE (R. L. Chambers, R. E. Donaghy, R. J. Mack, R. S. Moore, C. D. Williams, WMD)

Fabrication of the four LTA's was completed and shipment of the LTA's to the Quad Cities Nuclear Power Station was in time for the scheduled refueling outage of Quad Cities Unit 1 at the end of Cycle 4 (January, 1979). The LTA's have been inserted into the core of Quad Cities Unit 1 at the beginning of Cycle 5, which started on February 27, 1979.

5.3.1 Cu-Barrier

After introduction of several modifications designed to optimize the copper plating process, plating was initiated on both bright-etched and autoclave-oxidized tubing for the LTAs. Each plated tube was inspected for the following copper quality attributes:

Plate Thickness

Copper thickness was measured nondestructively using an eddy-current technique. The acceptance criterion was set at 0.0004 ± 0.0001 inches (10 ± 2.5 μm).

Visual Appearance

Visual appearance evaluations were conducted at a 1x magnification. A variable focus boroscope was utilized to inspect the full length of the tubing. The integrity of each tube was judged against a physical standard. This standard was chosen on the basis of loadability tests conducted on a tube exhibiting significant blistering.

Copper Adherence

Bond and scribe testing were employed to establish whether the copper plate was adherent.

Inspection results revealed excellent control on copper thickness. Visual appearance and adhesion of tubing copper plated on unoxidized Zircaloy were judged to be acceptable. By comparison, many of the tubes plated on an oxidized surface exhibited blistering and a lack of plating adhesion. Based on loading test results, these tubes were judged to be acceptable for assembly into the lead test bundles.

Subsequent to copper plating and inspection operations, these tubes were cut to length prepared for end plug welding, *i.e.,* chemical removal of copper from the end of the tubes, dried and transferred to the fuel loading area.

After loading the fuel pellets, the fuel rods were outgassed, final end plug welded, characterized and assembled into bundles. Standard bundle inspections were performed in preparation for shipment.

5.3.2 Zr-Liner

Following processing (coextrusion, reduction and inspection), the crystal bar and sponge zirconium lined tubes were autoclaved on the outer surface only. This was accomplished by welding temporary end plugs on the tubes prior to exposure to the steam environment.

After the autoclave treatment, the temporary end plugs were removed and the tubes were inspected for length, dried and transferred to the fuel loading area. Pellet loading was conducted without major difficulty; however, it was determined that loading proceeded more smoothly when short stacks of pellets were pushed into the tube rather than insertion of the entire column as currently done on standard production hardware. This response can be related to the relatively soft, non-oxidized characteristic of the pure zirconium liner.

After loading, the fuel rods were outgassed, and the final endplug welded. The fuel rods were characterized and assembled into bundles. Standard bundle inspections were performed in preparation for shipment.

5.3.3 Quality Measurements

The major activities in the second half of 1979 were the inspection of copper plated tubes, inspection and characterization of the full length and segmented fuel rods, rods with copper plating and zirconium liners, and preparation of the documentation required to support release of the four fuel bundles for shipment.

The primary method for inspection of the copper plated tubes was the eddy-current technique previously discussed. Tubes were subjected to eddy-current inspection before and after plating. Tubes showing satisfactory thickness and uniformity of copper were also subjected to visual inspection for the presence of stains and blisters; and samples of the tubes were subjected to tests for adhesion of the copper, using a bend technique or a scribe technique defined in the quality planning and product specifications.

After loading of the rods with fuel pellets of the prescribed enrichment, the rods were prepressurized and closure-welded and then subjected to routine x-ray inspection, enrichment scanning, visual and dimensional inspections. The rods were also dimensionally characterized by equipment similar to that which will be used for site inspection after bundle irradiation (see Section 5.4).

Finally the bundles were assembled using routine procedures, and submitted to standard inspection prior to release for shipment.

Throughout the quality activities, deviations from specification requirements were judged by a Material Review Board (MRB) activity provided by the appropriate Quality and Design organizations. In some situations special tests were carried

out to support MRB dispositions. For example: (a) microblisters and (b) stains on the copper near the end-plug regions (where copper had been removed by an acid treatment). In case (a) loading tests showed that the microblisters were highly resistant to damage by UO_2 pellets during rod loading, and a repetitive frictional sliding test showed the copper integrity to be fully retained after extended sliding interaction with UO_2 pellets. In case (b) Auger Spectroscopy showd the stains to be a thin (approximately 1500 Å) layer of copper oxide, formed by interaction with traces of nitric acid during the end-plug zone cleaning operation. Documentation of these special tests is included in the program documentation data package.

The details of all inspection work, and MRB dispositions where these were required, are recorded in the Quality Notices covering fabrication of the cladding, rods, and bundles.

5.4 TASK 4.0 IRRADIATION AND EVALUATION (S. Sen and B.U.B. Sarma, NTD)

To monitor and evaluate the performance of the barrier LTAs a data acquisition system, which tracks the detailed power history of the reactor operations, was installed at the site. This comprised installation of a magnetic tape unit and also the software package for the Fuel Performance Analyses and Data Acquisition System (FPADAS).[1] Checkout and verification of the program system were completed prior to the scheduled shutdown of the Quad Cities 1 reactor (end of Cycle 4, January, 1979).

	A	B	C	D	E	F	G	H
1	VA00102	VE00102	ZE00105 TIE ROD	VK00103	VK00111	ZE00103 TIE ROD	VK00108	VE00104
2	VE00101	VK00109	VV00102	ZP00102	VV00111	VV00113	VV00103	VK00105
3	ZE00104 TIE ROD	VV00101	VV00116	VV00109	ZA00109	ZA00110	ZP00104	ZK00102 TIE ROD
4	VK00101	ZP00101	VV00106	SEGMENT ROD ZX00106 ZX00103 ZX00101 ZX00112	WATER ROD	ZA00105	ZA00108	VV00110
5	VK00110	VV00105	ZA00101	WATER ROD	ZA00107	ZA00113	ZP00103	VV00115
6	ZE00102 TIE ROD	VV00114	ZA00104	ZA00114	ZA00106	ZA00112	ZA00115	ZK00104 TIE ROD
7	VK00106	VV00117	ZP00105	ZA00103	ZP00106	ZA00111	SEGMENT ROD ZX00116 ZX00115 ZX00114 ZX00113	XN00102
8	VE00105	VK00107	ZK00101 TIE ROD	VV00107	VV00104	ZK00103 TIE ROD	XN00101	VK00104

XXXXXXX -- ROD SERIAL NUMBER

-- FULLY CHARACTERIZED ROD

Figure 5.1-1. Fuel Rod Serial Numbers and Locations of Fully Characterized Rods, Zirconium Liner (Crystal Bar Zirconium) Coreduced with Zircaloy Bundle Serial Number LJB586

	A	B	C	D	E	F	G	H
1	VB00101	VG00103	ZG00103 TIE ROD	VL00105	VL00111	ZG00102 TIE ROD	VL00101	VG00104
2	VG00101	VL00106	VW00102	ZS00102	VW00108	VW00105	VW00112	VL00102
3	ZG00104 TIE ROD	VW00101	VW00111	VW00107	ZB00113	ZB00111	ZS00104	ZL00105 TIE ROD
4	VL00103	ZS00101	**SEGMENT ROD XS00106 XS00105 XS00102 XS00101**	SEGMENT ROD	WATER ROD	ZB00107	ZB00102	VW00113
5	VL00110	VW00104	ZB00106	WATER ROD	ZB00105	ZB00101	ZS00105	VW00110
6	ZG00101 TIE ROD	VW00115	ZB00103	ZB00104	ZB00115	ZB00108	ZB00109	ZL00104 TIE ROD
7	VL00108	VW00106	ZS00106	ZB00110	ZS00107	ZB00114	**SEGMENT ROD XS00111 XS00109 XS00108 XS00107**	VS00101
8	VG00105	VL00109	ZL00102 TIE ROD	VW00109	VW00103	ZL00101 TIE ROD	VS00102	VL00107

XXXXXX – ROD SERIAL NUMBER

– FULLY CHARACTERIZED ROD

Figure 5.1-2. Fuel Rod Serial Numbers and Locations of Fully Characterized Rods, Zirconium Liner (Low Oxygen Sponge Zirconium) Coreduced with Zircaloy Bundle Serial Number LJB587

	A	B	C	D	E	F	G	H
1	VC00101	VH00102	ZH00104 TIE ROD	XP00108	XP00106	ZH00101 TIE ROD	XP00105	VH00104
2	VH00101	XP00103	VX00109	ZT00102	VX00108	VX00104	VX00110	XP00109
3	ZH00102 TIE ROD	VX00113	VX00101	VX00105	ZC00102	ZC00109	ZT00103	ZM00102 TIE ROD
4	XP00110	ZT00101	VX00117	SEGMENT ROD ZV00110 ZV00109 ZV00108 ZV00107	WATER ROD	ZC00114	ZC00103	VX00112
5	XP00107	VX00116	ZC00101	WATER ROD	ZC00108	ZC00104	ZT00107	VX00114
6	ZH00103 TIE ROD	VX00111	ZC00111	ZC00112	ZC00110	ZC00107	ZC00113	ZM00103 TIE ROD
7	XP00101	VX00107	ZT00104	ZC00105	ZT00105	ZC00106	SEGMENT ROD ZV00104 ZV00103 ZV00102 ZV00101	VT00101
8	VH00102	XP00104	ZM00101 TIE ROD	VX00118	VX00115	ZM00104 TIE ROD	VT00102	XP00102

XXXXXX -- ROD SERIAL NUMBER

-- FULLY CHARACTERIZED ROD

Figure 5.1-3. Fuel Rod Serial Numbers and Locations of Fully Characterized Rods, Copper Barrier on Etched Zircaloy, Bundle Serial Number LJB588

	A	B	C	D	E	F	G	H
1	VD00101	VJ00104	ZJ00104 TIE ROD	VN00106	VN00110	ZJ00101 TIE ROD	VN00103	VJ00103
2	VJ00101	VN00101	VZ00103	ZU00102	VX00109	VZ00111	VZ00101	VN00107
3	ZJ00103 TIE ROD	VZ00102	VZ00113	VZ00117	ZD00103	ZD00114	ZU00104	ZN00104 TIE ROD
4	VN00102	ZU00101	VZ00105	SEGMENT ROD ZW00111 ZW00110 ZW00109 ZW00108	WATER ROD	ZD00108	ZD00110	VZ00110
5	VN00109	VZ00114	ZD00101	WATER ROD	ZD00109	ZD00112	ZU00105	VZ00115
6	ZJ00102 TIE ROD	VZ00108	ZD00111	ZD00102	ZD00106	ZD00113	ZD00107	ZN00105 TIE ROD
7	VN00108	VZ00107	ZU00106	ZD00105	ZU00103	ZD00104	SEGMENT ROD ZW00107 ZW00106 ZW00105	VU00102
8	VJ00102	VN00104	ZN00101 TIE ROD	VZ00106	VZ00112	ZN00103 TIE ROD	VU00101	VN00105

XXXXXX — ROD SERIAL NUMBER

— FULLY CHARACTERIZED ROD

Figure 5.1-4. Fuel Rod Serial Numbers and Locations of Fully Characterized Rods, Copper Barrier on Autoclave-Oxidized Zircaloy. Bundle Serial Number LJB589

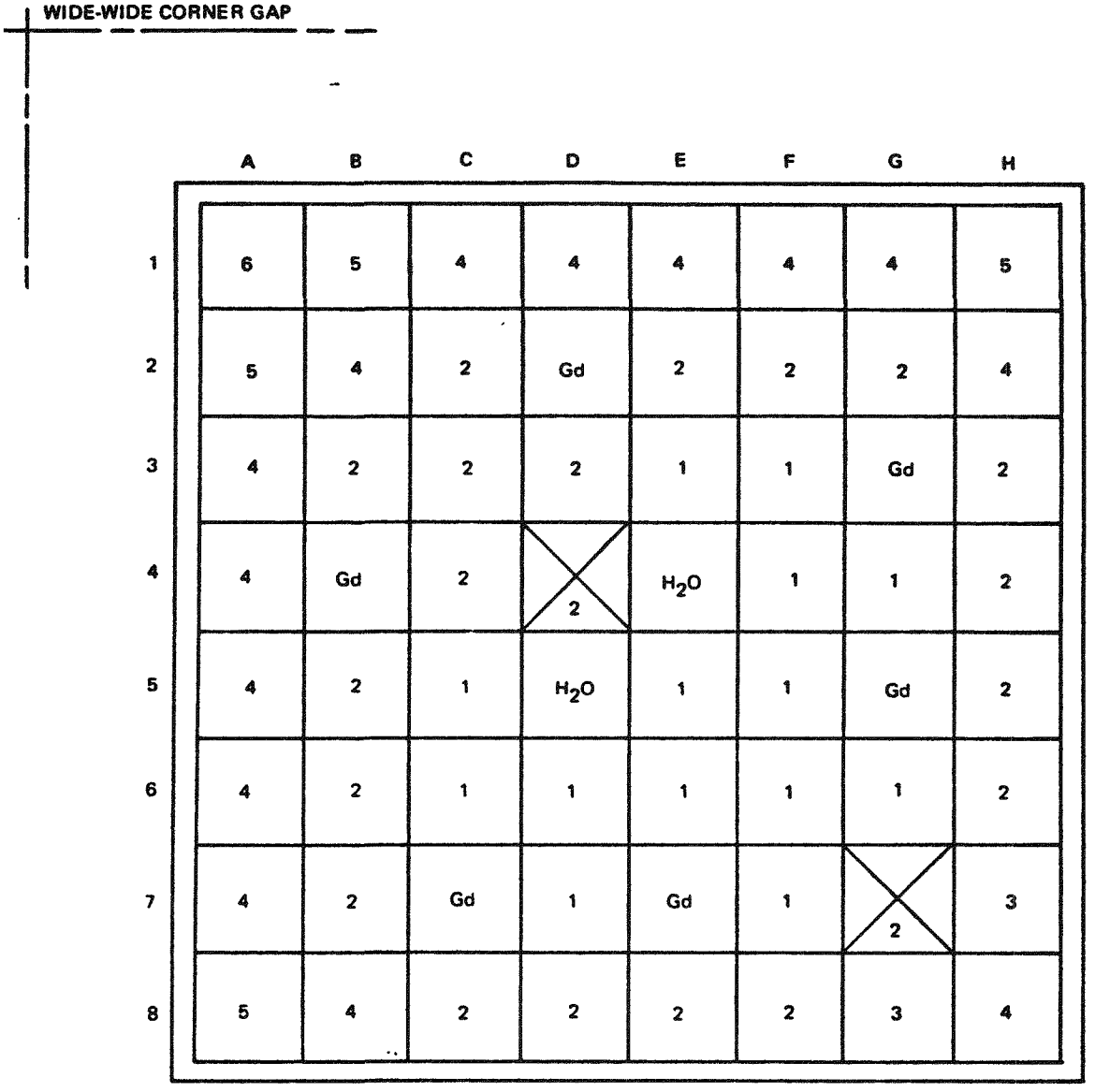

ROD TYPE	U-235 (wt%)	Gd_2O_3 (wt%)	NUMBER OF RODS
1	3.8	–	14
2	3.0	–	21
3	2.4	–	2
4	2.0	–	14
5	1.7	–	4
6	1.3	–	1
Gd	3.0	2.0	6
H_2O	WATER RODS	–	2

⊠ = SEGMENTED ROD POSITIONS

Figure 5.1-5. Cross Section of Bundle with 2.82% Average Enrichment and 6 Rods with 2 Wt% Gd_2O_3

ACKNOWLEDGMENTS

The contributing authors of Section 5 gratefully acknowledge help by many of their colleagues, particularly:

R. A. Day of the GE Advanced Reactor Systems Department for his efforts in developing eddy-current techniques suitable for monitoring the performance of the barrier LTAs.

C. C. Guitton of BWRSED for assistance with design and licensing of the LTAs.

W. von Ketron and C. A. McKinney of WMD for assistance with the plating of the Cu-barrier cladding.

W. T. Grubb, L. King and L. Niedrach of CRD for their help on matters pertaining to the chemistry of the plating processes.

S. L. Rowley, of WMD for scheduling the fabrication of the LTAs.

D. R. Rutkin and C. H. Ballard of NTD for their help in establishing the data acquisition system and in arranging for pre-irradiation characterization of the LTAs.

6. REFERENCES

1. *Demonstration of Fuel Resistant to Pellet-Cladding Interaction, Second Semiannual Report, January-June 1978,* compiled by H. S. Rosenbaum, September 1978 (GEAP-23773-1).

2. *Demonstration of Fuel Resistant to Pellet-Cladding Interaction, First Semiannual Report, July-December 1977,* compiled by H. S. Rosenbaum, February 1978 (GEAP-23773).

3. R. K. Haling, "Operating Strategy for Maintaining an Optimum Power Distribution throughout Life," TID-7642, ANS Topical Meeting, San Francisco, CA, September 26-27, 1963.

4. D. S. Tomalin, R. B. Adamson, R. P. Gangloff, "The Performance of Irradiated Copper and Zirconium Barrier-Modified Zircaloy Cladding under Simulated PCI Conditions," September 1978, to be published in ASTM STP 681, 1979, (NEDO-12715).

5. R. P. Gangloff, "The Behavior of Unirradiated Zr-lined and Cu-plated Zircaloy-2 Tubing under Simulated Pellet-Cladding Interaction Conditions," GEAP-25093, to be issued.

6. D. E. Newbury, "Quantitative Analysis by Secondary Ion Mass Spectrometry," in *Quantitative Surface Analysis of Materials,* ASTM STP 643, American Society for Testing and Materials (1978).

7. E. F. Sturcken and W. G. Duke, "Measurement of Preferred Orientation of Thin-Walled Zircaloy-2 Tubes," Dp-607, E. I. du Pont de Nemours & Co., Savannah River Laboratory (November 1961).

8. J. J. Kerns, "Thermal Expansion and Preferred Orientation in Zircaloy," WAPD-TM-472, Westinghouse Electric Co., Bettis Atomic Power Laboratory, (November 1965).

9. L. G. Shulz, *J. Appl. Phys.,* **20,** 1030 (1949).

10. H. S. Rosenbaum and J. E. Lewis, *J. Nucl. Mater.,* **67,** 273 (1977).

11. B. D. Cullity, *Elements of X-ray Diffraction,* Addison-Wesley, Reading, Massachusetts, 1959, P. 269.

12. D. Cubicciotti and J. S. Sanecki, J. Nucl. Mater., **78**, 96 (1978).

DISTRIBUTION

U.S. DOE Distribution (150)
Category UC-78

D. J. Groetch
Knolls Atomic Power Laboratory
P.O. Box 1072
Schenectady, NY 12301

H. W. Schadler, Manager
Metallurgy Laboratory
General Electric Company
Research and Development Center
P.O. Box 8
Schenectady, NY 12301

F. W. Buckman
Consumers Power Company
1945 Parnall Road
Jackson, MI 49201

M. D. Freshley (3)
Battelle Pacific Northwest Laboratory
Battelle Blvd.
Richland, WA 99352

C. R. Hann
Battelle-Northwest Laboratory
Richland, WA 99352

K. Woods
Exxon Nuclear Company, Inc.
Richland, WA 99352

C. E. Crouthamel
Exxon Nuclear Company, Inc.
Richland, WA 99352

G. Sofer
Exxon Nuclear Company, Inc.
Richland, WA 99352

T. Snead
Duke Power Company
P.O. Box 2178
Charlotte, NC 28342

J. Korthever
Duke Power Company
P.O. Box 2178
Charlotte, NC 28342

J. T. A. Roberts
Electric Power Research Institute
P.O. Box 10412
Palo Alto, CA 94303

F. E. Gelhaus
Electric Power Research Institute
P.O. Box 10412
Palo Alto, CA 94303

J. R. Tomonto
Florida Power and Light Company
P.O. Box 013100
Miami,FL 33101

Gordon Bond
GPU Service Corporation
260 Cherry Hill Road
Parsippany, NJ 07054

W. J. Tunney
Long Island Lighting Company
175 East Old Country Road
Hicksville, NY 11801

Howard Sobel
American Electric Power Service Corp.
Nuclear Materials and
Fuel Management Section
2 Broadway
New York, NY 10004

Orville Cypret
Arkansas Power Light
P.O. Box 551
Little Rock, AK 72203

J. Tulenko
Babcock Wilcox Company
Nuclear Power Generation Division
P.O. Box 1260
Lynchburg, VA 24505

R. N. Duncan
Combustion Engineering, Inc.
100 Prospect Hill Road
Windsor, CT 06095

W. M. Kiefer (6)
Commonwealth Edison Company
P.O. Box 767
Chicago, IL 60690

M. L. Lee
Consolidated Edison Company of New York
4 Irving Place
New York, NY 10003

D.B. Wehmeyer
Detroit Edison Company
2000 Second Avenue
Detroit, MI 48226

S. W. Wilczek, Jr.
Niagara Mohawk Power Corporation
300 Erie Boulevard West
Syracuse, NY 13202

J. P. Cagnetta
Northeast Utilities Service Company
P.O. Box 270
Hartford, CT 06101

John Hallam
Nuclear Services Corporation
1700 Dell Avenue
Campbell, CA 95008

G. F. Daebeler
Philadelphia Electric Company
2301 Market Street
P.O. Box 8699
Philadelphia, PA 19101

Kashmiri Mahna
Public Service Electric and Gas Company
80 Park Place
Newark, NJ 07101

R. R. O'Laughlin
Public Service Indiana
1000 East Main Street
Plainfield, NH 46168

R. J. Mullin
Tennessee Valley Authority
1410 Commerce Union Bank Building
Chattanooga, TN 37402

D. L. Larkin
Washington Public Power Supply System
P.O. Box 968
Richland, WA 99352

R. S. Miller
Westinghouse Electric Corporation
Nuclear Fuel Division
P.O. Box 355
Pittsburgh, PA 15230

R. M. Grube
Yankee Atomic Electric Company
20 Turnpike Road
Westboro, MA 01581

E. Straker
Science Applications, Inc.
8400 Westpark Drive
McLean, VA 22101

R. Omberg
Hanford Engineering Development Laboratory
P.O. Box 1970
Richland, WA 99352

W. Lipinski
Argonne National Laboratory
9700 South Cass Avenue
Argonne, IL 60439

W. R. Harris
Rand Corporation
1700 Main Street
Santa Monica, CA 90406

T. Rowe
Oak Ridge National Laboratory
P.O. Box X
Oak Ridge, TN 37830

U.S. Department of Energy
NASAP Control Office
Room F-409 (Mail Stop B-107)
Germantown, MD 20767

I.I. Spiewak
Oak Ridge National Laboratory
P.O. Box X
Oak Ridge, TN 37830

B. A. Pasternak
Booz-Allen Applied Research
4330 East-West Highway
Bethesda, MD 20014

D. R. O'Boyle
Commonwealth Edison Company
P.O. Box 767
Chicago, IL 60690

L. A. Niemark
Argonne National Laboratory
9700 South Cass Avenue
Argonne, IL 60439

R. W. Weeks
Argonne National Laboratory
9700 South Cass Avenue
Argonne, IL 60439

Carl Johnson
Argonne National Laboratory
9700 South Cass Avenue
Argonne, IL 60439

J. Horak
Oak Ridge National Laboratory
P.O. Box X
Oak Ridge, TN 37830

W. A. Weinreich
Bettis Atomic Power Laboratory
P.O. Box 79
West Mifflin, PA 1512

H. Ochen
Electric Power Research Institute
P.O. Box 10412
Palo Alto, CA 94304

P. E. MacDonald
EG&G Idaho, Inc.
P.O. Box 1625
Idaho Falls, ID 83401

Bettis Atomic Power Laboratory
Technical Library
P.O. Box 79
West Mifflin, PA 15122

Knolls Atomic Power Laboratory
Techical Library
P.O. Box 1072
Schenectady, NY 12301

E. L. Courtright
Battelle Pacific Northwest Laboratory
Battelle Blvd.
Richland, WA 99352

P. M. Lang, Chief
Nuclear Reactor Programs Branch (3)
Division of Nuclear Power Development
U.S. Department of Energy
Mail Stop B-107
Washington, DC 20545

W. V. Johnston, Chief
Fuel Behavior Research Branch
Division of Reactor Safety Research
U.S. Nuclear Regulatory Research Commission
Washington, DC 20555